Hochschule **RheinMain**
University of Applied Sciences
Wiesbaden Rüsselsheim

Hochschule RheinMain

Faculty of Engineering
Bachelor of Environmental Engineering

Bachelor Thesis

Alfred-Wegener-Institut

Screening of several *Amphidinium* species and strains for amphidinols and related secondary metabolites

Presented by
Jannik Weber
Examiner: Prof. Dr. Ursula Deister
Supervisor: Dr. Bernd Krock

Name	Jannik Weber	**Student. Nr.**	1032617
Start	22.03.2021	**Due Date**	21.06.2021

I. Acknowledgements

First and foremost, I'd like to express my gratitude to both my examiner Prof. Dr. Ursula Deister, from my home university Hochschule Rhein-Main, Rüsselsheim, for agreeing to examine my thesis to begin with and more importantly for the continuous support not only during the writing process, but also during my studies and exchange semester, as well as to my supervisor Dr. Bernd Krock from Alfred-Wegener-Institut (AWI), for making my thesis possible at AWI and for always being open about my questions even throughout the pandemic, answering them in a helpful and thought provoking manner.

Furthermore, I would like to thank Thomas Max and Annegret Müller from the section "Ecological Chemistry" of AWI. Thomas introduced me into the workways of mass spectrometry and gave me guidance throughout my measurements. His patient approach helped me in becoming more independent in my own works. Anne explained the functionality of various laboratory instruments to me, and she always had an open ear for my questions regarding the laboratory procedures.

A big thank you goes to my brother, Niklas, for always being there as a big brother and to my "Dampfloks" Eduardo and Vincent for making my time in Bremerhaven an athletic and memorable one.

Finally, I want to thank my parents and grandparents. Without their openness towards new challenges and their financial support this thesis would not have happened.

II. List of abbreviations

AMs	Amphidinols
ASP	Amnesic shellfish poisoning
CICESE	Ensenada Center for Scientific Research and Higher Education
DA	Domoic acid
DSP	Diarrheic shellfish poisoning
EPI	Enhanced product ion
ESI	Electrospray ionization
FS	Full scan
HAB	Harmful algal bloom
HPLC-MS	High performance liquid chromatography mass spectrometry
IOC	Intergovernmental Oceanographic Commis-sion
LC-MS/MS	Liquid chromatography with tandem mass spectrometry
LoD	Limit of detection
LPD	Luteophanol D
m/z	Mass to charge ratio
MS	Mass spectrometry
MS 1	First mass analyzer
MS 2	Second mass analyzer
NL	Neutral loss
NMR	Nuclear magnetic resonance
PSP	Paralytic shellfish poisoning
RCF	Relative centrifugal force
S/N	Signal to noise ratio

SRM	Selected reaction monitoring
t_R	Retention time
UHPLC-MS/MS	Ultra-High Performance Liquid Chromatography coupled with tandem mass spectrometry
UPLC-MS/MS	Ultra-performance liquid chromatography coupled with tandem mass spectrometry
UNCW	University of North Carolina, Wilmington
UNEP	United Nations Environment Program

Table of Content

1 Introduction

Throughout the evolutionary development, a remarkable instinct against imminent danger has proven to be a very efficient survival strategy for prey and predatory animals. Similar findings can be found during the human development as well, with the significant difference that humans started being able to identify and understand approaching dangers, in contrast to just sensing them. The change from instinct to understanding diminished the threat of danger and could even transform former dangers into advantages in certain cases. This analogy can be applied to the reasoning behind the selected topic for this bachelor thesis.

Amphidinium is a genus of dinoflagellates, proven to have several biological activities, such as being antifungal, cytotoxic, antimicrobial and ichthyotoxic (Mooney et al., 2010). Even though these biologic activities are confirmed, they do not apply to the entire genus *Amphidinium*, as not every species produces the so called "amphidinols" which are the toxins resulting in the stated biologic activities. In this work a total of eleven different species, with a total of 69 strains of the algal genus *Amphidinium*, originating from the Ensenada Center for Scientific Research and Higher Education (CICESE) based in Ensenada, Mexico and an algal resources collection facility, providing samples from worldwide distributed locations, based in the university of North Carolina Wilmington located in the USA, were examined using mass spectrometry with the intention to identify the given strains as toxic or non-toxic and to possibly discover new variations of amphidinols in the process. This work builds on the master thesis "LC-MS/MS Method for the Discovery and Identification of Amphidinols Produced by *Amphidinium*" written by Marvin Wellkamp in February 2020. One part of the master thesis was the development of a priorly non-existing LC-MS/MS-method that allows the chemical evidence of the presence of amphidinols in a few samples as well as the determination and quantification of amphidinols. This methodological development laid the basis for a screening- of amphidinols in a larger context, which is the aim of the present study.

In addition to the analysis of a large number of *Amphidinium* species for the presence of amphidinols and related secondary metabolites, potentially new and unknown amphidinols should be explored. Due to their size, it is likely that amphidinols have a higher number of structural variations than currently known. Hypothetically, this putative variety increases the possibility to discover new amphidinol variations during the analytical process. The vast majority of samples of this study have not been analyzed for amphidinols so far, therefore the knowledge about existing amphidinols in these strains still has not been explored.

The thesis is structured in five chapters. These being fundamentals describing the biology of the algal genus *Amphidinium*, the impact it has as part of harmful algal blooms on the ecosystem, as well as the operating modes of mass spectrometry and the concept behind the developed LC-MS/MS method, methods and materials, results, discussion, and a concluding summary. The extraction process is presented in detail in the methods and material chapter. Since the provided samples are composed of sets from two locations, the origin of both sample sets is shown as well. Measured toxin levels, distribution of the detected amphidinols and possibly new discoveries are presented under results. Explanations for the findings and proposed structures of amphidinols are made in the discussion part. A final summary concludes the thesis, and a short outlook sets the direction for the subsequent scientific procedure.

2 Fundamentals

2.1 Algal genus *Amphidinium*

Members of the genus *Amphidinium* are among the most abundant dinoflagellates worldwide (Jørgensen et al., 2004). The genus is incredibly diverse, whilst being highly conserved morphologically, it grows easily in culture and thrives in a wide variety of habitats (Jørgensen et al., 2004), temperatures (Murray and Patterson., 2002), and trophic modes (Jørgensen et al., 2004; Murray et al., 2004; Murray and Patterson., 2002), therefore *Amphidinium* has been used as a 'model' dinoflagellate in research for dinoflagellate genetics, polyketide production and photosynthesis (Murray et al., 2012). Dinoflagellates are a unique group of microbial eukaryotes that play a variety of important ecological roles, notably as the core of aquatic food webs, in symbioses with invertebrates such as corals, and as the agents responsible for producing harmful algal bloom toxins (HABs) (Murray et al., 2015). HABs result in a variety of disruptive effects in the environment as well as for the inhabiting species as shown in chapter 2.2. Some *Amphidinium* species can become so abundant as to cause sand discoloration and together with benthic diatoms and cyanobacteria, autotrophic *Amphidinium* species are likely to be some of the most important contributors to primary production in the interstitial zone (Jørgensen et al., 2004). They also produce toxins, named amphidinols, and bioactive compounds that both can have harmful effects. The first report of an amphidinol was the description of amphidinol (1), a potent antifungal agent, in cultures of the dinoflagellate *Amphidinium klebsii* by Satake et al., (1991). *Amphidinium* blooms can cause fish kills and the produced toxins may increase the effects of Ciguatera fish poisoning in affected areas or even cause them in the first place (Baig et al., 2006; Rhodes et al., 2010, Hallegraeff, 1993). These toxins can also have beneficial effects, producing compounds that exhibit antifungal or antimicrobial properties, making them interesting for the biotechnology field, because of their potential in the pharmaceutical area (Karafas et al., 2017).

2.1.1 Biology and bioactive properties

Amphidinium was first described based on the species *A. operculatum* by Claparede and Lachmann in 1859. “The epicone of the species is small and triangular-shaped and is located on a broadly rounded hypocone which is compressed-ventrally. The large nucleus is in the posterior part of the hypocone” (Claparede, Lachmann, 1859).

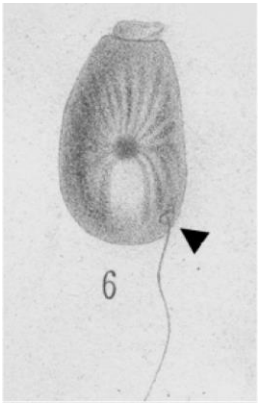

Image 1: Original illustration of *A. operculatum* by Claparede and Lachmann (1859)

This first description of *A. operculatum* was updated with a more detailed description by Jørgensen et al., (2004) and Murray et al., (2004) after examining the original illustrations. “The cells are ovoid to ellipsoidal in shape, with the greatest width between the cell center and the posterior end, which is dorsoventrally flattened. Cells are 29–50 µm long and 21–28 µm wide. The right side of the hypocone is convex, whereas the left is almost straight. A small epicone overlays the anterior central part of the hypocone. In ventral view, the epicone is irregular triangular with the anterior left tip clearly deflected to the left. The epicone is 7–10 µm wide and anteriorly flat. The angle of the anterior right tip is almost 90 degrees, with the anterior left tip forming an angle of approximately 30 degrees. The deeply incised cingulum originates 0.3 cell lengths from the anterior of the cell. The cingulum is displaced and slightly descending, with an angle of approximately 45 degrees between the proximal and distal ends”. After the reworks on the taxonomy of *Amphidinium* by Jørgensen et al., (2004) and Murray et al., (2004) only species, which possess a

small, crescent-shaped epicone which is deflected to the left, belong to the genus *Amphidinium*. The previous taxonomic definition of *Amphidinium* contained 120 species (Murray and Patterson, 2002), from these species only 20 qualified for the redefined conditions of *Amphidinium* by Jørgensen et al., (2004) and Murray et al., (2004). The 120 species were therefore subdivided into the two categories, these being "*Amphidinium* sensu lato" for the remaining 100 species and "*Amphidinium* sensu stricto" for the 20 species, that meet the newly defined requirements. (Jørgensen et al., 2004).

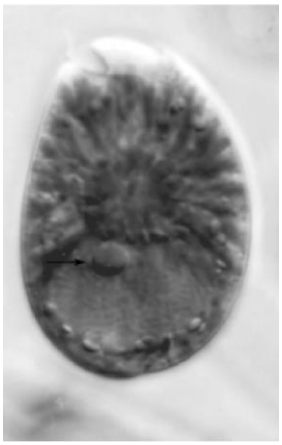

Image 2: *A. operculatum* (Murray et al., 2004)

The biology of *A. carterae* was also described as part of the publication of Murray et al., (2004). "The cells are oval from the ventral side and dorsoventrally flattened. The cells are 10–20 µm long, 9–13 µm wide, and approximately 6µm in breadth. The epicone is crescent shaped from the ventral side and clearly deflected toward the left. The cingulum begins 0.3–0.4 of the cell length from the apex, midway across the ventral face, rising initially, and then descending on the ventral side" (Murray et al., 2004).

Image 3: *A. carterae* (Murray et al., 2004)

Compounds produced by *Amphidinium* include macrolides, short linear polyketides, and long-chain polyketides. Amphidinols (AMs) are one common type of polyketide compound produced by *A. carterae* and closely related species, with approximately 20 analogues known, displaying a variety of properties including hemolytic and antifungal activity (Murray et al., 2015). Since the first family member was reported as a potent antifungal agent in 1991 by Satake et al., amphidinols and the closely related analogues, luteophanols, lingshuiols, carteraols, formed an important group of natural bioactive marine products. Known for its hemolytic, cytotoxic, algicidal and ichthyotoxic activity, karlotoxin (Mooney et al., 2009), is a linear amphipathic polyketide, produced by the genus *Karlodinium*, similar in activity to the hemolytic toxins of amphidinols. Karlotoxin acts as a membrane disrupting molecule containing cholesterol, resulting in swelling and ultimately osmotic cell lysis (Mooney et al., 2010). The amphidinols mode of action involves binding to lipids in the bilayer membrane, with the polyene part, which increases membrane permeability (Satake et al., 2017). Further investigation of *Amphidinium* strains led to isolation of Luteophanols B, C, and D (Kubota et al., 1998, 2005). Luteophanol D is the only luteophanol compound investigated to date for its biological activity, and it has been reported to have antibacterial effects (Murray et al., 2015).

All species except for *A. fijiensis* and *A. massartii* showed toxicity in a brine shrimp assay as shown in table 1 below along with other additional morphological features.

The most toxicity resulted from extractions of *A. gibbosum* where there was substantial cell death after 24 h and complete cell death after 48 h. Strains of *A. tomasii*, *A. theodori*, *A. magnum*, and *A. carterae* displayed the most initial cell death, aside from *A. gibbosum*, and each had less than 90% cell viability after 24 h, with *A. tomasii* showing the most initial toxicity among these with only 74% cell viability at 24 h (Karafas et al 2017).

Table 1: Morphological features of *Amphidinium* species (Karafas et al., 2017)

Genus	Length [µm]	Width [µm]	Shape	Cell division	Metabolic movement	Toxic
A. carterae	10 – 20	9 – 13	Round, elliptical	Motile	No	Yes
A. massartii	6 – 21	5 – 17	Round, oval, elliptical	Motile	No	No
A. thermaeum	8 – 30	8 – 20	Round, oval	Cysts	Yes	Yes
A. pseudomassartii	13 – 21	8 – 19	Round, elliptical	Motile	No	Yes
A. theodori	13 – 21	10 – 17	Elliptical, oval	Cysts	Yes	Yes
A. fijiensis	10 – 23	6 – 15	Round elliptical oval, pear – shaped	Cysts	Yes	No
A. trulla	18 – 31	17 – 23	Oval, elliptical	Motile	No	Yes
A. tomasii	19 – 42	13 – 25	Round oval elliptical	Motile	No	Yes
A. paucianulatum	17 – 41	12 – 35	Elliptical, pear – shaped	Motile	No	Yes

Genus	Length [µm]	Width [µm]	Shape	Cell division	Metabolic movement	Toxic
A. magnum	26 – 47	14 – 36	Oval	Motile	No	Yes
A. gibbosum	24 – 43	17 – 23	Elliptical, "hump-back"	Motile	No	Yes

Light, salinity, and temperature have been shown to affect hemolytic activity by a strain of *A. carterae* in culture, with higher salinities and temperatures being associated with the highest hemolytic activity (Zimmermann, 2006, Murray et al., 2015). Furthermore, closely related species from different geographic regions can have very different toxin profiles (Rhodes et al 2010).

2.2 Harmful algal blooms

Virtually every coastal region of the world is affected by harmful algal blooms (HABs) (Hallegraeff, 1993) commonly called red tides. Since the latter term includes many blooms that discolor the water but cause no harm and excludes blooms of highly toxic cells that cause problems at low and essentially invisible cell concentrations, the term HAB is preferred (Anderson et al., 2012). The term harmful algal blooms (HABs) was coined by the Intergovernmental Oceanographic Commission (IOC) of UNESCO to describe any proliferation of microalgae, regardless of the concentration, that is perceived as a nuisance because of its negative socio-economic impact on public health, fisheries resources, and coastal commodities (Díaz et al., 2019). HABs are most common in coastal marine ecosystems, but they may also affect the open ocean as well as brackish or freshwater ecosystems (Anderson et al., 2012). Among the 5000 species of extant marine phytoplankton, some 300 species can at times occur in such high numbers that they obviously discolor the surface of the sea leading to the name 'red tides', while only ca. 40 species are able to produce potent toxins (Hallegraeff, 1993). HAB events are typically associated with rapid

proliferation and/or high biomass accumulation of toxic microalgae at the sea surface or in the water column, but even low cell numbers of highly toxic planktonic species or accumulations of cells on benthic substrates may cause problems (Anderson et al., 2012).

Even nontoxic algal blooms can have devastating impacts, for instance, when they lead to kills of fish and invertebrates by generating anoxic conditions in sheltered bays (Hallegraeff et al., 2010). HABs are often nearly monospecific events. Correctly assessing the precise taxonomic identity of the causative organism thus becomes crucial in deciding whether knowledge on toxicology, physiology, and ecology gained from similar blooms in other parts of the world can be applied to the local situation. Nevertheless, most toxigenic HAB taxa belong to the dinoflagellates (Anderson et al., 2012).

2.2.1 Reasons for occurrence of HAB

The reasons behind the expansion of HABs include natural dispersal of species by currents and storms; through human activities such as animal and plant agricultural runoff and non-point nutrient pollution, ballast water discharge and shellfish seeding. In addition, to the quantity of nutrients supplied through point and non-point sources of pollution, the relative abundance of the major nutrients such as nitrogen, phosphorus, and silicate, and a variety of micronutrients such as trace metals or vitamins and the chemical form of those nutrients (e.g., inorganic versus organic) are all important (Anderson et al., 2008, Anderson et al., 2012). The ballast water transport of plankton species is problematic, because even though the planktonic stages of diatoms and dinoflagellates show only limited survival during the voyage in dark ballast tanks, their resistant resting spores are well suited to survive these conditions (Hallegraeff, 1993). One single ballast tank was estimated to contain more than 300 million toxic dinoflagellate cysts which could be germinated into confirmed toxic cultures. HABs can be initiated even from cells present at low con-

centrations, sometimes persisting in the background for months before a bloom develops. Other HABs are delivered into a specific region through advection after developing elsewhere (Raine et al., 2010).

A concern is the relationship between HABs and the growing eutrophication of coastal waters (Anderson et al., 2002). Historically, the conceptual understanding of HABs in eutrophic systems has been based on the simplistic notion that more nutrients yield higher algal biomass. However, the composition and relative proportional availability of nutrient pools, the range of physiological responses by different phytoplankton are all important controlling responses to cultural eutrophication by HABs. The sources of nutrients that may stimulate blooms include sewage, atmospheric and groundwater inputs, and agricultural and aquaculture runoff (Anderson et al., 2012). Even though the problems derived from HAB events varies tremendously, depending on factors such as the geographic region, the affected seafood, and the frequency and intensity of the blooms, the losses suffered by local and regional economies, whether directly or indirectly, are often enormous, and include the aquaculture, fisheries, and tourism sectors. According to the UNEP Global Environmental Outlook, the annual worldwide economic impact of algal biotoxins on human health from seafood alone is ~US$4.0 billion (Díazet al., 2019).

2.2.2 Ichthyotoxicity

According to Hallegraeff (2003), there are three main types of HAB-causing microorganisms:

i. non-toxin-producing species that affect the recreational value of the sites where they proliferate, by causing discoloration of the water or enormous amounts of foam, or by causing high rates of fish mortalities via the drastic reduction of dissolved oxygen in water, due to the explosive increase in microalgal cell density.
ii. toxin producing species that can cause a variety of neurological and gastrointestinal disorders in humans, including paralytic (PSP), diarrheic (DSP), and

amnesic (ASP) shellfish poisoning as well as Ciguatera fish poisoning through their uptake by the food chain, thus posing an important threat to public health and shellfish exploitations; Ciguatera is a tropical fish food poisoning syndrome well known from coral reef areas in the Caribbean and Australia. Humans consuming contaminated fish can suffer from the previously mentioned gastrointestinal and neurological illnesses and in extreme cases can die from respiratory failure.

iii. species that are not toxic to humans but affect fish in culture, by physically damaging the fish (Hallegraeff, 2003, Díazet al., 2019).

HABs threaten the viability of cultured fish by several mechanisms:

i) respiratory dysfunction either by mechanical damage to the gill epithelium caused by the microalgae themselves or by the depletion of dissolved oxygen in the water column following bacterial degradation.

ii) the toxicity of dinoflagellate neurotoxins (Van Deventer et al., 2012).

iii) the oxidation of cell membranes by ROS and PUFA produced by the fish in response to the toxins (Marshall et al., 2003; Mardones et al., 2015).

iv) the toxin-mediated disruption of osmoregulatory capacity (Díazet al., 2019).

Algal species, like the dinoflagellates *Cochlodinium*, *Karenia*, and *Karlodinium*, even though nontoxic to humans, can produce exudates or reactive oxygen species that can damage the gill tissues of fish (Hallegraeff et al., 2010). The clogging of fish gills by algal mucus has sometimes been invoked, but more commonly fish suffocate themselves through production of excessive gill mucus generated as a protective response to environmental irritants (Anderson et al., 2012). Whereas wild fish stocks can swim away from problem areas, caged fish in intensive aquaculture operations are trapped and thus can suffer catastrophic mortalities. Of greatest concern to human society are algal species that produce potent neurotoxins that can find their way through shellfish and fish to human consumers where they produce a variety of the mentioned gastrointestinal and neurological illnesses (Hallegraeff, 1993, Hallegraeff, 2010).

Ichthyotoxic chemical molecules have rarely been conclusively identified as the causative agent of fish kills, except for brevetoxins of *Karenia brevis* and karlotoxins of *Karlodinium veneficum* (Anderson et al., 2012). In some cases, pumping of water to dilute the algal concentration, or immediate harvesting of marketable fish before they can be killed by algal blooms, may also be an option since the hemolytic toxins do not accumulate in fish flesh (Hallegraeff, 1993).

2.2.3 Impact of HAB illustrated by the situation in Chile

The described effects of HABs can be illustrated well by the ongoing impacts on the coastal country Chile. The Chilean economy is especially vulnerable to the negative impacts of HABs, as aquaculture and pecten culture have become two of the most dynamic and successful economic activities in the country. Chile is the second largest producer of salmon and trout worldwide after Norway. In northern and southern Chile and especially in the Patagonian fjords, HABs have followed the global trend of increasing impact, with recurrent problems over the last four decades (Díazet al., 2019). Due to their high frequency and recurrence, the most important toxic episodes have been those caused by the presence of domoic acid (DA), the toxin responsible for amnesic shellfish poisoning (ASP). ASP events are recurrent in the inner sea of the Los Lagos region, the site of > 95% of the national production of the Chilean blue mussel with an annual mean of 25 × 104 t. This important aquaculture industry is second in Chile after salmon farming. An HAB outbreak in the summer of 2016 imposed important economic losses at 45 Chilean salmon farms (Paredes et al., 2016), with the death of 39.942 t of fish, resulting in unemployment of 1700 people, due to the inactivity of the processing plants and the ban on mussel harvesting. In that year, the estimated economic losses were close to 2 million US$.

In southern Chile, HABs have had serious effects on salmon farming. Moreover, the decline in the supply of Chilean salmon led to a globally significant 25% increase in salmon prices (FAO, 2016). HAB events are increasingly causing serious harm to economic sectors related to the exploitation of coastal resources (shellfish culture and fish farming) in Chile (Díaz et al., 2019).

2.3 Functionality of UHPLC-MS/MS

Liquid chromatography is based on adsorption equilibriums between substances, that are solved in a liquid mobile phase and a solid stationary phase resulting in the separation of components from a mixture. The process of separation is carried out in pipes or capillaries, in which the mobile phase flows along the stationary phase. This instrument is called a chromatographical column. A column can be operated efficiently if the carrier material is extremely fine-grained. The adsorption of free molecules from the mobile phase onto the stationary phase and the subsequent desorption determines the transport speed for a substance through the column. A prolonged column results in increased retention times for the same substance. The retention time of substances depends on the intensity of the interaction with the adsorbent and stationary phase. The different retention times result in the temporal separation at the end of the column. To achieve the separation, a mixture of mobile phase containing the relevant substances is transported through the column, this mixture is called eluate. The substances elute in succession from the column after a successful separation according to the interaction with the adsorbent. Substances with a strong interaction to the stationary phase experience a stronger retention during the column transport than substances with weaker interaction. The amount of time, a substance requires to be detected after the injection is the retention time. Dead time on the other hand, is the time required for the pure mobile phase to pass through the column. The dead time is the minimum time of elution. The quality of mass separation achieved in the column is termed mass resolution or simply resolution. In general, many factors influence the absolute MS response such as the cleanliness of ion source, ion optics and collision cell, the ion source flow rates, collision cell pressure and ultimate MS vacuum, leading to significant day-to-day variation in MS responses (J. Pitt, 2009). Therefore, internal standards are usually required for accurate quantitative results.

High performance liquid chromatography mass spectrometry (HPLC-MS) has become a routine technique, which can be applied to a wide range of biological molecules, that allow highly sensitive and accurate assays (J. Pitt, 2009). Ultra High Performance Liquid Chromatography (UHPLC-MS) is based on HPLC-MS and retains the same practicality and principles, whilst increasing the attributes of speed, sensitivity, and resolution. UHPLC uses columns packed with smaller particles (less than 2 µm), higher flow rates and an increased pressure of up to 15.000 psi, which decreases the column length to 50 mm instead of 150 mm for example, resulting in reduced solvent consumption and shorter measuring times. These changes reduce the number of theoretical plates, leading to a reduced resolution. The smaller particles overcompensate the reduction of theoretical plates since the particle size enables a duplication of the remaining theoretical plates, thereby resulting in an increase of theoretical plates in comparison to standard HPLC. The usage of the smaller particles extends the performance of liquid chromatography to Ultra High Performance Liquid Chromatography (UHPLC) (Chandarana et. al., 2016) (Reddy et al., 2010).

Mass spectrometers analyze electric charged particles, to achieve this the analyte molecule is converted into a charged or ionized state. Mass spectrometry analyzes the ions and any fragment ions based on their mass to charge ratio (*m/z*). After converting the analyte into an ionized state, it can be specifically accelerated or deflected by electric or magnetic fields to allow a selection of predetermined ions. An uninterrupted interaction between ions and the magnetic fields must be always ensured. The eluate carrying the to be separated compounds, is pumped through the system with high pressure to maintain a permanent liquid stream, leading to the name of the instrument: High performance liquid chromatography. (J. H. Gross, 2019). A substance with a known mass is infused into the quadrupole of a mass spectrometer. Afterwards the magnetic fields in the quadrupole are modulated to ensure that the known mass has the highest intensity. If the modulation is successful the calibration is optimal, and the mass spectrometer can be used reliably.

2.3.1 Structure of Tandem Mass Spectrometry

Tandem MS is best understood as a concept of operating functional units that are lined up in succession and spatially separated, as illustrated in figure 1. The functional units are in the following order: ion source, first mass analyzer (MS 1), collision cell, second mass analyzer (MS 2) and detector. Neutral particles are ionized in the source, selected in MS 1, fragmented in the collision cell, separated in MS 2, and detected in the detector. This process is applicable for selected reaction monitoring (SRM-Scan) and for collision induced dissociation but does not apply for a precursor and neutral loss scan.

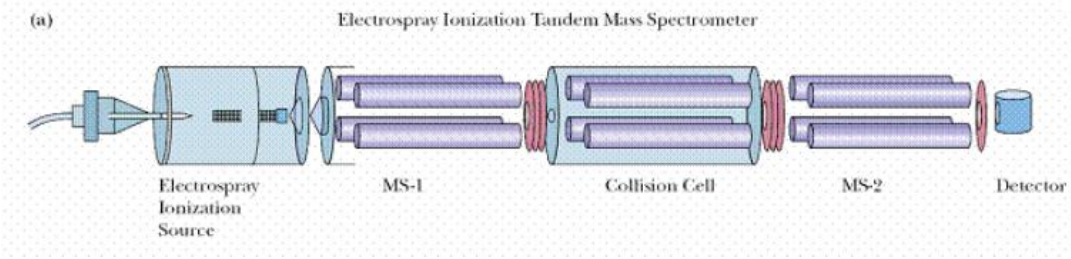

Figure 1: Schematic structure of a triple quadrupole tandem mass spectrometer[1]

The coupling of mass spectrometry with liquid chromatography was limited over many years, due to the relative incompatibility of existing mass spectrometry ion sources with a continuous liquid stream (J. Pitt, 2009). The development of the electrospray ion source by Fenn in 1988 changed this situation (Fenn et al., 1989).

The electrospray ionization (ESI) developed by Fenn is used to transfer the eluate from the liquid chromatography directly into the mass-spectrometric analyzers. The basis for ESI is charge separation in the electrolyte solution produced by strong electrical fields. The mobile phase of the HPLC is flowing through the ESI capillaries, which are carrying a high voltage of several kilovolts. The high voltage transmits a surface charge onto the droplets of the mobile phase through the sprayer gas. The former liquid has changed into an electrical charged aerosol, called electrospray

[1] tandem mass spectrometry protein sequencing - MS-MS: First mass spec. acts as filter. MS-2 works as detector for the fragment | Mass spectrometry, Chemistry, Tandem (pinterest.de)

ionization. After the aerosol is created, it is continuously decreased in size by the temperature and desolvation gas, compressing the charges tightly at the surface. This compression results in the so-called Coulomb-explosion, which partly ionizes the analyte and creates further unsolvated ions, by overcoming the tension at the tips of the aerosol droplets and tearing them into a few µm fine beam. The electrospray is rapidly evaporated due to the heat and usage of dry nitrogen. The residual electrical charge of the electrospray is transferred to the analytes (J. Pitt, 2009) (J. H. Gross, 2019). Heat and the usage of a desolvation gas, like nitrogen, is necessary to prevent the liquid spray from freezing. The ionized analytes are transferred into the first analyzer.

Both the first and second analyzer are quadrupole analyzers consisting of a set of four axis-parallel metal rods, which are arranged in the corners of a square. One pair of two diagonally opposite rods are connected to the same pole of a radiofrequency AC voltage source. In addition, a DC voltage is superimposed above. The combination of constant and varying voltages, allow the transmission of a *m/z* value along the axis of the rods. By varying the voltages with time, it is possible to scan across a range of *m/z* values, resulting in a mass spectrum. Usually, quadrupole analyzers operate between scan speeds of 4000 *m/z* to 10000 *m/z* per seconds. The quadrupoles can also be set to monitor a specific *m/z* value, then switch to a new specific *m/z* value and further on. This technique is achieved by stepping through the voltages and is useful in improving the detection limits of targeted analytes, because more detector time is available for detecting specific ions, instead of scanning across ions that are not produced by the analyte. The stepping between specific ions is carried out in a few milliseconds, which allows a range of *m/z* values to be stepped through for the detection of analytes. Due to losses in the collision cell the absolute signal is decreased in tandem MS. Despite the signal decrease, tandem MS has advantages in a very high specificity, meaning a greatly reduced chemical noise and a superior signal to noise ratio compared to single MS. If an analyte however

fragments poorly or produces many, low intensity fragments, the signal to noise ratio of tandem MS could be worsened compared to single MS detection.

The reaction zone behind MS 1 can be an open flight tube and the reaction length corresponds to the time, the ions require to pass through the zone. If the ions possess enough internal energy for a spontaneous dissociation after passing MS 1, the fragment ions can be transferred into MS 2. In the case of more stable precursor ions, the fragmentation must be forced through energy supply. This energy supply is forced upon the ions in the collision cell, where an inert gas, like nitrogen, causes a collision-induced collapse whilst the ions are flying through the collision cell. The collisions cause vibration stimulation leading to dissociation of the ions. The combination that is obtained by placing a collision cell between two quadrupole mass analyzers is called a triple quadrupole mass spectrometer and is an example of tandem mass spectrometry in which two stages of mass analysis are independently applied (J. Pitt, 2009) (J. H. Gross, 2019).

The detector detects the mass separated ions and measures their relative abundance. The detector amplifies the ion charge into electrical signals, which are then transmitted to a computer with a MS software for data handling and for the calculations required for quantifications (Sargant et al., 2013).

2.3.2 Measurement modes

Table 2 shows the four different measurement modes or measurement modes, that were used for the measurements of amphidinols.

Table 2: Measurement modes of triple quadrupole mass spectrometers (J. Pitt, 2009)

Name	First Quadrupole	Third Quadrupole	Applications
Product ion Scan	Fixed	Scanned	Structural studies, identification of unknowns

Name	First Quadrupole	Third Quadrupole	Applications
Precursor Scan	Scanned	Fixed	Detection of structurally related analytes that produce a commo fragment ion
Neutral loss scan	Scanned	Scanned with fixed offset relative to first quadrupole	Detection of structurally related analytes that eliminate a common neutral molecule on collision
Selected reaction monitoring (SRM)	Fixed	Fixed	High sensitivity detection of a panel of targeted analytes

The SRM measurement mode selects an ion with a specific or fixed mass to charge ratio (*m/z* value) in the first quadrupole. The selected ion is fragmented in the collision cell resulting in a specific fragment ion. The third quadrupole detects the fragment ion, which corresponds to the defined ion value set in the quadrupole. Due to the possibility to select a fixed ion value in the third quadrupole, the measurement mode is called selected reaction monitoring (S. Baecher, 2014). In order to scan multiple ions, multiple SRM measurements are made in succession, that are subsequently put together into an overall scan.

A product ion scan detects every fragment ion of a fixed precursor ion, while the precursor scan detects every precursor ion of a fixed fragment ion. Both measurement modes function in the opposite way.

The neutral loss scan results in a signal if a precursor ion with a known *m/z* value fragments by losing a predefined neutral loss.

The final measurement mode is the full scan, which does not follow the pattern of table 2. Only one mass analyzer is used, and no fragmentation takes place in the collision cell. During the recording of a complete mass spectrum (full scan), the time of measurement is very limited, in order to capture a complete mass range in a few 100 milliseconds. Chromatography with a fast-scanning frequency reduces the sensitivity in full scan mode. A full scan is suitable for qualitative work, like the identification of unknown compounds (J. H. Gross, 2019).

2.4 Method development

The method development was partly the base of the master's thesis "LC-MS/MS Method for the Discovery and Identification of Amphidinols Produced by *Amphidinium*" written by Marvin Wellkamp in 2020. Since this thesis is based on the works of the mentioned master thesis, it is crucial to understand the development process of the used LC-MS/MS-based method, to comprehend the screening process of *Amphidinium* species undertaken in this work and the steps required in finding new variations of amphidinols. Therefore, the baselines of the method development, which are relevant in the works of this thesis, are explained below.

Every substance collapses into fragments in a specific way, allowing a clear identification in the process. Similar substances that can be summed up into a primary group, also collapse into similar fragments. Similarities within fragmentation schemes of individual amphidinols were a basic requirement for the development of a functioning NL-method. It has been shown that a similarity between the fragmentation schemes was a bond break between two hydroxyl groups near tetrahydropyranring B. The break always occurred for every amphidinol between the same carbon atoms. The bond break was named C-1' / C-1 because it divided the lipophilic part and the hydrophilic part of the amphidinols. The numbering was continued to the end of the lipophilic part (C-1') and hydrophilic part (C-1). The numbering of the C-1' / C-1 bond break was essential, because the official carbon numbering from the beginning to the end of the polyketide chain results in different carbon

numbers of an identical structural position of the molecule due to the different sizes of the carbon chains of the amphidinols (Wellkamp et al., 2020).

Figure 2 shows the chemical structure and a fragmentation scheme for amphidinol 21 reported by Satake et al., 2017. The C-1’ / C-1 bond break was added, and the numbering of the molecule was adapted, with the C-1’ to C-22’ being the lipophilic part, whilst C-1 to C-64 builded the hydrophilic part.

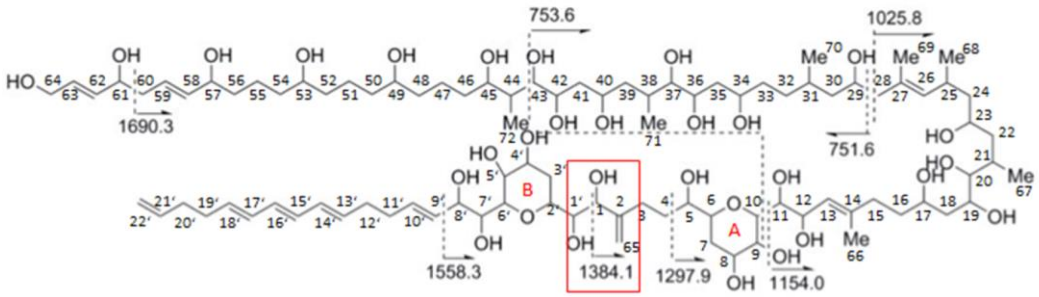

Figure 2: Product ion and fragmentation scheme from amphidinol 21. The C-1' / C-1 bond break was marked in red (Wellkamp et al., 2020)

Figure 3 shows the original recorded amphidinol 21 with the initial numbering system. The numbering system was not separated between the lipophilic and hydrophilic part, therefore the C-1’ / C-1 bond break was not marked in the initial recording.

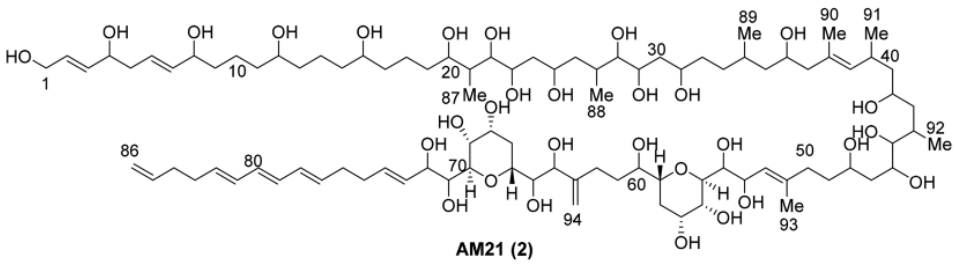

Figure 3: Original recording of amphidinol 21 by Satake et al., 2017.

The high abundancy of the described C-1’ / C-1 bond break was supported by neighboring atoms and bonds. These were the opposite vicinal hydroxyl groups at C-1’ and C-1, the tetrahydropyranring B at C-2’ and the double bond between C-2 and C-65 for amphidinol 21, which can be seen in figure 2. Such a double bond between

carbon atoms was unique in the amphidinols and was responsible, along with the other neighboring atoms and bonds, for the high abundancy of the C-1' / C-1 bond break. Every fragment that was formed in the hydrophilic part, broke once more at the C-1' / C-1 bond resulting in a second fragment. These double fragments were named pair fragment.

During the development of a method that allowed the detection of unknown amphidinols, it was decided to use a neutral loss method. This decision was made because the third quadrupole of a precursor scan only detects a fragment with a defined mass. Fragments that were created by the C-1' / C-1 bond break included tetrahydropyranring A, most of the connecting C_6-chain and the hydrophilic part. This was problematic for the method, due to the high diversity of the hydrophilic part, resulting in many varieties with different masses. This variety suggested that new amphidinols did not necessarily include one of the found fragments, and therefore would not be detected. This prevents the use of one comprehensive method since many methods would have been required to cover all the variations. The third quadrupole of a neutral loss scan detects every fragment created by the loss of a neutral fragment with a defined mass. In the case of amphidinols the C-1' / C-1 bond break resulted in the loss of a neutral fragment. This neutral fragment included the entire lipophilic part starting from the C-1' atom. The lipophilic part had only a few variations, compared to the hydrophilic part, with a total of seven variations found in the 37 described amphidinols from the literature. The seven variations differed in the number of carbon atoms, hydroxyl groups and double bonds. It was also important to divide the amphidinols into groups of sulfated and non-sulfated, as the method needed to be adjusted slightly to allow for a successful detection of amphidinols. Sulfated amphidinols lose their sulfate group before they are fragmented (Wellkamp et al., 2020). Table 3 lists the masses of the seven non-sulfated neutral losses, as well as information about the chemical structure.

Table 3: Non-sulfated neutral loss types

#	Neutral loss [Da]	Number of C- atoms	Number of hydroxyl groups	Number of double bounds
1	392.13	22	5	5
2	426.23	22	7	4
3	418.24	24	5	6
4	398.28	22	5	2
5	440.25	23	7	4
6	442.23	22	8	4
7	338.18	18	5	4

For the calculation of the fragmentation from sulfated amphidinols a mass of 120 Da was added to make up for the loss of the sulfate group. The adjusted masses can be seen in table 4.

Table 4: Sulfated neutral loss types

#	Neutral loss [Da]
1.1	512.13
2.1	546.23
3.1	538.24
4.1	518.28
5.1	560.25
6.1	562.12
7.1	458.18

Table 22 and 23 listed in the appendix display the results found by Wellkamp et al., (2020) for the used chromatographic and mass spectrometry parameters, which were used throughout every measurement stated in this thesis.

2.5 Purpose of work

The purpose of the present study was the quantification and identification of amphidinols and secondary metabolites, from 69 individual samples of the algal genus *Amphidinium,* using several UHPLC-MC/MS measurement modes. Such an amount of *Amphidinium* samples provided the opportunity for a large-scale analysis of the present toxin profiles for each sample. This was especially relevant because the toxin profiles of the received samples were still completely unknown, making it difficult to raise hypothesis about the chemical or biological properties of the samples.

The analysis of the toxins can be separated into two different phases. In the first phase the samples were quantified by the SRM method (Wellkamp et al., 2020) to provide clarification about the existing toxins in each sample, and additionally about the amount of toxin per cell contained in each sample.

In the second phase the samples were measured through the neutral loss and full scan methods developed by Wellkamp et al., 2020 to possibly detect new unknown variations of amphidinols. Due to the large size of amphidinols, the probability of the presence of yet unknown structural variations was high. The detection of new amphidinol variations through neutral loss and full scan measurements however would not be sufficient, because the candidates were yet to be correctly identified as amphidinols. Therefore, creating enhanced product ion scans would be necessary for every found candidate, which made it possible to reject the candidate or to correctly identify them as amphidinols. The purpose behind the identification was to enhance the existing SRM method with additional amphidinol variations, making measurements of future *Amphidinium* samples more efficient and complete.

3 Material and Methods

3.1 Origin of samples and sample collection

For the quantitative determination, a Luteophanol D standard with a concentration of 10.56 ng/µl was provided. The standard material was isolated from the *Amphidinium carterae* strain ACRN03 and was made available by F. Garcia-Camacho from the University of Almeria, Spain (Molina-Miras et al., 2018).

A total of eleven different *Amphidinium* species, containing a total number of 69 strains, originating from two locations, were examined. The species were the following: *A. operculatum*, *A. theodori*, *A. massartii*, *A. carterae*, *A. tomasii*, *A. fijiensis*, *A. gibbossum*, *A. thermaeum*, *A. paucianulatum*, *A. magnum* and new isolates from Baja California, Mexico that were not identified yet. Table 20 in the appendix shows the species and cell count of the 13 strains, which were collected in Ensenada, Mexico. The majority of samples however originated from various worldwide locations, since they were provided by the algal resources culture collection facility from the university of North Carolina Wilmington in the USA. Table 21 in the appendix lists the culture conditions, cell count and the species of the remaining 56 strains from the collection facility in North Carolina. The strains from Mexico were composed of four different species, whilst the strains from North Carolina had nine different species. The species *A. theodori* and *A. massartii* were present in both sample sets.

Table 5 shows a complete list of all the transitions for amphidinols (AM), which were built into the SRM method. The method contained a total of 55 transitions, out of which 39 were already stated throughout the literature, as well as 16 newly discovered amphidinol variations, named N1 to N16, by Wellkamp et al., 2020.

Table 5: Complete list of calculated transitions of known and newly discovered AM by Wellkamp et al., 2020, that were implemented in the SRM method

Name	Q1-Mass (m/z)	M(m/z)	Toxin	Q1-Mass (m/z)	Q3-Mass (m/z)
AM – 1	1512	974	KAR – B	1462	1064
AM – 2	1398	1006	LP – A	1278	754

Name	Q1-Mass (m/z)	M(m/z)	Toxin	Q1-Mass (m/z)	Q3-Mass (m/z)
AM – 3	1350	932	LP – B	1344	904
AM – 4	1324	932	LP – C	1344	904
AM – 5	1394	976	LP – D	1330	904
AM – 6	1368	976	LS	1374	976
AM – 7	1254	742	LS – A	1296	904
AM – 9	1350	932	LS – B	1266	754
AM – 10	1296	904	SP	1266	754
AM – 11	1500	988	N1	1268	876
AM – 12	1426	914	N2	1430	1038
AM – 13	1452	914	N3	1458	1066
AM – 14	1288	742	N4	1316	876
AM – 15	1186	760	N5	1346	946
AM – 17	1306	816	N6	1346	946
AM – 18	1382	964	N7	1346	928
AM – 19	1462	946	N8	1364	946
AM – 20 (M)	1346	904	N9	1364	946
AM – 20 (S)	1653	1260	N10	1364	946
AM – 21	1798	1406	N11	1364	946
AM – 22	1668	1330	N12	1326	946
AM – A	1362	964	N13	1326	928
AM – B	1442	946	N14	1344	946
AMD – G	1300	768	N15	1344	946
CAR – E	1422	1030	N16	1344	946
KAR – A	1480	1082			

3.2 UPLC-MS/MS

An ultra-performance liquid chromatography (UPLC®) instrument coupled with tandem mass spectrometry (UPLC-MS/MS) was used to identify and quantify the toxin levels of amphidinols. The UPLC-system includes an AQUITY UPLC column oven, an AQUITY I UPLC class autosampler and an AQUITY I UPLC class binary pump. The separation was created through a Purospher®STAR RP-18 endcapped (2 µm) Hibar® HR 50-2.1 UPLC-column (Merck Millipore, Darmstadt Germany). An 0.5 µm OPTS-SOLV® EXP™ precolumn (Sigma-Aldrich, Hamburg, Germany) was used, to ensure the safety of the column. The entire system was coupled to the Xevo® TQ-XS mass spectrometer (Waters GmbH, Eschborn, Germany). The software MassLynx (Version 4.2,

Waters) was used in order to collect and analyze the data. The quantification and calculations of detection limits of the measured data required the additional software TargetLynx XS (Waters). The detection limits were defined as the threefold of the signal-to-noise ratio (S/N), which were also directly calculated in TargetLynx XS (M. Wellkamp, 2020).

3.3 Extraction process

The samples were present in three different matrices, therefore requiring three different extraction processes. All three extraction processes achieved the same result; an extract with a defined end volume that allowed mass spectrometry measurements and subsequent determination of the amphidinol cell quota of each analyzed strain.

3.3.1 Cell Pellets

Twelve samples consisted of cell pellets. The solid pellets were poured into cyrovials (SARSTEDT, Nümbrecht, Germany). After the sample transfer, the original microtube (Eppendorf, Hamburg, Germany) was rinsed with 1 ml of methanol (HPLC-grade, Merck, Darmstadt, Germany), which was added to the cryovial with the sample. In addition, ca. 0.9 g Lysing Matrix D (Thermo Savant, Illkirch, France) was added to the sample with a laboratory spatula. The cells were lysed by reciprocal shaking at a speed of 4.5 m/s for 45 seconds in a Bio 101 FastPrep Instrument (Thermo Savant). Following this step, the vials were centrifuged for 15 minutes at 16100 relative centrifugal force (RCF) to separate the liquid from the solids (5415 R, Eppendorf), where after 500 µl of the supernatants were transferred using a pipette into a 0.45 µm spin filter (Merck Millipore, Darmstadt, Germany), which was centrifuged for 30 seconds at 2300 RCF. The filtrate was transferred into a 2 ml HPLC-crimp vial (Agilent Technologies, Waldbronn, Germany). The remaining 500 µl of supernatant were put into the previously used spin filter, which was centrifuged again for 30 seconds at 2300 RCF. The second filtered supernatant was combined with the first one. The sample was left open overnight inside the laboratory fume hood to evaporate the entire methanol in the vial. After the sample was dried up overnight,

it was reconstituted to a defined volume of 500 µl methanol, the vial then was crimped with a silicone-septum (11 mm Silver Aluminum Crimp Cap, PTFE/silicone septa, Agilent Technologies) and was vortexed to ensure that every solved substance from the raw extract inside the vial was dissolved again.

3.3.2 Lyophilized cell cultures

The samples were covered with patches of salt, which implies that entire cultures rather than singular cell pellets were freeze-dried. During the thawing process residues of water formed inside the falcon tubes, thereby revealing an incomplete lyophilization process.

Samples 14 to 20 all had less biomass and were extracted in a different manner after the beginning steps. 5 ml of deionized water (Milli-Q, Merck Millipore, Darmstadt, Germany) was added to the pellets, which then were vortexed and centrifuged for 20 minutes at 3220 RCF and 10 °C. The watery supernatant was also transferred into a separate centrifuge tube, 1 ml of the supernatant however was transferred back to the pellet, after which the entire content of the centrifuge tube was put into a cryovial. The vial was centrifuged for ten minutes at 16100 RCF. Half of the supernatant was put into the previously used separate centrifuge tube, whereas the other half was used to rinse the original centrifuge tube to collect any remaining biomass. This half was then added back into the vial to ensure an entire transfer of biomass. The now refilled vial was centrifuged again for ten minutes at 16100 RCF, with the emerging supernatant being added to the separate centrifuge tube entirely this time.

The samples were extracted further in the fast prep instrument (Thermo Savant) following the identical steps as described in the cell pellet extraction process, the only difference was that only 500 µl methanol were added to the sample in the beginning.

Sample 13 differs slightly from the other samples since it was sent in a 50 ml centrifuge tube, due to a higher volume of biomass compared to the other samples,

which were sent in 20 ml centrifuge tubes, therefore the extraction process varies between sample 13 and samples 14-20. 15 ml of filtered water (Merck-Millipore) was added to sample 13, which then was vortexed and centrifuged for 20 minutes at 3220 RCF (5810 R, Eppendorf) and 10 °C. The watery supernatant was taken off the pellet with a pipette and kept in a spare falcon tube due to the hypothesis that amphidinols could be dissolved in the initial thawing process. 2 ml of methanol were added on the pellet, and the centrifuge tube was vortexed for 30 seconds. After vortexing, the pellet was still in large part one piece, due to its biomass. The pellet was broken up into smaller pieces with a lab spatula using mechanical force. Subsequently the centrifuge tube was secured in a supporting flask and placed below an ultrasound rod for one minute at a 70% cycle with 50% power (SONOPLUS HD2070 MS72, Bandelin electronic, Berlin, Germany). The sample was again centrifuged for 15 minutes at 3220RCF. 500 µl of the supernatant was transferred into a spin filter at a time and centrifuged for 30 seconds at 16100 RCF. Each spin filter was discarded after one use, due to clogging of the filter. This step was repeated until the supernatant was transferred entirely into spin filters. The content of the centrifuged spin filters was put in a HPLC-sample vial. The samples were dried under gentle flow of nitrogen. A defined volume of 500 µl methanol was added to the dried sample. Due to the thickness of the filtered sample, another transfer into a new spin filter was needed. The spin filter was centrifuged again for 30 seconds at 2300 RCF, after which the sample was put into a new HPLC-sample vial and crimped.

3.3.3 Small filters

The samples arrived in the form of one to three filters per sample covered in biomass. One filter per sample was placed on a petri dish where one quarter was cut with a laboratory scalp. The petri dish and scalp were cleaned with methanol before a new filter was used. The quarter of the filter was rolled up using tweezers and placed inside a cryovial. The samples were extracted further in the fast prep instru-

ment (Thermo Savant) following the identical steps as described in the cell pellet extraction process with a few differences. 1.5 ml methanol were added to the vial in the beginning and the process was repeated twice with 1 ml methanol being added in the second iteration.

3.3.4 Large filters

These samples arrived identically to the small filters, however each sample consisted of five to eight larger filters (Image 4, step 1). All the filters were cut apart into small pieces on the petri dish using a standard scissor (Image 4, step 2). Both the petri dish and scissor were cleaned with methanol before new filters were used. The filter pieces were distributed evenly into two 50 ml centrifuge tubes. The centrifuge tubes were filled with 20 ml methanol and placed into the fridge to soften the filters overnight (Image 4, step 3).

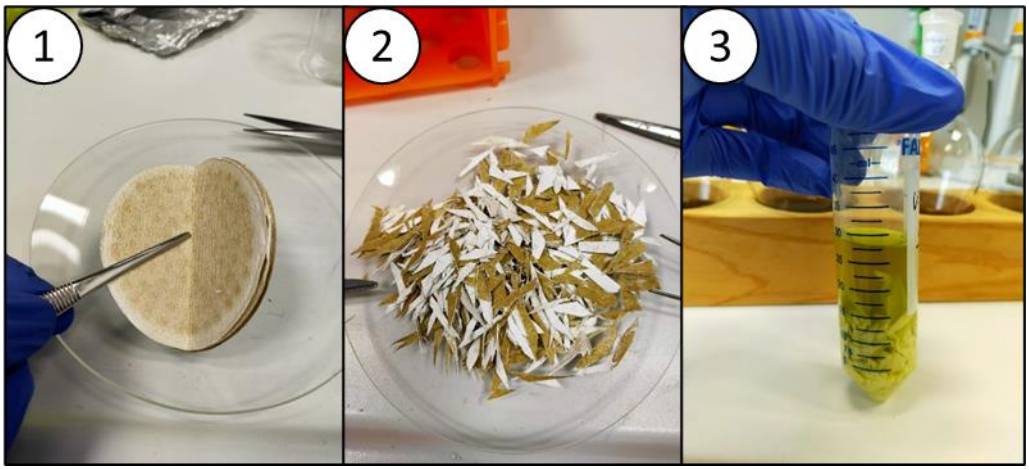

Image 4: Extraction steps 1 - 3 (Filter samples, cut up filter pieces, transfer into centrufige tube with methanol)

The centrifuge tube was secured in a supporting flask and placed below an ultrasound rod for one minute at a 70% cycle with 80% power (Image 5, step 4). Since there were two centrifuge tubes per sample this step must be carried out twice per sample. Both were placed in a 5810R centrifuge for ten minutes at 4000RCF. The supernatant was decanted through a funnel, which was then rinsed with 1 ml methanol, into a 100 ml pear-shaped flask (Schott, Mainz, Germany) (Image 5, step 5). The

remaining filter pieces were squeezed together with a pipette to transfer any soaked-up liquid into the pear-shaped flask. The now emptied centrifuge tubes were refilled with 20 ml methanol to start the second fraction of the extraction process. Both tubes were processed with the ultrasound rod, centrifuged, and transferred into the identical pear-shaped flask as before. The content of the flasks was split into two new centrifuge tubes, which were centrifuged for 10 minutes at 4000 RCF. The supernatant was transferred back into the pear-shaped flask using a pipette. The remains inside the centrifuge tubes were collected in a cryovial that was centrifuged for 10 minutes at 13200 RCF. The supernatant of the cryovial was added to the pear-shaped flask, completing the transferring process (Image 5, step 6).

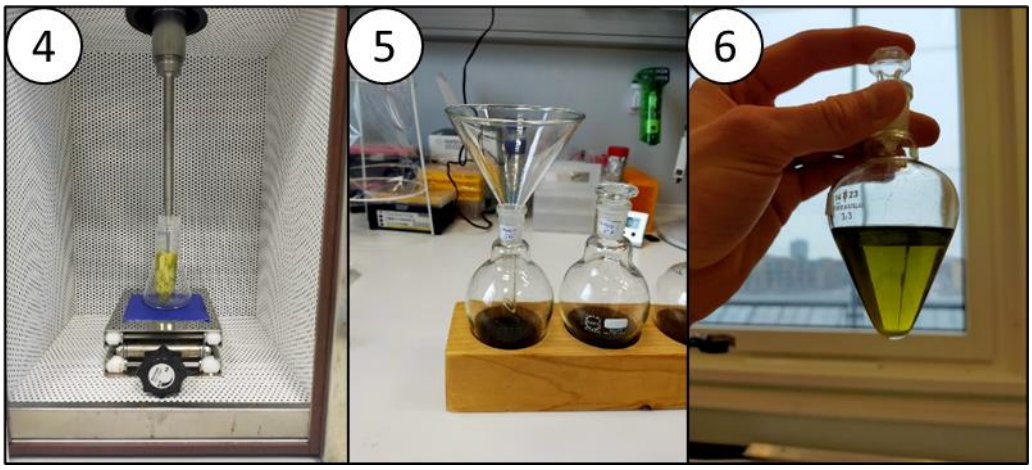

Image 5: Extraction steps 4 – 6 (ultrasonic rod, transfer into pear shaped flask, pear shaped flask before rotavapor transfer)

A rotavapor device (Heidolph, Schwabach, Germany) was used to reduce the volume of liquid until the sample almost runs dry (Image 6, step 7). Before the evaporation process could start, the entire rotavapor-system was rinsed and cleaned with methanol and the water bath was filled with filtered water set to maintain a temperature of 40 °C. The kryostat was turned on to cool the device and acted as a pump. The sample was placed in the rotavapor device and lowered through a lever until about half of the flask was covered in the water bath. To increase the speed of the evaporation a vacuum of 300 was set, reducing the duration to about an hour until the sample had evaporated nearly all the liquid (Image 6, step 8).

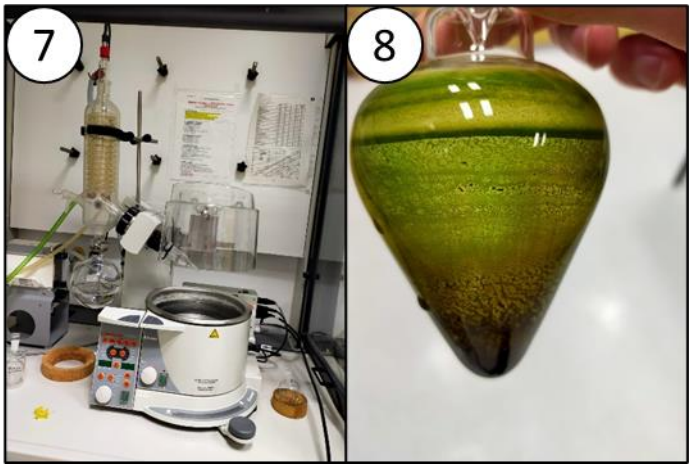

Image 6: Extraction steps 7 – 8 (rotavapor device, sample after processing in rotavapor device)

The dried residues in the flask were rinsed three times with 1 ml methanol. Per milliliter of methanol the flask was pivoted and vortexed for 30 seconds to flush most of the dried biomass out to the bottom of the flask. The residues after each rinsing step were transferred into an Eppendorf tube using a glass pipette (BRAND, Wertheim, Germany), however due to the size of the EPI only the first 2 ml were transferred (Image 7, step 9), and the EPI was left standing open under the laboratory fume hood to dry out. After the drying was finished the third 1 ml portion of extract was transferred over and left outside to dry out as well.

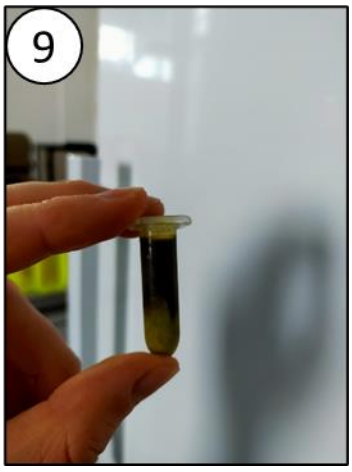

Image 7: Extraction step 9 (EPI after 2ml transfer)

The dry EPI was filled with 1 ml methanol, vortexed for 30 seconds, and 500 µl of the 1 ml methanol were transferred into a spin filter, that was centrifuged for 15

minutes at 21130 RCF (Eppendorf 5424R). The content of the spin filter was put into a HPLC-sample vial, afterwards the second 500 µl methanol were put in the same spin filter as used before and the previous steps were repeated. The filled HPLC-sample vial was vaporized until the samples had dried out using nitrogen. Finally, the originally completed vial from the extraction process using only a quarter of a filter was unified with the corresponding newly extracted sample. The now refilled sample was once more dried out using nitrogen, then the sample was filled up with a defined end volume of 1 ml methanol and crimped as the final step in the extraction process (Image 8, step 10).

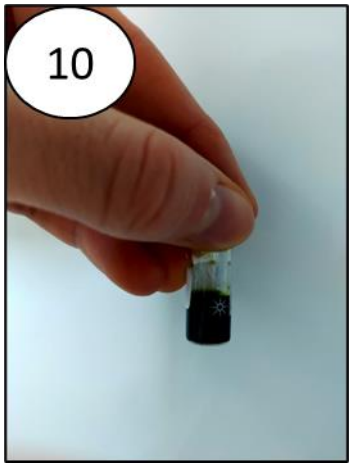

Image 8: Extraction step 10 (Finished sample after the extraction process)

4 Results

In this section the results of the UHPLC-MS/MS measurements were presented in four different subchapters, each focusing on a separate measurement mode to examine the 69 different *Amphidinium* strains.

4.1 Selected reaction monitoring (SRM) – Measurement mode

The following tables in this section list the different strains in which various amphidinols, were detected through the SRM method, as well as the calculation of their respective cell quote using the equations stated in section 4.1.1. The detected amphidinols were sorted according to their species throughout the tables. A detected amphidinol was marked with a "X" in the appropriate column.

Table 6 shows every detected amphidinol of the sample set originating from Ensenada, Mexico. The sample set contained 13 strains, out of which seven strains produced a total of 14 different amphidinols, comprised of the species *A. operculatum, A. massartii* and New Isolates, which are yet to be identified. Out of these seven strains, five were unidentified new isolates and one strain respectively belonged to *A. operculatum* and *A. massartii*. Table 20 in appendix A lists the full sample set originating from Ensenada, Mexico, whilst table 24 shows the cell quote in fg/cell of each detected amphidinol for every strain shown in table 6.

Table 6: Detected amphidinols produced by *Amphidinium* strains originating from Ensenada, Mexico

Name	t_R [min]	AA60 *A. operculatum*	AA39 A. massartii	AA181 New Isolates	AA177 New Isolates	AA172 New Isolates	AA165 New Isolates	AA111 New Isolates
AM – 2	3,78	X		X	X	X	X	X
AM – 4	3,87			X	X	X		
AM – 5	4,07			X	X	X		
AM – 6	3,18	X						
AM – 7	3,3			X	X	X		
AM – 9	4,10			X	X	X		
AM – 11	3,43			X	X	X		

Name	t_R [min]	AA60 *A. oper-cula-tum*	AA39 A. mass-artii	AA181 New Isola-tes	AA177 New Isola-tes	AA172 New Isola-tes	AA165 New Isola-tes	AA111 New Isola-tes
AM – 14	2,61	X		X	X			
AM – 15			X					
AM – 17	4,17	X				X	X	
N7	4,40	X						
N8/N9	4,17	X						
N12	3,88			X	X			
N13	3,52		X	X				

Tables 7 to 11 show every detected amphidinol of the second sample set originating from the algal culture collection of the University of North Carolina, Wilmington, NC, USA (UNCW) that has collected strains from worldwide locations. The sample set contained 56 strains, out of which 25 strains produced a total of 41 different amphidinols, comprised of the species *A. tomasii, A. gibbossum, A. massartii* and *A. carterae*. Out of these 25 strains, 15 belonged to *A. carterae,* six to *A. massartii,* three to *A. tomasii* and one strain belonged to *A. gibbossum*.

Table 7 lists the three amphidinol producing strains from *A. tomasii*, as well as one strain respectively belonging to *A. gibbossum* and *A. massartii*. A detected amphidinol was marked with a “X” in the appropriate column.

Table 21 in the appendix lists the full sample set originating from the algal culture collection of the University of North Carolina, Wilmington, NC, USA (UNCW), whilst the tables 25 - 29 show the cell quote in fg/cell of each detected amphidinol for every strain shown in table 7 to 11.

Table 7: Detected amphidinols in *Amphidinium* strains from the species *A. tomasii, A. gibbosum, A. massartii* originating from the algal culture collection of UNCW, cultivating strains from worldwide locations

Name	t_R [min]	ARC90 *A. tomasii*	ARC197 *A. tomasii*	ARC388 *A. tomasii*	ARC104 *A. gibbossum*	CCMP1741 *A. massartii*
AM – 2	3,78	X				
AM – 4	3,87	X				
AM – 7	3,3			X		
AM – 11	3,43	X				
AM – 17	4,17	X				
AM – 20 (S)	3,60		X			
AM – 20 (M)	2,93					X
LP – B / LP – C	2,82					X
LP – D	2,81	X			X	X
LS – A	3,75					X
LS – B / SP	2,97					X
N1	2,97					X
N12	3,88	X				
N13	3,52	X				
N14 – N16	4,48	X				

Table 8 lists the additional five amphidinol producing strains from *A. massartii*. A detected amphidinol was marked with a "X" in the appropriate column.

Table 8: Detected amphidinols from the species *A. massartii* originating from the algal culture collection of UNCW, cultivating strains from worldwide locations

Name	t_R [min]	CCMP2774 *A. massartii*	CCMP2813 *A. massartii*	CCMP1342 *A. massartii*	ARC149 *A. massartii*	ARC414 *A. massartii*
KAR – A	3,17				X	
KAR – B	3,96				X	
LP – D	2,81					X
LS – B / SP	2,97			X		

Name	t_R [min]	CCMP2774 *A. massar-tii*	CCMP2813 *A. massar-tii*	CCMP1342 *A. massar-tii*	ARC149 *A. mass-artii*	ARC414 *A. mass-artii*
N8 – N11	4,04	X	X			
N14 – N16	2,96					X

Table 9 lists the first five amphidinol producing strains from *A. carterae*. A detected amphidinol was marked with a "X" in the appropriate column.

Table 9: Detected amphidinols from the species *A. carterae* originating from the algal culture collection of UNCW, cultivating strains from worldwide locations

Name	t_R [min]	ARC101 *A. carte-rae*	ARC100 *A. carte-rae*	CCMP122 *A. carte-rae*	CCMP2199 *A. carte-rae*	CCMP119 *A. carte-rae*
AM – 2	3,98	X	X			
AM – 4	3,83		X			
AM – 6	3,95		X			
AM – 11	3,10		X			
AM – 17	3,06		X			
AM – 18	4,07			X		
AM – 19	3			X		
AM – 20 (M)	4,23			X		
AM – 22	3,81			X		
AM – A	4,17			X	X	
AM – B	3,32			X		
LP – D	2,81					X
LS	4,40			X		
N5 / N6	4,47			X		
N7	4,56			X		
N8 – N11	4,37			X		
N12	3,76	X	X	X		
N13	4,70	X	X	X		
N14 – 16	4,48			X		

Table 10 lists the next five amphidinol producing strains from *A. carterae*. A detected amphidinol was marked with a "X" in the appropriate column.

Table 10: Detected amphidinols from the species *A. carterae* originating from the algal culture collection of UNCW, cultivating strains from worldwide locations

Name	t_R [min]	ARC195 *A. carterae*	CCMP2100 *A. carterae*	ARC383 *A. carterae*	ARC98 *A. carterae*	ARC99 *A. carterae*
AM – 2	3,98		X		X	X
AM – 4	3,83	X	X	X	X	X
AM – 5	3,93		X			
AM – 7	2,98		X			
AM – 9	4,31		X	X	X	
AM – 11	3,10		X		X	X
AM – 14	2,97		X			
AM – 17	2,97				X	
AM – 20 (M)	2,93	X		X		
LP – A	2,97	X		X		
LP – B / LP – C	3,16	X		X		
LP – D	2,81	X		X	X	X
LS – A	3,75	X		X	X	
LS – B / SP	2,97	X		X		
N1	2,97	X		X		
N3	3,65			X		
N8 – N11	4,04		X			
N12	3,76		X		X	X
N13	3,78		X		X	X
N14 – N16	2,96				X	X

Table 11 lists the final five amphidinol producing strains from *A. carterae*. A detected amphidinol was marked with a “X” in the appropriate column.

Table 11: Detected amphidinols from the species *A. carterae* originating from the algal culture collection of UNCW, cultivating strains from worldwide locations

Name	t_R [min]	ARC410 *A. carterae*	ARC411 *A. carterae*	ARC412 *A. carterae*	ARC413 *A. carterae*	CCMP2400 *A. carterae*
AM – 4	3,83	X			X	
AM – 9	4,31					X
AM – 12	3,87		X	X		

Name	t_R [min]	ARC410 *A. carte-rae*	ARC411 *A. carte-rae*	ARC412 *A. carte-rae*	ARC413 *A. carte-rae*	CCMP2400 *A. carte-rae*
AM – 20 (M)	2,93	X			X	
CAR – E	4,39	X	X	X		
LP – A	2,97	X				
LP – B / LP – C	3,16	X			X	
LP – D	2,81	X			X	
LS – A	3,75	X	X	X	X	
LS – B / SP	2,97				X	
N1	2,97				X	
N3	3,65	X				
N12	3,76	X				

4.1.1 Calculations

The calculations of the stated SRM results were split into two different categories, these being the raw calculations and the cell quote calculation. Before the raw calculations were carried out, the limit of detection (LoD) for the entire measurements was calculated. To calculate the LoD the concentration of the used LPD standard was required as well as the signal to noise ratio from MassLynx (Equation 1).

$$LoD = c(LPD) * \frac{3}{Signal\ to\ noise\ ratio}$$

Equation 1

The LoD was multiplied by the sample volume in µl (equation 2). In equation 3 the LoD was converted into the correct unit (fg/sample).

$$LoD\ \left[\frac{ng}{sample}\right] = LoD * sample\ volume\ [\mu l]$$

Equation 2

$$LoD\ \left[\frac{fg}{Sample}\right] = LoD\ \left[\frac{ng}{Sample}\right] * 1000000$$

Equation 3

The first step of the raw calculation was to measure the LPD standard, if no peak could be detected, the entire measurement was discarded. If the LPD-standard was detected, the area of the produced peak was measured by MassLynx (Figure 4).

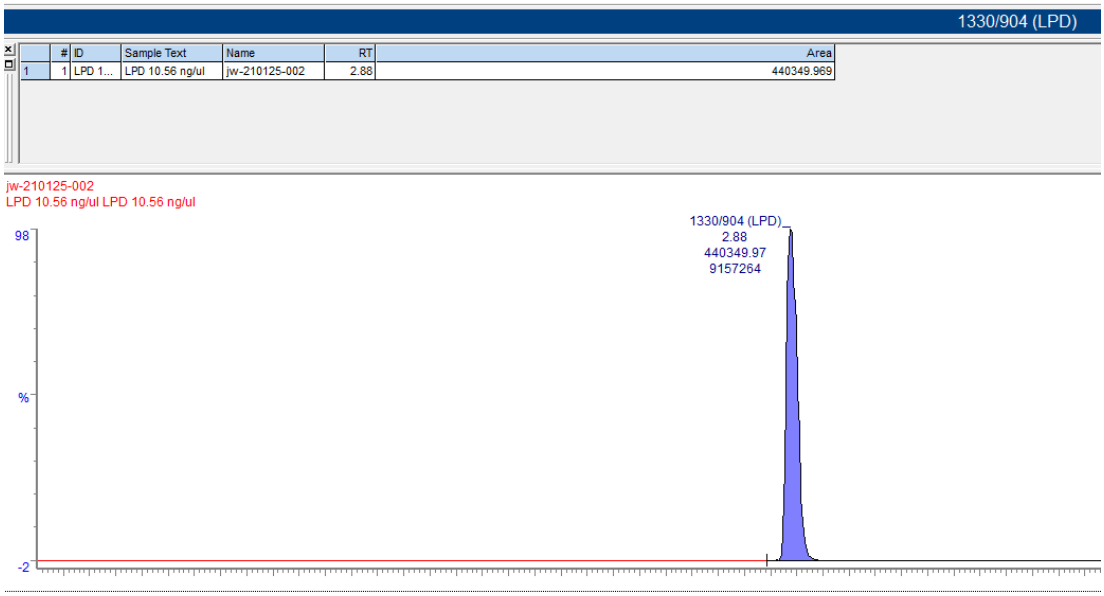

Figure 4: Successful detection of the LPD standard in MassLynx

The measured area was multiplied by the LPD-standard concentration and subsequently divided by the area of the LPD-standard.

$$\frac{Toxin\ [ng]}{Volume\ [\mu l]} = \frac{Peak\ Area * c(LPD)}{Peak\ Area\ (LPD)}$$

Equation 4

Equation 4 states the described calculation, which was carried out for every sample, leading to the amount of toxin present in one µl. This result was multiplied by the corresponding sample volume, resulting in the amount of toxin contained in a sample, as stated in equation 5:

$$\frac{Toxin\ [fg]}{Sample} = \frac{Toxin\ [ng]}{Volume\ [\mu l]} * Sample\ volume\ [\mu l] * 1000000$$

Equation 5

In the second part of the calculations, the LoD was required again to calculate the LoD for the cell count of each sample (equation 6).

$$LoD\ (cell\ quote) = \frac{LoD\ [\frac{fg}{sample}]}{Number\ of\ Cells}$$

Equation 6

The LoD for the cell quote was important, because a measurement in which the cell quote of a toxin in a sample was not higher than the fivefold of the LoD (cell quote) the result was marked as non-detected and was not considered in further measurements. Equation 7 shows the calculation of the cell quote in fg/cell.

$$Cell\ quote\ \left[\frac{fg}{cell}\right] = \frac{Toxin\ [fg]/sample}{Number\ of\ cells}$$

Equation 7

4.2 Neutral loss (NL) – Measurement mode

Table 3 in chapter 2.4 lists the seven non-sulfated neutral loss types, whilst table 4 lists the seven sulfated neutral loss types. All 14 neutral loss types were a result of the C-1' / C-1 bond break between the lipophilic and hydrophilic part of an amphidinol, as described in chapter 2.4 as well. Every strain of the complete sample set was examined through the neutral loss method created by Wellkamp et al., 2020 about the presence of a predefined neutral loss.

Table 12 shows the results of the neutral loss measurement. A total of 30 neutral losses, comprised by ten individual neutral losses, and 27 Q1-Masses were found in 17 individual strains. The strains AA111 (2), ARC101 (2), AA165 (4), AA172 (2), CCMP2100 (2), CCMP1821 (2) and AA60 (3) displayed neutral losses in more than one Q1-Mass. The number of Q1-Masses was stated in brackets behind the strain name. The strains AA165, ARC101 and ARC410 had two neutral losses in one Q1-Mass.

Table 12: Detected neutral losses and corresponding Q1-Masses found in various strains

Strain name	t_R [min]	Q1-Mass (m/z)	Neutral loss
ARC117	3,32	1105	418
AA113	3,75	1114	518

Strain name	t_R [min]	Q1-Mass (*m/z*)	Neutral loss
AA111	2,93	1138	338
AA111	3,90	1140	392
CCMP2774	3,33	1152	398
ARC101	3,89	1226	398
AA38	2,03	1238	440
AA165	2,92	1242	392 / 512
AA165	3,80	1264	392
AA39	2,90	1297	426
AA172	3,79	1305	442
ARC101	2,94	1328	392 / 512
CCMP1784	3,09	1329	562
CCMP2100	2,90	1358	426
CCMP2100	2,95	1360	426
AA60	3,75	1384	392
AA165	3,90	1392	442
AA165	3,90	1396	392
ARC410	2,93	1398	338 / 512
AA60	2,92	1418	426
CCMP1821	3,81	1420	418
CCMP122	3,20	1446	518
AA60	2,92	1486	512
CCMP1821	3,84	1492	398
ARC411	3,39	1627	338
ARC99	3,79	1725	398
AA172	3,77	1765	440

The ten detected neutral losses were listed in table 13, as well as their respective occurrence.

Table 13: Occurrence of individual detected neutral losses in the complete sample set

Neutral loss	Occurrence
392	6 / 30
398	4 / 30
426	4 / 30
512	4 / 30
338	3 / 30
418	2 / 30
440	2 / 30
442	2 / 30

Neutral loss	Occurrence
518	2 / 30
562	1 / 30

4.3 Full scan (FS) – Measurement mode

The full scan measurement was used to ensure that every possible amphidinol variations would be captured in the detector, even if the detected variation did not possess any of the defined neutral losses stated in table 3 and 4. During the full scan every existing Q1-Mass in each strain between the *m/z* value of 1000 to 1800 was detected.

In table 14 every Q1-Mass detected through the full scan measurement, except for identical masses, which were already listed in table 5 and 12, was listed. A total of 41 additional Q1-Masses, produced by 27 individual strains, were detected during the measurement. The strains AA113 (2), CCMP2774 (2), ARC101 (2), ARC411 (4) and CCMP2400 (2) produced more than one Q1-Mass. The number of Q1-Masses was stated in brackets behind the strain name.

Table 14: Additional detected Q1-Masses through the full scan measurement mode

Strain name	t_R [min]	Q1-Mass (*m/z*)
ARC173	4,22	1016
ARC412	3,73	1017
CCMP2199	4,40	1022
AA113	4,16	1028
ARC388	3,39	1032
ARC173	3,19	1033
AA113	4,16	1044
CCMP2774	2,89	1046
ARC101	4,15	1061
ARC411	3,06	1068
AA139	3,73	1074
CCMP2813	2,88	1090
ARC197	2,76	1092
ARC151	2,57	1115
ARC411	2,74	1119
ARC150	3,10	1126
ARC89	3,27	1127
AA113	3,78	1135

Strain name	t_R [min]	Q1-Mass (*m/z*)
CCMP1784	3,77	1180
1BF	2,89	1214
CCMP2973	4,12	1230
ARC101	3,40	1272
ARC383	3,21	1281
AA165	4,04	1290
ARC115	2,88	1304
ARC195	3,77	1322
ARC195	3,59	1332
AA60 (50 mL)	3,03	1334
ARC71	3,63	1336
ARC410	3,53	1378
CCMP2774	3,48	1386
CARM	4,58	1411
ARC72	3,36	1459
ARC149	3,99	1478
CCMP2400	4,08	1484
ARC411	4,35	1506
CCMP2400	3,14	1514
ARC411	3,26	1608
CCMP1342	2,90	1626
ARC388	3,75	1650
ARC387	3,66	1730

A list of every detected Q1-Mass by the neutral loss and full scan method was stated in the appendix under table 30. Additionally, the Q1-Masses of known amphidinols were also added into table 30.

4.4 Enhanced product ion (EPI) scan – Measurement mode

A customized enhanced product ion scan was created for every strain, that was stated in the complete list of every detected Q1-Mass in table 30. In total 79 individual EPI scans were created to identify the possible amphidinol candidates, and to correctly assess them as such. An EPI scan detects every fragment ion of a fixed Q1-Mass.

Out of the total 79 recorded EPI scans, table 15 lists a total of nine different Q1-Masses produced by eight strains, which were selected as possible amphidinol candidates. Every possible Q1-Mass was previously unknown to produce amphidinols. Table 16 lists a total of three different Q1-Masses, which were already known to produce amphidinols, however the fragmentation pattern differed. Each EPI scan was discussed in detail in the following chapter, to identify the candidates based on their fragmentation patterns.

Table 15: Possible amphidinol candidates possessing unknown Q1-Masses

Strain name	t_R [min]	Q1-Mass (*m/z*)	Detection mode
ARC101	3,89	1226	Neutral loss
AA165	2,92	1242	Neutral loss
CCMP2100	2,90	1358	Neutral loss
AA60	3,75	1384	Neutral loss
CCMP122	3,20	1446	Neutral loss
AA60	2,92	1486	Neutral loss
CCMP1821	3,84	1492	Neutral loss
ARC411	4,35	1506	Full scan
ARC411	3,26	1608	Full scan

Table 16: Possible amphidinol candidates possessing known Q1-Masses

Strain name	t_R [min]	Q1-Mass (*m/z*)
ARC383	2,97	1266
ARC410	2,93	1398
ARC412	3,87	1426

5 Discussion

The main aspect in this chapter is to establish possible fragmentation patterns of the newly found amphidinols candidates stated in table 15 and 16, chapter 4. At first, however, a short discussion about the results of the SRM measurement, as well as possible errors and required additional steps is given.

5.1 Selected reaction monitoring (SRM)

5.1.1 Overview about the detected amphidinols from each *Amphidinium* species and error analysis of the measurements

From every detected *Amphidinium* species, the strain with the most abundant amphidinol content was selected and portrayed in figure 5 and in the diagrams (figure 6). The diagrams revealed a strong difference between the cell quote of varying *Amphidinium* species. The highest amount of toxin was found in a strain of *A. carterae* with a total sum of 4137 fg/cell, in comparison the highest toxin amount found in a strain of *A. gibbosum* was just 2 fg/cell produced by LPD. A similarity between every strain, with a slight exception for AA181, was that one amphidinol produced more than half of the entire toxin amount in the presented strains. Even in the strain AA181, AM9 almost produced half of the detected toxins (47%). The highest diversity of produced toxins was found in the strains ARC383 (*A. carterae*) and AA181 (unidentified New Isolates) with a variety of ten detected amphidinols. Even though both strains produced the same number of toxins, the distribution of the toxins was a bit different. The toxins AM9 (47%), AM2 (37%) and AM7 (15%) together produced about 99% of the entire toxins in the strain AA181, whilst in the strain ARC383 the toxins were produced in part by LSA (47%), LSB (41%), LPD (5%), LPB (3%), N1 (2%) and AM20 (M) (1%). In both strains the remaining toxins put together produced less than 1% of the entire toxin amount. The strain ARC383 (*A.carterae*) not only showed a higher toxin amount, but also a higher distribution rate throughout the toxin production, however both strains had two significant toxin producers in AM9 (47%), AM2 (37%) for strain AA181 and LSA (47%), LSB (41%) for strain

ARC383. The stated percentages of the toxins in both strains were approximated and therefore not exact.

The strain AA60 was the most abundant strain from *A. operculatum* with a toxin total of 28 fg/cell, produced by AM6 (79%), AM2 (14%) and AM14 (7%). The most abundant strain from *A. tomasii* was ARC90 with a toxin total of 83 fg/cell, produced by N12 (73%), N13 (11%), AM2 (8%) and five remaining toxins (8%). The final strain depicted in the diagrams was CCMP1741 from the species *A. massartii* with a toxin total of 1232 fg/cell, produced by LSB / SP (50%), LSA (44%), N1 (3%), LPD (2%), LPB / LPC (1%) and AM20 (M) (<1%). The stated percentages of the toxins in the strains were also approximated and therefore not exact.

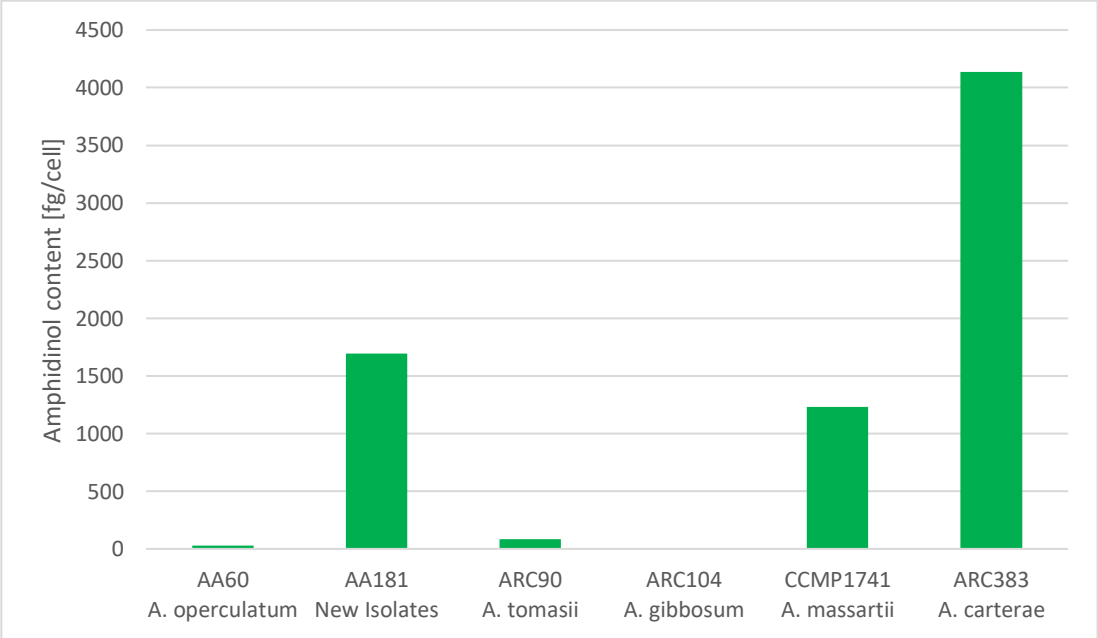

Figure 5: Calculated amphidinol content of the most abundant strains per species

Figure 6: Amphidinol profiles of the most abundant strains per *Amphidinium* species

The identification process of amphidinols detected through the SRM method was solely based on the defined transitions implemented in the method. This was not sufficient to be certain about the correct identification of a detected amphidinol. Therefore, an enhanced product ion scan (EPI) was created for every detected amphidinol in the SRM measurement. The strains that were possessing the highest abundance of each amphidinol were selected for the EPI scans. It was important to note that only a singular strain was measured for the identification of a specific amphidinol. The presence of the identified amphidinol in the remaining strains was done through the measured retention time. A similar retention time measured in the remaining strains compared to the EPI strain was seen as confirmation of the identified amphidinol. The figures listed under section D of the appendix show the spectra, which confirmed the amphidinols through the recorded EPI scans. Table 31 in the appendix list the confirmation status of every detected amphidinol in the SRM measurement. However, to be certain about the presence of the presumed amphidinol, EPI scans would have to be created for every single strain. This missing information must be considered, if assumptions/hypothesis or future works were based on the stated toxin profiles. However, even a successfully conducted qualitative analysis of the detected amphidinols would not have made the results representative or comparable with future amphidinol measurements, as explained below.

The measurements were quantified by a non-certified LPD-standard. During the initial shipment, parts of the solvent evaporated due to a transport error. The volume loss was corrected as best as possible to maintain the correct concentration of the sample, however it was impossible to guarantee absolute accuracy of the stated standard concentration (Wellkamp et al., 2020). Furthermore, the amphoteric properties of Luteophanol D could have led to interactions with the vessel walls, resulting in further losses of the standard substance. The preparation of the eluents was also prone to slight variations because every measuring day required new eluents,

resulting in different retention times between individual measurements for example. As described in chapter 3.3 most of the samples arrived as filter samples containing a high amount of biomass. Even after the extraction process the samples still exceeded the optimal amount of biomass for UHPLC-measurements. This meant that some parts of the UHPLC, like the cone or needle, were polluted by the samples, resulting in changed chromatographic conditions between measurements. The samples were also extracted over a prolonged time, which led to different storage periods for individual samples. Since it was possible that some form of interaction between sample and vessel wall took place, the influence on a sample was strongly influenced by the storage periods. For each measurement, the sample caps had to be penetrated by the UHPLC-needle leaving a tiny hole in the cap during the process. The solvents inside the samples were able to evaporate in small margins through the created needle hole, which resulted in deviations from the original stated sample volume. A longer storage period probably increased the evaporation effect.

5.2 Exemplary presentation of the necessary procedures undertaken for the discovery of potential new amphidinol variations

This exemplary presentation of individual strains was meant to provide a better idea about the scope of this thesis and more importantly to disclose the procedures used for the analysis of the neutral loss, full scan, and enhanced product ion measurements. The following procedures were undertaken using the software MassLynx (Version 4.2, Waters). The measurements were completed in identical order as listed in the results chapter.

The analysis of the neutral loss measurements can be seen in figure 7 below.

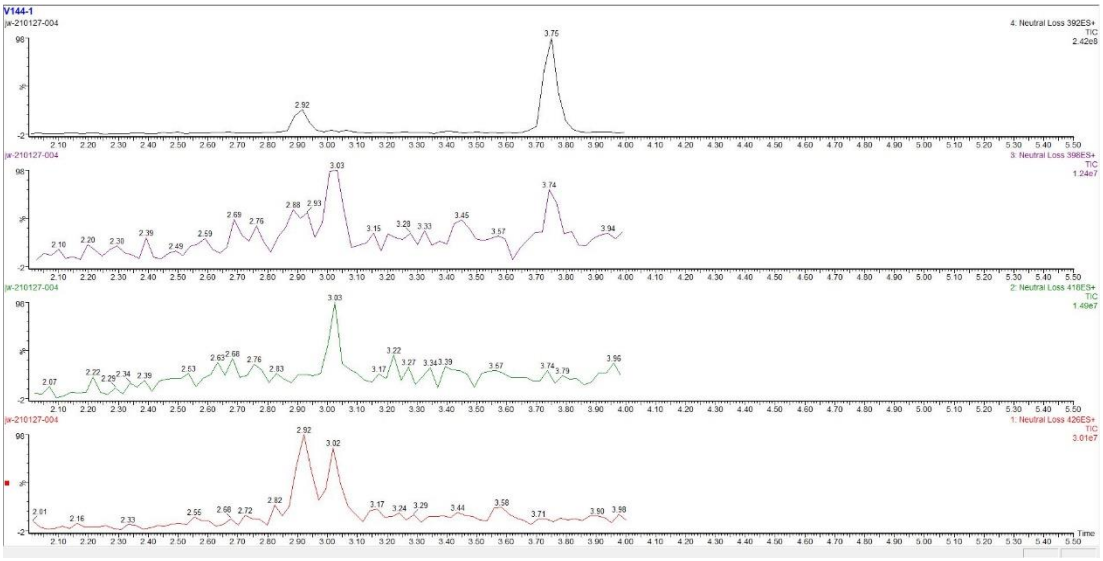

Figure 7: Overview about the chromatograms created by the four neutral losses (392Da, 398Da, 418Da and 426Da) in strain AA60

Figure 7 shows the four individual chromatograms of the neutral losses 392Da, 398Da, 418Da and 426Da. Each chromatogram was checked for existing peaks. A peak was defined to show at least a signal to noise ratio of three, this meant that the peak height had to be at least three times higher than the surrounding noise-peaks, which were always present during a measurement. The example shown in figure 7 had three peaks, which were subsequently checked individually for Q1-Masses. The first peak can be seen in the top chromatogram of the 392Da neutral loss, with a retention time of 3,75min. The second peak was produced by the neutral loss 418Da after a retention time of 3,03min. The final peak was detected after 2,92 min in the chromatogram of the 426Da neutral loss. The peak at 3,03min created by the neutral loss 398Da was not considered further, since it did not fulfill a signal to noise ratio of at least three.

The detected peaks were examined regarding the occurrence of Q1-Masses. Figure 8 shows the corresponding Q1-Mass to the first peak of the 392Da neutral loss with a mass of 1383.40 *m/z*.

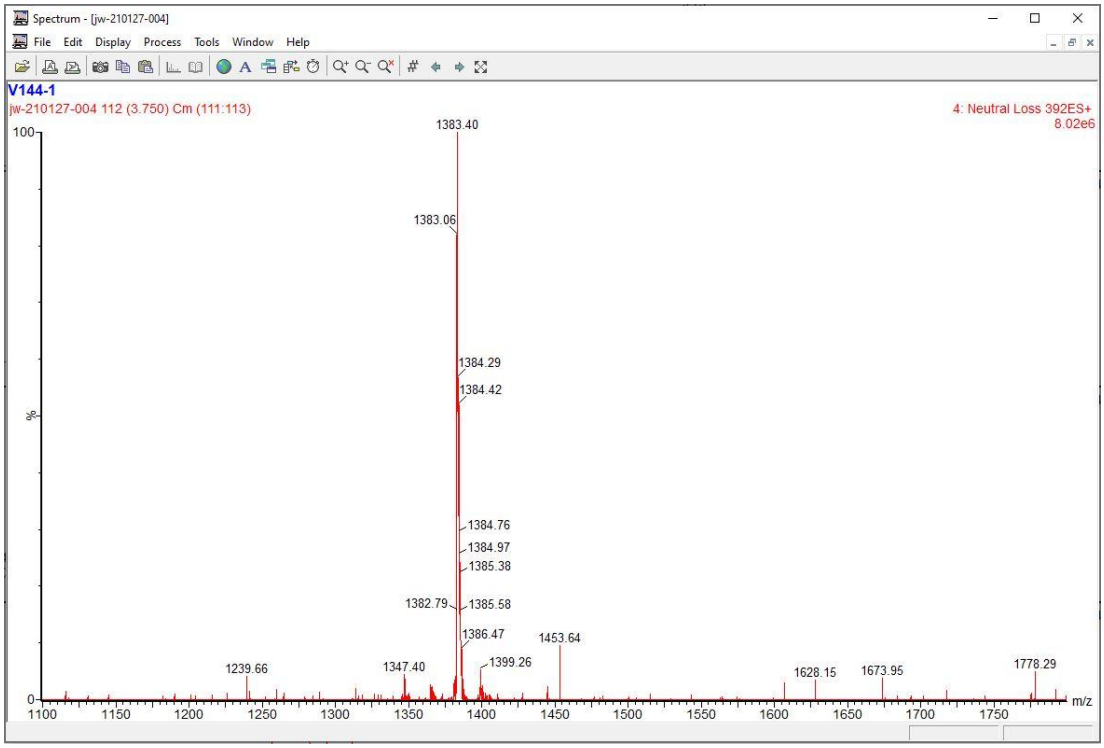

Figure 8: Corresponding spectrum of the neutral loss 392Da

The mass had by far the highest abundance compared to any of the other masses and was thereby considered as a positive detection. The detected mass was added to the list of Q1-Masses, which were measured again using an EPI scan for further investigation about the discovery of a possible new amphidinol variations. In contrast to the positive detection of the Q1-Mass 1383.40 *m/z* shown in figure 8, figure 9 depicts the discarded spectrum of the second peak produced by a 418Da neutral loss.

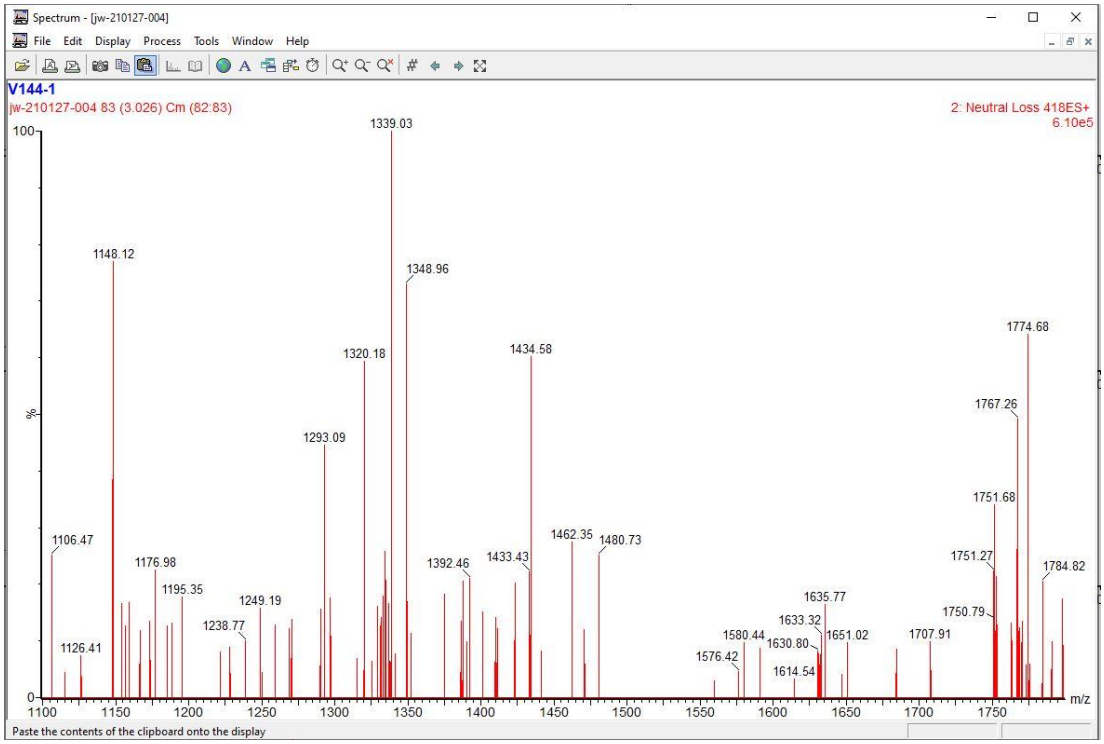

Figure 9: Corresponding spectrum of the neutral loss 418Da

Not a single mass possessing a high abundance was present in the spectrum, therefore no Q1-Mass was noted for this peak. Figure 28 in the appendix shows another positive detection of a Q1-Mass from the measured strain. The mass of 1417.37 *m/z* had a high abundancy in the spectrum of the third peak, produced by the neutral loss of 426D. This procedure was repeated for the remaining ten neutral losses as shown in the figures 29, 30 and 32 listed in the appendix. Figure 31 shows the detection of the Q1-Mass 1485.36 *m/z* found in the peak produced by the neutral loss of 512Da. After every single neutral loss was checked for the presence of peaks and subsequently for the presence of an abundant Q1-Mass in the corresponding spectrum, the next strain was processed in an identical manner. This procedure was repeated for every strain of the sample set. The entire list of potential Q1-Masses producing possible unknown amphidinol variations that were detected through the neutral loss method was stated in table 12.

Table 12 was also used for the preparations of the full scan measurement. Theoretically the same Q1-Masses detected through the neutral loss measurement should

also be detected through the full scan measurement. After the full scan was conducted and analyzed only twelve out of the 27 Q1-Masses were likewise detected in the full scan measurement. Table 17 lists the confirmed Q1-Masses, that were detected in both the neutral loss and full scan measurement.

Table 17: Q1-Masses detected in both the neutral loss and full scan measurement

Strain name	t_R [min]	Q1-Mass (*m/z*)	Neutral loss
AA113	3,75	1114	518
CCMP2774	3,33	1152	398
ARC101	3,89	1226	398
AA165	2,92	1242	392 / 512
AA165	3,80	1264	392
ARC101	2,94	1328	392 / 512
CCMP2100	2,90	1358	426
AA60	3,75	1384	392
AA165	3,90	1396	392
ARC410	2,93	1398	338 / 512
AA60	2,92	1418	426
AA60	2,92	1486	512

The remaining 15 Q1-Masses were not detected during the full scan. Noteworthy was that none of the 15 unconfirmed Q1-Masses, were included in the selection of possible amphidinol variations, since none of them possessed an EPI spectrum showing similarities to known fragmentation patterns of amphidinols. The full scan

confirmation of Q1-Masses detected in the neutral loss measurement, could therefore be seen as an important criterion that must be met in the discovery process of new amphidinol variations.

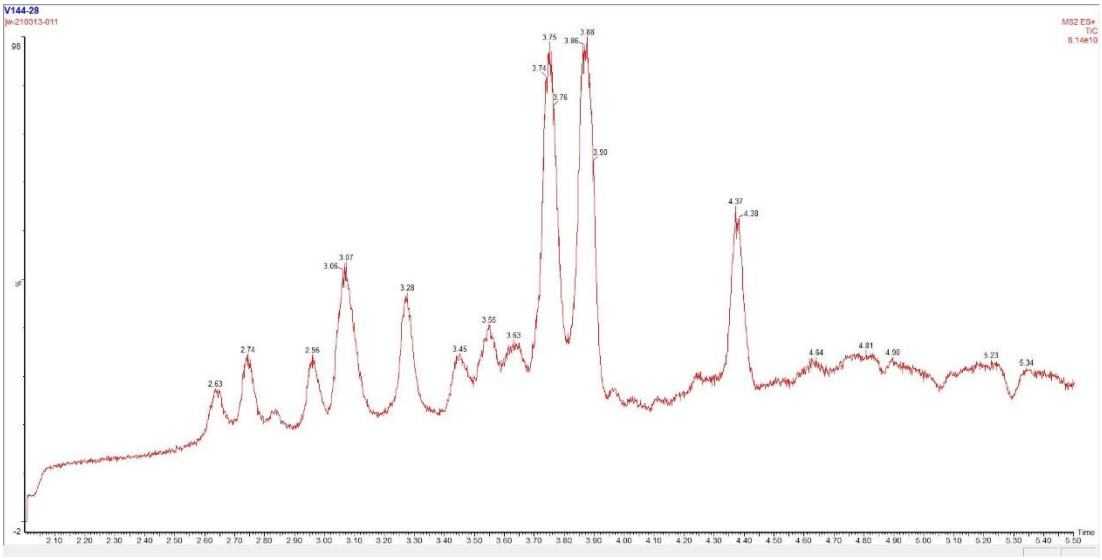

Figure 10: Overview about the full scan chromatogram of strain ARC411

Figure 10 shows the full scan chromatogram of strain ARC411. The chromatogram was analyzed slightly different than the previous neutral loss measurement. The different approach was undertaken because of the vast number of peaks present in a chromatogram. MassLynx marked eleven peaks in the chromatogram of figure 10 with retention times. Every peak, that showed a retention time was checked for the presence of an abundant Q1-Mass. Figure 11 shows the spectrum of the peak occurring after 3,28min. The detection process for the Q1-Masses in the corresponding spectrums was identical to the neutral loss procedure. In the case of figure 11 the Q1-Mass 1607.50 *m/z* was detected.

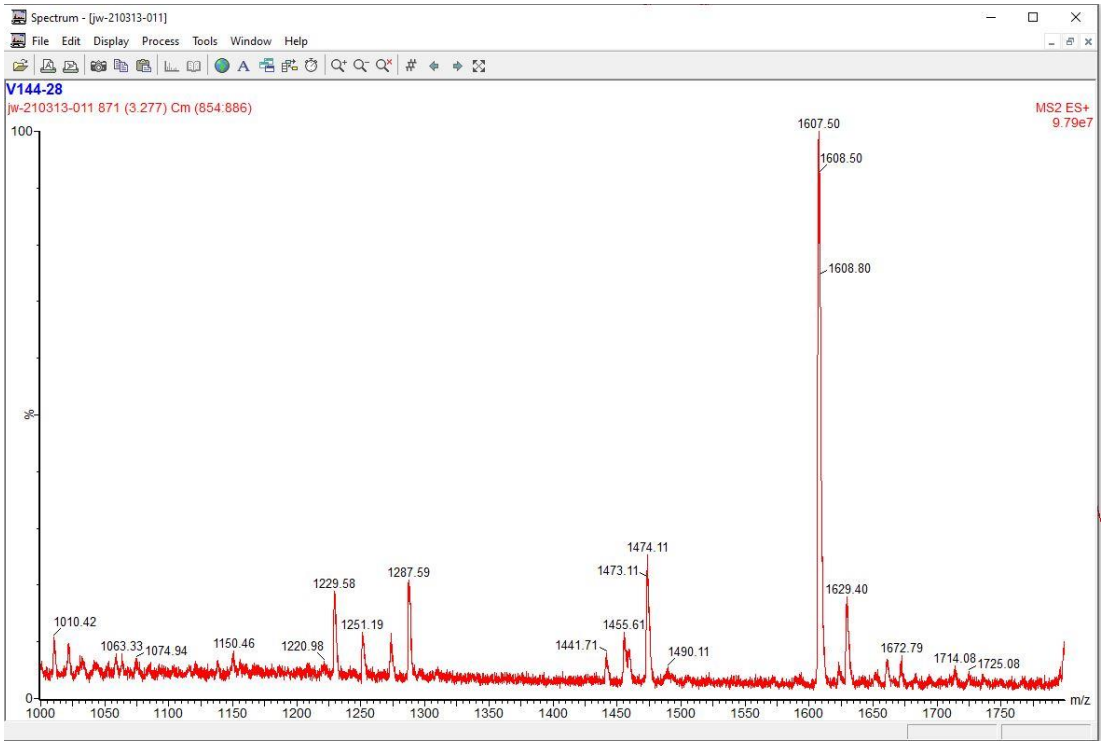

Figure 11: Corresponding spectrum of the peak occurring after 3,28 min in strain ARC411

Figures 33 and 34 in the appendix show the two additional detected Q1-Masses 1425.61Da and 1505.61Da, which were detected in the spectrums of the two peaks occurring after 3,88 min (1425.61Da) and 4,37 min (1505.61Da). Additionally figure 35 shows the discarded spectrum of the 3,75 min peak. These four spectra demonstrated the importance of every peak occurring in a full scan measurement, since the discarded spectrum occurred in the second highest peak after 3,75 min, whilst the spectrum possessing the Q1-Mass 1607,50 *m/z*, which was included in the EPI scan, occurred in the relatively small peak after 3,28 min. Detected Q1-Masses possessing the same mass as already known amphidinols were not listed in table 14, since these masses were included in the EPI scan, nonetheless. The strains with the highest cell count per amphidinol, as calculated during the SRM measurement, were selected for the subsequent EPI scan. Table 18 below lists the confirmed Q1-Masses of known amphidinols by the full scan measurement.

Table 18: Q1-Masses of known amphidinols confirmed through the full scan

Strain name	t_R [min]	t_R - Fullscan [min]	Q1-Mass (*m/z*)
AA177	3,3	3,3	1254
ARC383	2,97	2,97	1266
ARC410	3,84	3,75	1296
CCMP2100	3,87	3,83	1324
CCMP2100	4,10	4,31	1350
AA177	4,07	4,07	1394
AA181	3,78	4,09	1398
ARC412	3,87	3,87	1426
CCMP122	3,81	3,81	1668

After every peak was checked, the next strain in the sample set was processed according to the same principles. The complete list of every detected Q1-Mass from the neutral loss, full scan measurement and known amphidinols was shown in table 30 in the appendix.

At last, the EPI scans were created individually for every Q1-Mass listed in table 30. Figure 12 below shows the first step of the creation process. The detected Q1-Mass, named “Daughters of” in MassLynx, was added with two decimal digits. The starting mass stayed consistently at 100 *m/z* for every created EPI scan. The end mass had a value of about 100 *m/z* more than the recorded Q1-Mass. The scanning time was calculated as followed:

$$Scan\ time = \frac{End\ mass - Start\ mass}{10000}$$

Equation 8

10000 was the set scanning rate of the mass spectrometer and was therefore also consistent. The collision energy was also consistent at 75 eV. The time frame of the EPI scan was based on the respective retention time. The start was selected to be one minute earlier than the retention time, whilst the end was set to be one minute after the stated retention time. A time window of 2min was therefore used in every EPI scan.

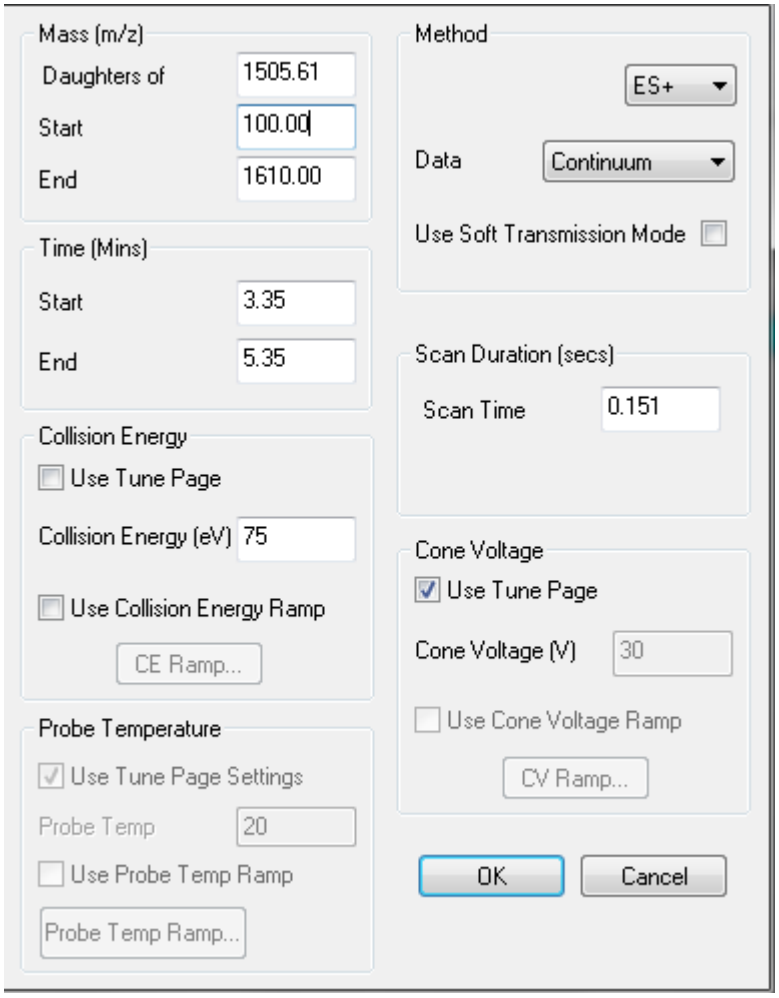

Figure 12: Settings for the EPI scan of 1506Da

Figure 13 shows the "Method event" settings of the EPI scan. The flow state into the liquid chromatography was set to start 0,01 min after the starting time of the measurement and was switched from the chromatography path into the waste path 0,01 min before the measurement window ended.

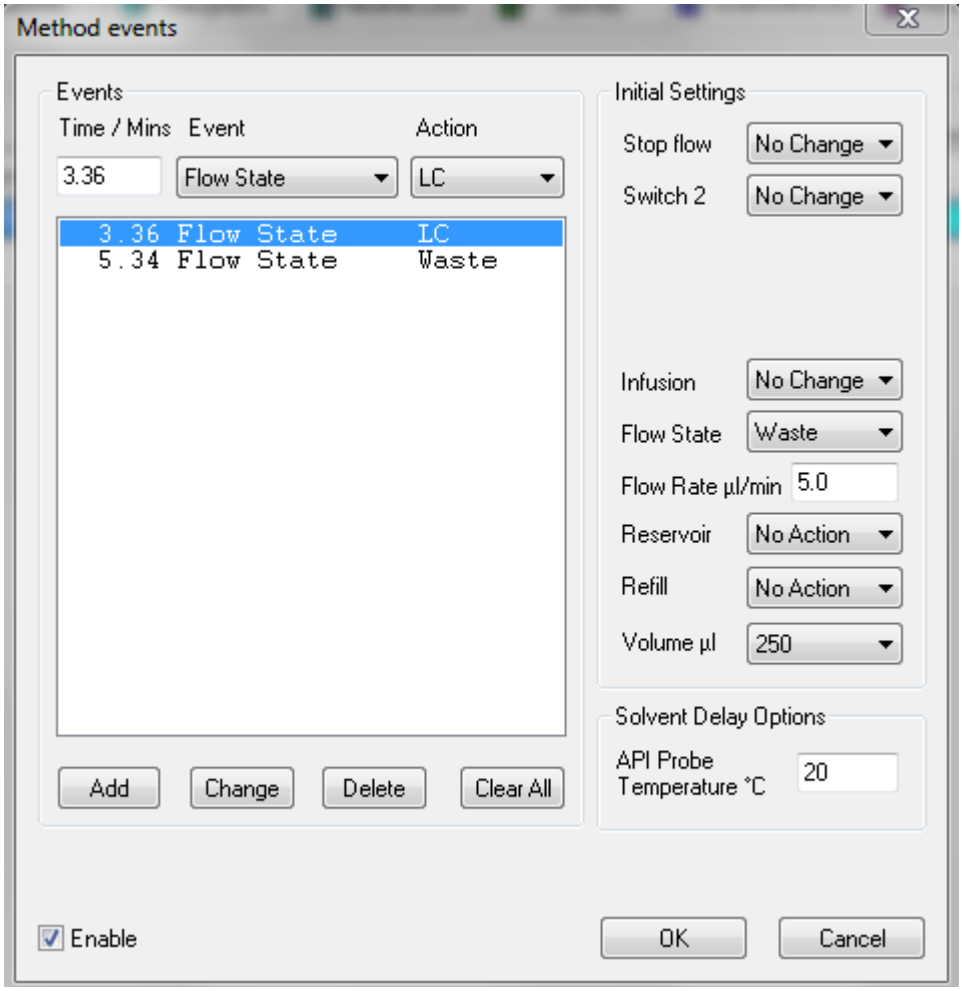

Figure 13: Method event for the EPI scan of 1506Da

Both setting windows had to be completed correctly for every individual EPI scan. The completed EPI scan marked the end of the necessary procedures which were undertaken for the discovery of potential new amphidinol variations.

5.3 Fragmentation pattern proposals for possible detected amphidinol variations

After the completion of the described measurements in the previous section a total of twelve substances were detected, which could possibly be new variations of amphidinols. Since amphidinols fragment according to similar fragmentation patterns, it was possible to compare the fragmentation patterns of the detected candidates with established and confirmed fragmentation patterns described throughout the literature for existing similarities between them. The stated fragmentation patterns

were only proposals for possible structures of the detected substances. A complete clarification of the structure could only be done by a nuclear magnetic resonance (NMR) spectroscopy, which was not the case for the presented fragmentation patterns in this thesis.

During the research about similarities between the amphidinols, additionally to the neutral losses of the lipophilic part, a highly conservative structure was found starting at C-1 to C-14 in the hydrophilic part of every amphidinol. C-14 was marked in the proposed fragmentation pattern of U1. No changes in the chemical structure occur for any amphidinol in this part. This was important for the creation of the proposed fragmentation patterns since changes in the amphidinol structure could only occur starting at C-15 until the end of the hydrophilic part and in the lipophilic part. Furthermore, it was found that amphidinol structures rarely consist of long C-chain without any functional groups, such as a hydroxyl- or methyl group.

U1

U1 had a retention time of 3,95 min and a mass of 1226Da. The mass fragmented into 834Da at the C-1' / C-1 bond break because the lipophilic part, or neutral loss, starting from C-1' had a mass of 392Da. The 834Da fragment created by the C-1' / C-1 bond break, had the highest abundancy in the fragmentation spectrum. The fragmentation pattern presented in figure 14 was not able to explain the remaining small abundant fragments such as 1062Da and 762Da. Only the fragment 1008 was coherent with the stated proposal, therefore the proposal was insufficient.

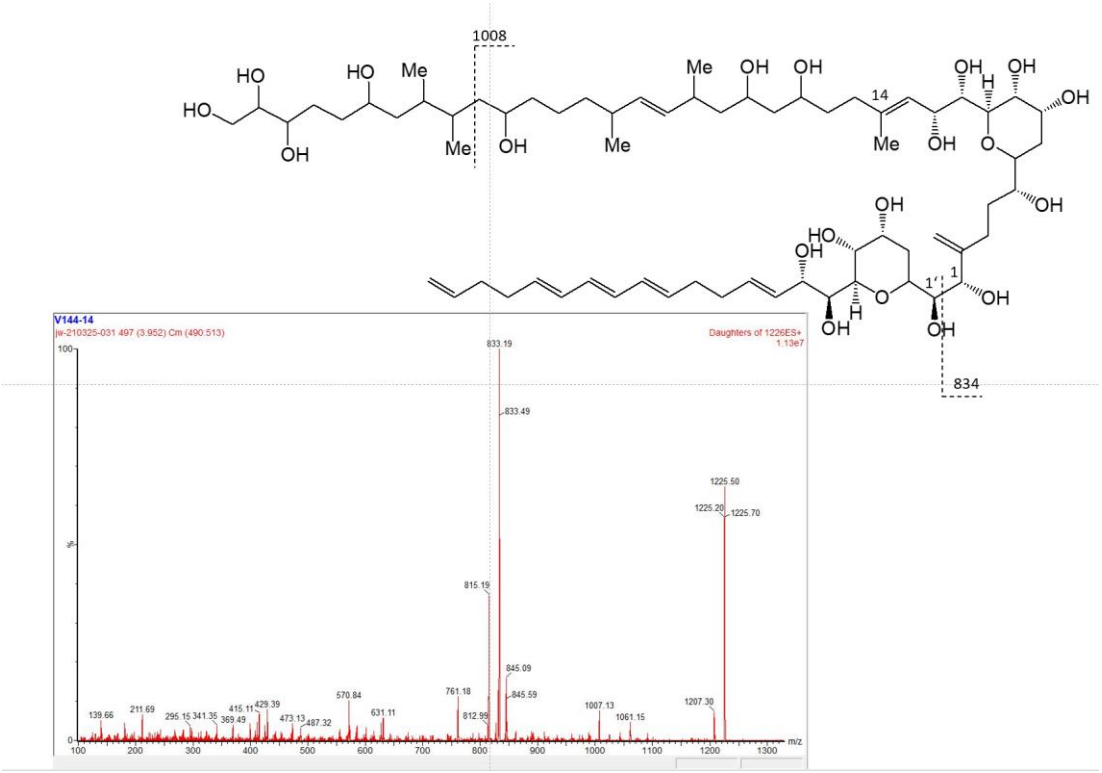

Figure 14: Enhanced product ion scan of 1226Da (3,95 min) of the strain ARC101, named U1. Additionally, the fragmentation spectrum and a fragmentation pattern proposal were stated

U2

U2 had a retention time of 3,01 min and a mass of 1242Da. The EPI scan showed some similarities between the substance and amphidinol 12. U2 produced the fragment 1122Da, which was 120Da lighter than the Q1-Mass. This mass was identical to the mass of sodium hydrogen sulfate $NaHSO_4$. The fragmentation pattern of amphidinol 12 (Figure 16) contained the same loss of 120Da, which was expected since amphidinol 12 was known as a sulfated amphidinol. U2 also possessed the two abundant fragments 850Da and 730Da. The mass 1122Da fragmented again at the C-1' / C-1 bond break, which divided the lipophilic part with a mass of 392Da from the hydrophilic part, creating the 730Da fragment. The 850Da fragment had a difference of 272Da to the 1120Da fragment, which was marked in the hydrophilic part.

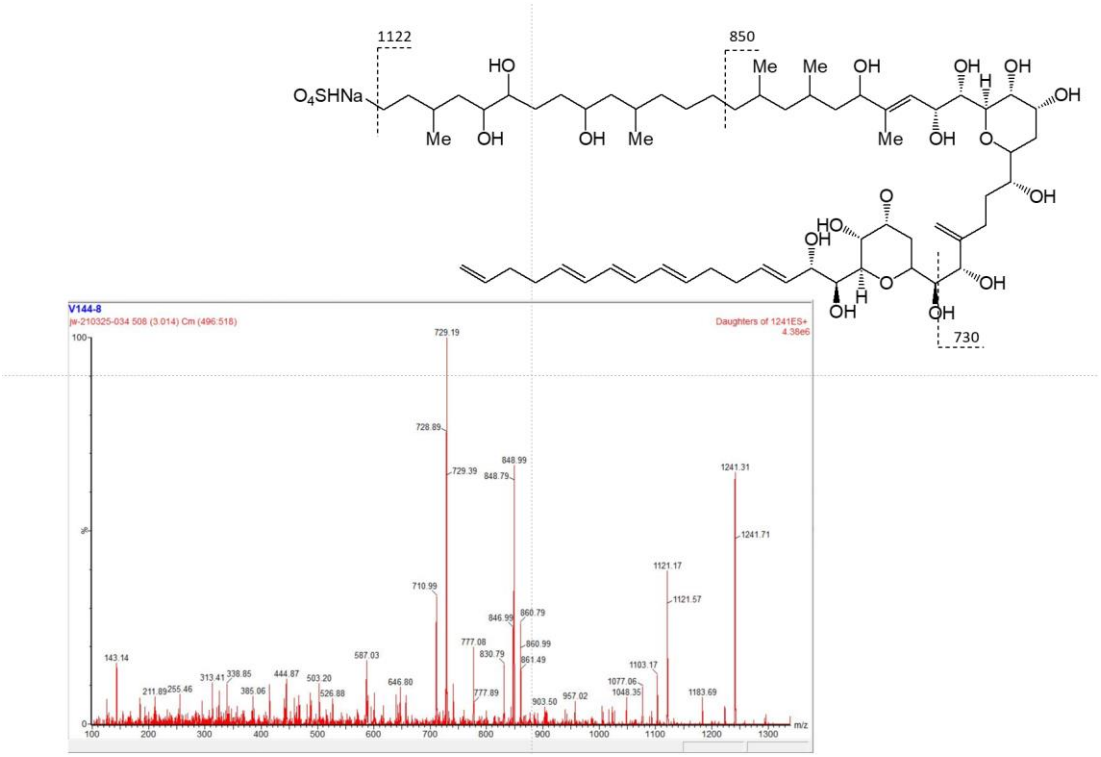

Figure 15: Enhanced product ion scan of 1242Da (3,01 min) of the strain AA165, named U2. Additionally, the fragmentation spectrum and a fragmentation pattern proposal were stated

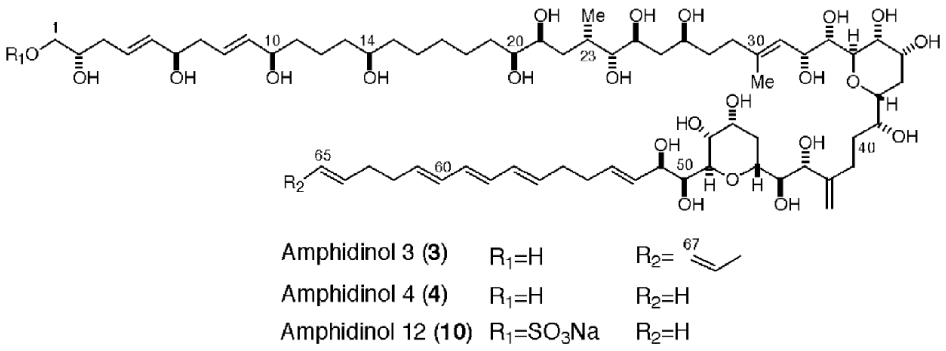

Figure 16: Fragmentation pattern of amphidinol 12 described by Echigoya et al., 2005

U3

The substance, named U3, was detected at 3,03 min with a mass of 1266Da. The mass was identical to the LSB/SP, however the fragment ion of LSB/SP 754Da, was missing in the spectrum, proving that the spectrum was different from the existing

toxin. The fragmentation spectrum was very similar to the previously described substance U2 with the addition of 24Da in total mass. The 120Da fragment in U2 was also produced by U3 (1146Da) and the fragment 874Da had the same 272Da difference to the 1146Da fragment. The mass 1146Da fragmented again at the C-1' / C-1 bond break, creating the 754Da fragment. The fragmentation pattern proposal of U3 was identical to U2, with an additional two carbon atoms in the hydrophilic part, containing two double bonds to achieve the correct mass of 1266Da.

Figure 17: Enhanced product ion scan of 1266Da (3,03 min) of the strain ARC383, named U3. Additionally, the fragmentation spectrum and a fragmentation pattern proposal were stated

U4

U4 was detected at a retention time of 2,97 min and had a mass of 1358Da. The lipophilic part had a value of 426Da and the abundant fragment 932Da was created by C-1' / C-1 bond break. A loss of 131Da and 253Da created the fragments 1228Da and 1105Da. Both fragments had a low abundancy in the spectrum but were marked accordingly in the hydrophilic part.

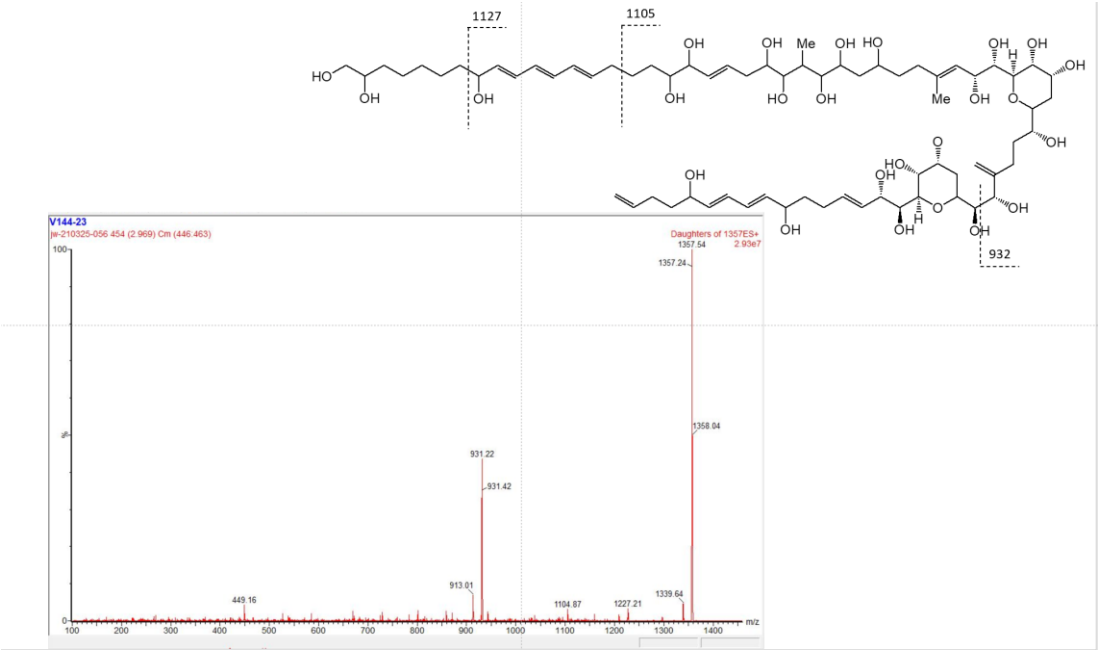

Figure 18: Enhanced product ion scan of 1358Da (2,97 min) of the strain CCMP2100, named U4. Additionally, the fragmentation spectrum and a fragmentation pattern proposal were stated

U5

U5 had a retention time of 3,82 min and a mass of 1384Da. The mass fragmented into 992Da at the C-1' / C-1 bond break, due to a neutral loss of 392Da. The 992Da fragment created by the C-1' / C-1 bond break, had the highest abundancy in the fragmentation spectrum. The fragmentation pattern presented in figure 19 cannot clarify the remaining small abundant fragments such as 1219Da and 919Da. Only the fragment 1165Da was coherent with the stated proposal, therefore the proposal was insufficient.

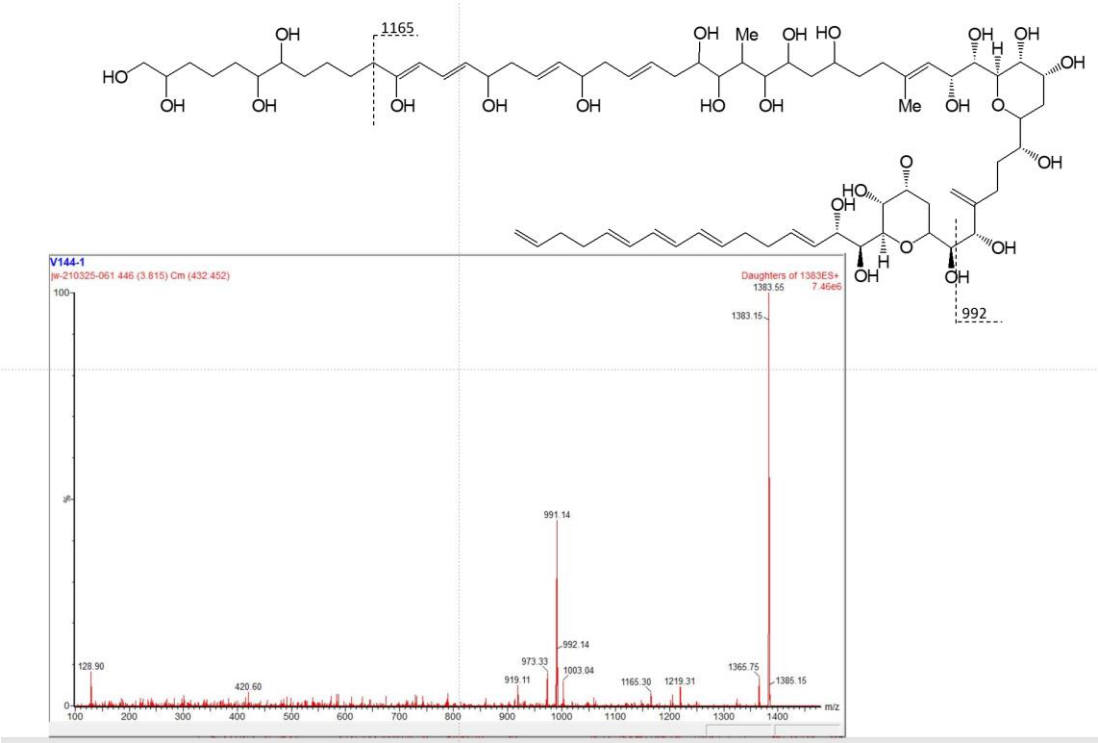

Figure 19: Enhanced product ion scan of 1384Da (3,82 min) of the strain AA60, named U5. Additionally, the fragmentation spectrum and a fragmentation pattern proposal were stated

U6

The EPI spectrum of U6 was similar to the spectra of U2 and U3, which were based on amphidinol 12, however it only depicted two detected fragments. U6 had a retention time of 2,91 min and a mass of 1398Da. The first fragment 1288Da was 120Da lighter than the Q1-Mass of the EPI scan, which was again identical to the mass of sodium hydrogen sulfate $NaHSO_4$. The first fragment fragmented again at the C-1' / C-1 bond break, into the second fragment of 886Da, caused by the neutral loss of 392Da. Since both U2 and U3 were based on amphidinol 12, U6 was also compared against amphidinol 12. The substance was 28Da lighter than the similar amphidinol 12. To obtain the mass of 1398Da for U6., two carbon atoms were removed in the hydrophilic part of amphidnol 12.

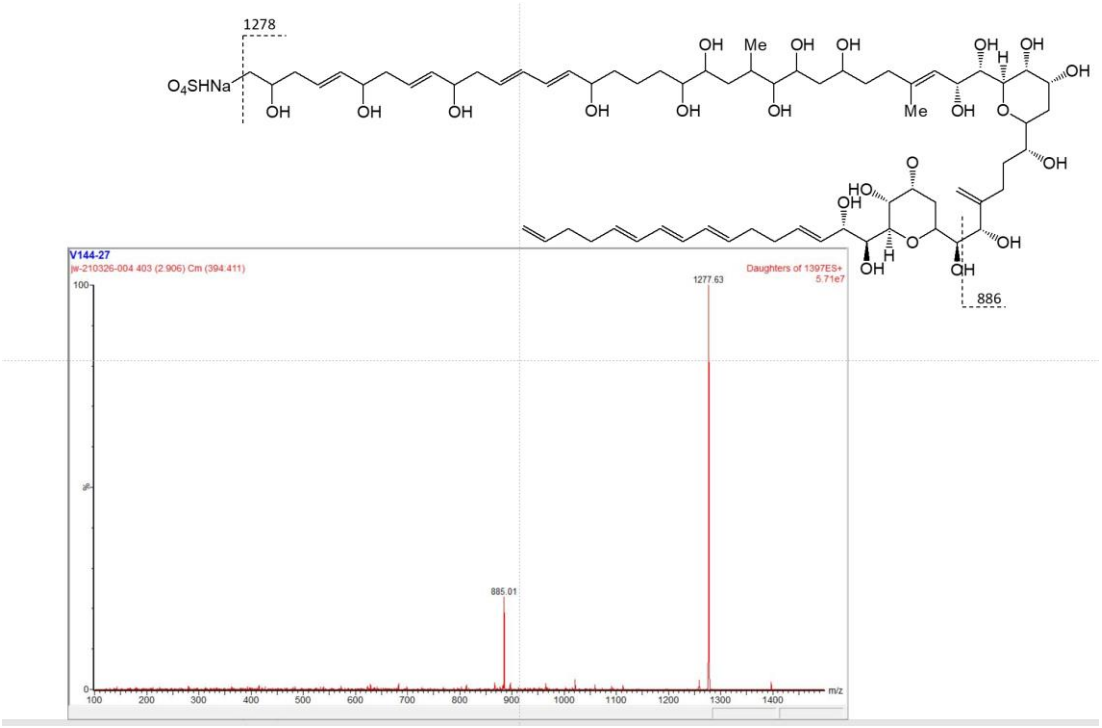

Figure 20: Enhanced product ion scan of 1398Da (2,91 min) of the strain ARC410, named U6. Additionally, the fragmentation spectrum and a fragmentation pattern proposal were stated

U7

U7 had a retention time of 3,91 min and a mass of 1426Da. The EPI scan revealed a similar fragmentation spectrum and a similar retention time to amphidinol 18 (figure 22). The similarities were found in the high abundant fragments (1208Da and 1150Da), which were created next to both sides of the carbonyl group in the hydrophilic part. Both fragments were so called “pair fragments” because another fragmentation for both fragments occurred again because of the C-1’ / C-1 bond break. The pair fragments were marked in the same colors. The fragment (1034Da) created by the C-1’ / C-1 bond break only showed a low abundant peak, like amphidinol 18. Compared to the mass 1382Da of amphidinol 18, U7 was 44Da heavier. However, the neutral loss was only 392Da, whereas the neutral loss of amphidinol 18 was 418Da. Therefore, the structure of U7 had to be 70Da heavier in the hydrophilic part. Four carbon atoms containing one double bond and one hydroxyl group were

added between the second fragment (1150Da) and the rest of the hydrophilic part until C-14.

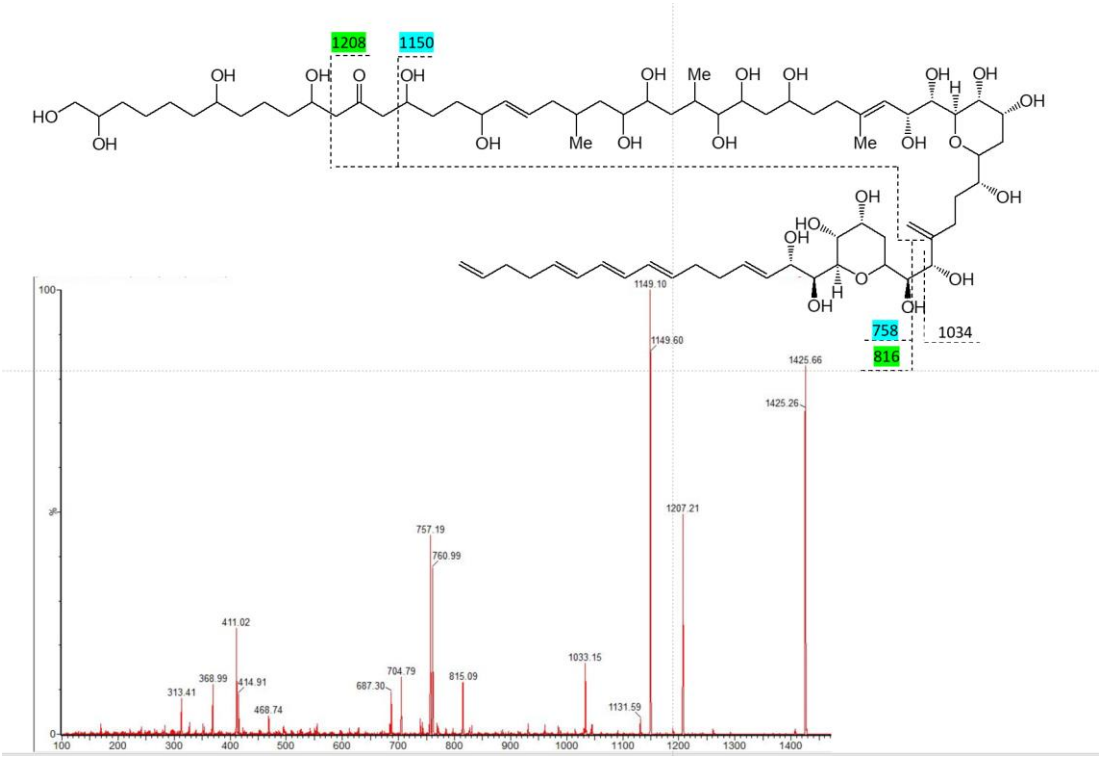

Figure 21: Enhanced product ion scan of 1426Da (3,91 min) of the strain ARC412, named U7. Additionally, the fragmentation spectrum and a fragmentation pattern proposal were stated

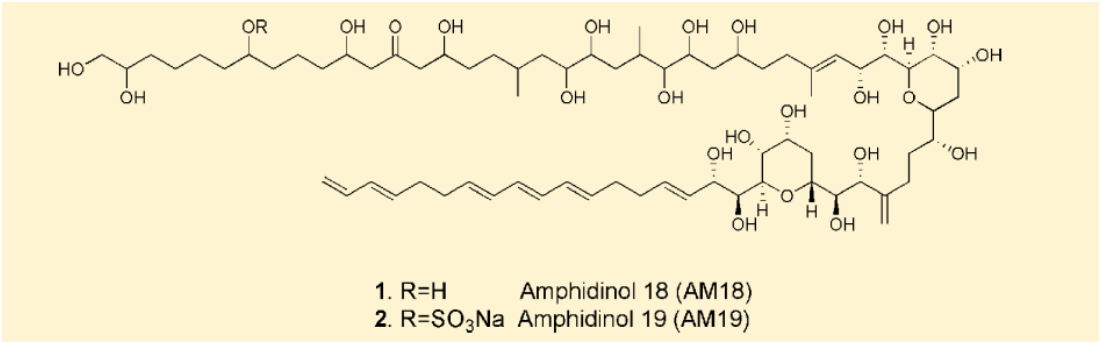

Figure 22: Fragmentation pattern of amphidinol 18 described by Nuzzo et al., 2014

U8

U8 had a mass of 1446Da and was detected at 3,24 min. The substance was similar to the other unknown substances, which lost a mass of 120Da due to the fragmentation of sodium hydrogen sulfate $NaHSO_4$. U8 was 48Da heavier than U6 but the lipophilic part had a mass of 398Da, which was 6Da heavier than the lipophilic part of U6. Therefore, the hydrophilic part had to be 42Da heavier compared to U6. Two additional methyl groups and one double bonded carbon atom were added after the break of $NaHSO_4$ and C-14. The two fragments 1126Da and 1086Da were 200Da and 240Da lighter than the fragment 1326Da, which was created by the loss of 120Da. The C-1' / C-1 bond break resulted in the fragment of 928Da.

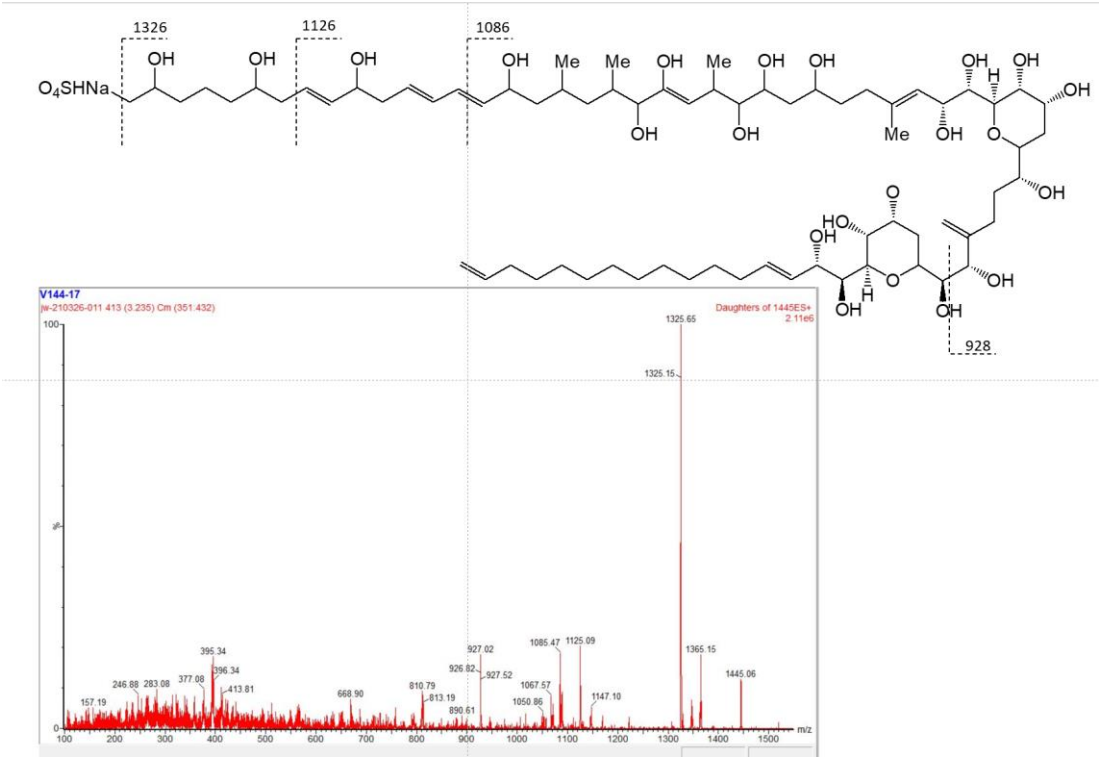

Figure 23: Enhanced product ion scan of 1446Da (3,24 min) of the strain CCMP122, named U8. Additionally, the fragmentation spectrum and a fragmentation pattern proposal were stated

U9

The substance U9 had a retention time of 3,02 min and a mass of 1484Da. The spectrum showed the same 120Da loss as found in previous spectra of unknown substances. The loss of 120Da resulted in the fragment 1366Da and was again ex-

plained through the fragmentation of a sodium hydrogen sulfate $NaHSO_4$. Otherwise, the substance was 40Da heavier than U8, however the neutral loss was 392Da and therefore 6Da lighter than the neutral loss of U8. Because of that the substance had to be 46Da heavier in the hydrophilic part compared to U8. The fragment 1094Da was 272Da lighter than the sulfate fragment 1366Da and was marked in the hydrophilic part. Two methyl groups and one carbon atom were added to the structure of U8, whilst two double bonds were removed to achieve an additional mass of 46Da in the hydrophilic part. The C-1' / C-1 bond break resulted in the fragmentation of the 1366Da fragment, creating the subsequent 974Da fragment.

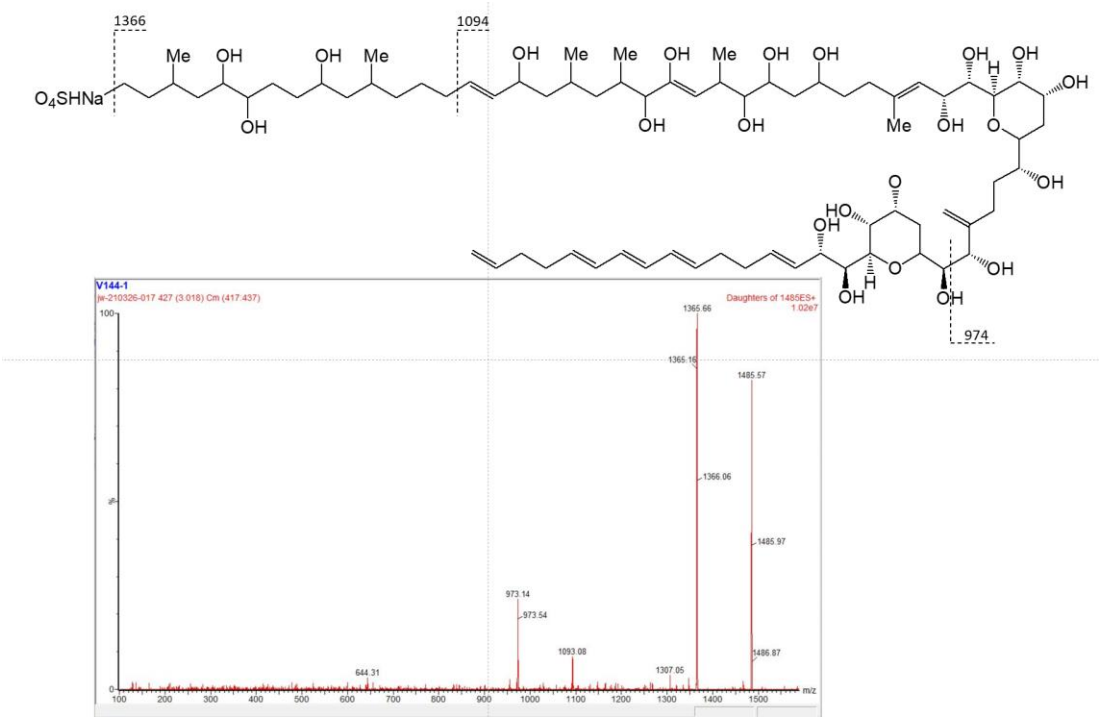

Figure 24: Enhanced product ion scan of 1486Da (3,02 min) of the strain AA60, named U9. Additionally, the fragmentation spectrum and a fragmentation pattern proposal were stated

U10

The substance U10 was included as a negative example of a substance missing an EPI spectrum, which showed any similarities to known amphidinols. The substance was detected at 3,86 min and had a mass of 1492Da. The recorded spectrum revealed an abundance of H_2O separations, which were highly unlikely for amphidinols. In general, amphidinols rarely fragment more than one water molecule at

once. This was certainly not the case in the spectrum of 1492Da. Because of the that no proposal for a possible fragmentation pattern was stated for U10.

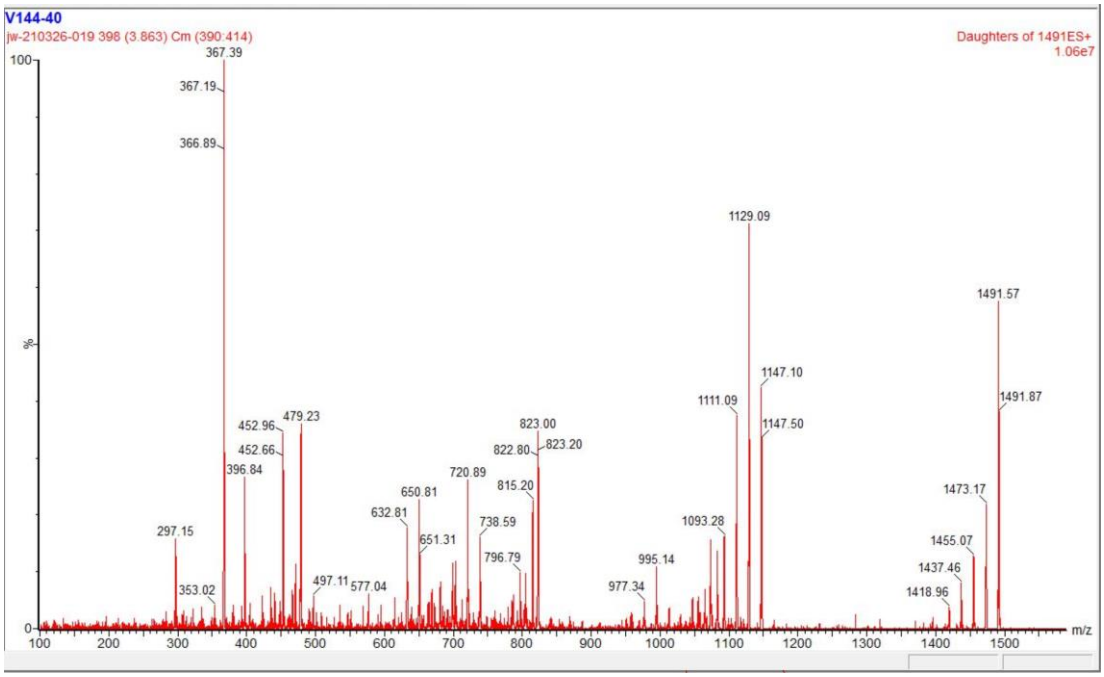

Figure 25: Enhanced product ion scan of 1492Da (3,86 min) of the strain CCMP1821, named U10. No fragmentation pattern proposal was stated for the recorded fragmentation spectrum

U11

U 11 had a retention time of 4,38 min and a mass of 1506Da. Just as substance U7, the EPI scan revealed a similar fragmentation spectrum and retention time to amphidinol 18 (figure 22). The similarities were found in the high abundant fragments (1208Da and 1150Da), which were created next to both sides of the carbonyl group in the hydrophilic part. The two fragments were again pair fragments that fragmented again at the C-1' / C-1 bond break. The pair fragments were marked in the same colors. The fragment (1082Da) created by the C-1' / C-1 bond break only showed a low abundant peak, like amphidinol 18. Compared to amphidinol 18, U10 was 124Da heavier. The substance U11 differed from U7 and amphidinol 18 in the lipophilic part. U11 had a neutral loss of 424Da, which was unusual since such a neutral loss did not exist in the neutral loss method. Because of the different neu-

tral loss, the hydrophilic part had to be 118Da heavier than amphidinol 18. Five carbon atoms and three hydroxyl groups were added between the second fragment (1150Da) and the rest of the hydrophilic part until C-14.

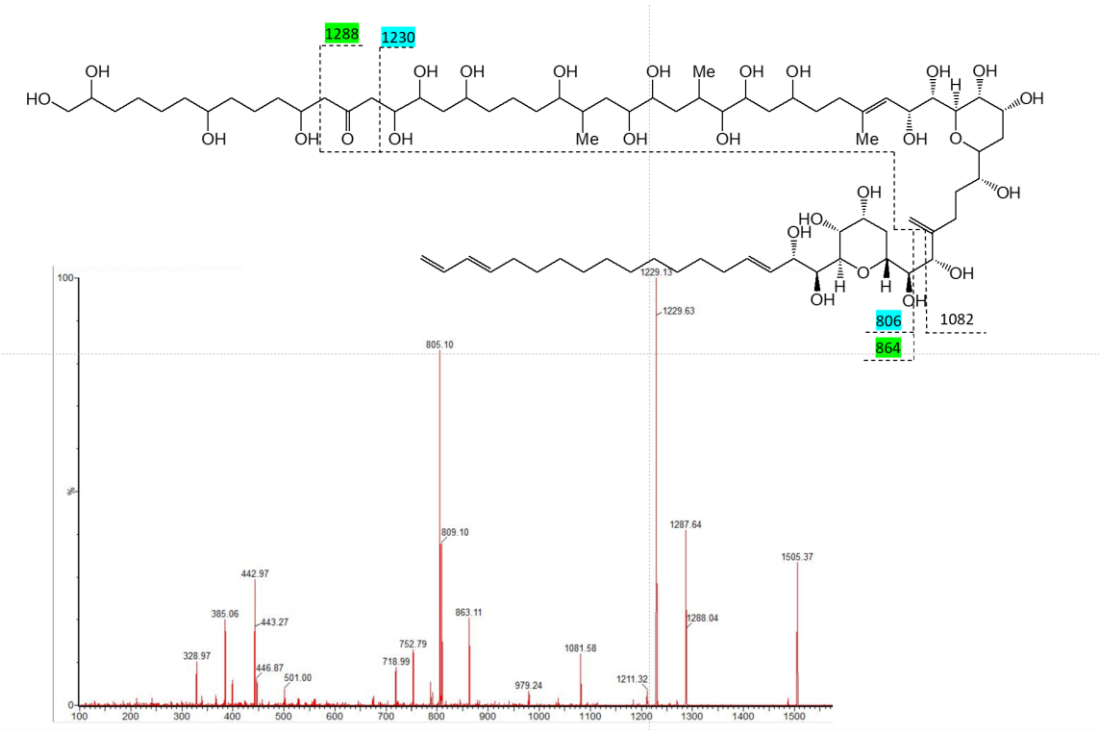

Figure 26: Enhanced product ion scan of 1506Da (4,38 min) of the strain ARC411, named U11. Additionally, the fragmentation spectrum and a fragmentation pattern proposal were stated

U12

U12 had a retention time of 3,31 min a mass of 1608Da and was detected in the same strain as U11, ARC411. The fragmentation spectrum revealed similarities to both amphidinol 12 and 18. The loss of 120Da, as well as pair fragments were present. The fragment 1488Da was explained again by the loss of $NaHSO_4$.The pair fragments 1288Da / 1230Da and 864Da / 806Da were explained by a break in the structure next to both sides of a carbonyl group. To conclude, the structure contained parts of amphidinol 12 (sulfate group) and 18 (carbonyl group) structure. The difference between the 1488Da fragment and 1288Da fragment was 200Da. Amphidinol 18 showed a difference of 218Da between the Q1-Mass and first fragment. However, the 218Da fragment of amphidinol 18 also contained a hydroxyl group at the end of the hydrophilic part, whereas U12 did not, since the sulfate group was

fragmented first. Therefore, a structure was created based on amphidinol 18, which was 2Da lighter up to the first pair fragment (1288Da). One carbon atom was removed, whilst two double bonds and one oxygen atom were added to adjust the mass in the described manner. Interestingly the pair fragment was identical to the pair fragment of U11, which meant that the neutral loss or lipophilic part had the same mass of 424Da in both substances. The C-1' / C-1 bond break did not only produce the two fragments 864Da and 806Da, but also the 1064Da fragment, which was produced by a break of the 1488Da fragment.

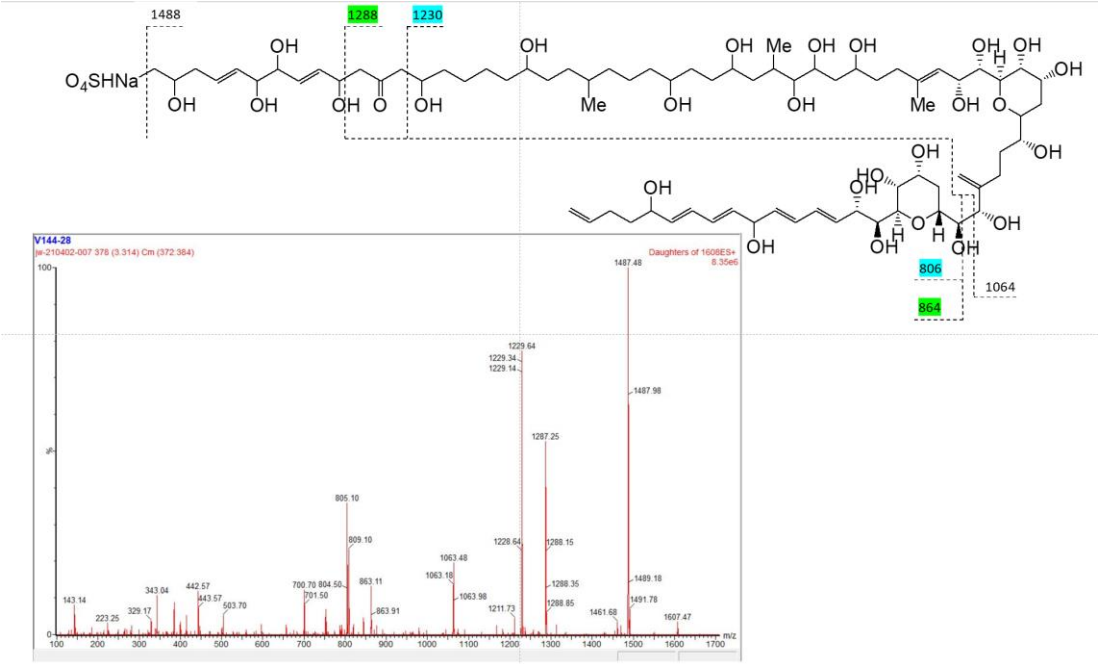

Figure 27: Enhanced product ion scan of 1608Da (3,31 min) of the strain ARC411, named U12. Additionally, the fragmentation spectrum and a fragmentation pattern proposal were stated

Summary U1 – U12

In total eleven out of the twelve detected substances were identified as possible amphidinol variations. Two out of the eleven proposed fragmentation patterns (U1 / U5) were insufficient in their explanation about the present fragments in the spectra and could therefore not be seen as a possible fragmentation pattern. This however did not change the possibility that the detected substances could be new am-

phidinol variations. Six substances lost a 120Da fragment, which was believed to occur due to the loss of sodium hydrogen sulfate $NaHSO_4$. The six substances therefore showed a similar fragmentation pattern as amphidinol 12.

In order to receive further information about the structure of the 120Da fragment an additional customized full scan measurement was created for every substance losing the stated 120Da fragment. The starting mass of the full scan was 20Da lighter than the Q1-Mass of the substance, whilst the end mass was 20Da heavier. The small scanning area (40Da) was used to analyze the Q1-Mass in more detail. The hypothesis was that the isotope pattern of sulfur, which is part of sodium hydrogen sulfate, could be detected and therefore confirmed. Sulfur possesses the four stable isotopes ^{32}S (95.02%), ^{33}S (0.75%), ^{34}S (4.21%), ^{36}S (0.02%). Unfortunately the resolution of the full scan measurement was not sufficient to undertake such an analysis and was therefore not investigated further.

Three substances showed very similar fragmentation spectra compared to amphidinol 18. The substances contained two fragments with a difference of 58Da between them. Both fragments appeared to fragment again at the C-1' / C-1 bond break in the spectrum. The substance U12 possessed both the similarities of amphidinol 12 and 18 and was therefore counted in both. A variety of four different neutral losses were detected in the substances, these being the 392Da, 426Da, 398Da as well as the newly found 424Da neutral loss. The newly found 424Da neutral loss was found in U11 and U12, which both were produced by the strain ARC411. The 392Da neutral loss occurred three times, whilst both the 426Da and 398Da neutral loss were only detected once. The stated transitions in Table 19 below included the fragmented mass of 120Da for the amphidinol variations similar to amphidinol 12, which were added to the present neutral loss in the substance. Every stated fragmentation pattern proposal contained the unchanged conservative C-1 to C-14 structure, which was marked exemplary in U1. Table 19 below lists the strain, retention time and proposed transitions of the detected eleven possible amphidinol variations.

Table 19: Overview about the transitions of the detected unknown substances, that possibly are amphidinol variations

Strain	t_R [min]	Transition (Q1- and Q3-Mass)
ARC101	3,89	1226 / 834
AA165	2,92	1242 / 730
ARC383	2,97	1266 / 754
CCMP2100	2,90	1358 / 932
AA60	3,75	1384 / 992
ARC410	2,93	1398 / 886
ARC412	3,87	1426 / 1034
CCMP122	3,20	1446 / 928
AA60	2,92	1486 / 974
ARC411	4,35	1506 / 1082
ARC411	3,26	1608 / 1064

6 Summary and Outlook

The presented thesis successfully provided the missing knowledge about the toxin profiles of every received sample strain by using the selected reaction monitoring method in an UHPLC-MS/MS instrument. Out of the 69 strains from eleven *Amphidinium* species, a total of 32 strains from six different species produced at least one amphidinol. During the quantification of the identified amphidinols the amount of toxin contained in a single cell, called cell quote, was calculated, which was crucial since *Amphidinium* species not only show hemolytic, cytotoxic and ichthyotoxic activities (Mooney et al., 2010), but were reported to create harmful algal blooms that can have devastating impacts on public health, fisheries resources, and coastal commodities (Díaz et al., 2019). A linkage between the calculated cell quote in the amphidinols and the toxicity effects could be investigated in future bioassays.

The stated hypothesis concerning the possibility to discover previously unknown amphidinol variations in the introduction of this work proved to be correct. The analysis of the complete sample set undertaken by the neutral loss and full scan methods resulted in 79 masses possibly containing amphidinol variations, that subsequently were examined about similarities to known amphidinols by using an enhanced product ion scan (EPI). Out of the 79 recorded EPI scans, eleven substances were identified as possible new amphidinol variations based on their fragmentation spectrum. Finally, fragmentation pattern proposals were stated for every of the eleven unknown substances.

Future works should implement the discovered amphidinol variations into the existing SRM method, and additionally quantify the discovered variations about their toxin profile and cell quote since the proposed fragmentation patterns were the last step completed in this thesis. Otherwise, the procedure for the discovery of new amphidinol variations proved to work well and can therefore be applied to new sample strains in upcoming projects.

List of References

Anderson DM, Burkholder JM, Cochlan WP, Glibert PM, Gobler CJ. (2008): Harmful algal blooms and eutrophication: examining linkages from selected coastal regions of the United States. In: Harmful Algae 8, 39–53

Anderson, D. M., Cembella, A. D., and Hallegraeff, G. M. (2012): *Progress in understanding harmful algal blooms: paradigm shifts and new technologies for research, monitoring, and management*. In: Ann. Rev. Mar. Sci. **4**, 143–176. doi: 10.1146/annurev-marine-120308-081121

Anderson, D.M., Glibert, P.M., Burkholder, J.M. (2002): *Harmful algal blooms and eutrophication: nutrient sources, composition, and consequences.* In: Estuaries **25** (4b), 562–584

Bächer, Silvia (2014): Massenspektrometrische Methoden in der Laboratoriumsmedizin. Dissertation, LMU München: Medizinische Fakultät. 10.5282/edoc.17801

Baig, H. S., Saifullah, S. M. & Dar, A. (2006): *Occurrence and toxicity of Amphidinium carterae Hulburt in the North Arabian Sea.* In: Harmful Algae, **5**, 2: 133-140.

Chandarana, C., Manani, L., Patel, V. & Prajapati, P. (2016): UPLC: A Prominent Analytical Technique For Pharmaceuticals. In: International Journal of Pharmaceutical Sciences Review and Research. Article No. **34**, Pages: 192-201.

Claparede, E & Lachmann, J. (1859): Etudes sur les infusoires et les rhizopodes. In: Memoires de l'Institut National Genevois, **6**: 410.

Díaz, P. A., Alvarez, A., Varela, D., Perez-Santos, I., Díaz, M., Molinet, C., et al., (2019): *Impacts of harmful algal blooms on the aquaculture industry: Chile as a case study.* In: Perspect. Phycol. **6**, 39–50. Doi: 10.1127/pip/2019/0081

Dodge, J. D. 1982. Marine Dinoflagellates of the British Isles. Her Majesty's Stationary Office, London, 303 pp.

Echigoya, R.; Rhodes, L.; Oshima, Y.; Satake, M. The structures of five new antifungal and hemolytic amphidinol analogs from Amphidinium carterae collected in New Zealand. Harmful Algae 2005, 4, 383–389.

FAO (2016): *GLOBEFISH – Analysis and information on world fish trade.*

Fenn J. B., Mann M, Meng CK, Wong SF, Whitehouse CM. Electrospray ionization for mass spectrometry of large biomolecules. Science 1989; **246**:64-71.

Gross, J. H. (2019). Massenspektrometrie: Spektroskopiekurs kompakt (1. Auflage). https://doi.org/10.1007/978-3-662-58635-8

Hallegraeff, G. (2003): *Harmful algal bloom: a global overview.* In: Hallegraeff, G., Anderson, D.M. & Cembella, A.D. (eds.), Manual on Harmful Marine Microalgae. Monographs on Oceanographic Methodology. UNESCO Publishing., France, pp. 25–50.

Hallegraeff, G. (2010): *Ocean climate change, phytoplankton community responses, and harmful algal blooms: a formidable predictive challenge.* In: J. Phycol. **46**: 220–235.

Hallegraeff, G. M. (1993): *A review of harmful algal blooms and their apparent global increase*. In: Phycologia, **32**, 2.

Jørgensen, M. F., Murray, S. & Daugbjerg, N. (2004): Amphidinium Revisited. I. Re-denition of Amphidinium (Dinophyceae) Based on Cladistic and Molecular Phyloge-netic Analyses. In: Journal of Phycology, **40**, 2: 351-365.

Karafas, S., Teng, S. T., Leaw, C. P. & Alves-de Souza, C. (2017): *An evaluation of the genus Amphidinium (Dinophyceae) combining evidence from morphology, phyloge-netics, and toxin production, with the introduction of six novel species*. In: Harmful Algae, **68**: 128-151.

Kubota, T., Takahashi, A., Tsuda, M., Kobayashi, J., (2005): *Luteophanol D, new poly-hydroxyl metabolite from marine dinoflagellate Amphidinium sp.* In: Mar. Drugs **3**, 113–118.

Kubota, T., Tsuda, M., Doi, Y., Takahashi, A., Nakamichi, H., Ishibashi, M., Fukushi, E., Kawabata, J., Kobayashi, J., (1998): *Luteophanols B and C, new polyhydroxyl compounds from marine dinoflagellate Amphidinium sp*. Tetrahedron **54**, 14455–14464.

Mardones, J.I., Dorantes-Aranda, J.J., Nichols, P.D. & Hallegraeff, G.M. (2015): *Fish gill damage by the dinoflagellate Alexandrium catenella from Chilean fjords: Synergistic action of ROS and PUFA.* In: Harmful Algae **49**: 40–49.

Marshall, J., Nichols, P., Hamilton, B., Lewis, R. & Hallegraeff, G. (2003): *Ichthyotoxicity of Chattonella marina (Raphidophyceae) to damselfish (Acanthochromis polycanthus): the synergistic role of reactive oxygen species and free fatty acids.* In: Harmful Algae **2**: 273–281.

Molina-Miras, A., Morales-Amador, A., de Vera, C. R., López - Rosales, L., Sánchez-Mirón, A., Souto, M. L., Fernández, J. J., Norte, M., García - Camacho, F. & Molina-Grima, E. (2018): A pilot-scale bioprocess to produce amphidinols from the marine microalga Amphidinium carterae: Isolation of a novel analogue. In: Algal Research, **31**: 87-98.

Mooney, B. D., Hallegraeff, G. M. & Place, A. R. (2010): *Ichthyotoxicity of four species of gymnodinioid dinoflagellates (Kareniaceae, Dinophyta) and puried karlotoxins to larval sheepshead minnow.* In: Harmful Algae, **9**, 6: 557-562.

Mooney, B.D., De Salas, M.F., Hallegraeff, G.M., Place, A.R., (2009): *Survey for karlotoxin production in 15 species of gymnodinioid dinoflagellates (Kareniaceae Dinophyta).* J. Phycol. **45**, 164–175.

Mooney, B.D., Hallegraeff, G. M. & Place, A. R. (2010): Ichthyotoxicity of four species of gymnodinioid dinoflagellates (Kareniaceae, Dinophyta) and purified karlotoxins to larval sheepshead minnow. In: Harmful Algae, **9**, 6: 557-562.

Murray, S. & Patterson, D. J. (2002): The benthic dinoagellate genus Amphidinium in south-eastern Australian waters, including three new species. In: European Journal of Phycology, **37**, 2: 279-298.

Murray, S. A., Garby, T., Hoppenrath, M. & Neilan, B. A. (2012): *Genetic diversity, morphological uniformity and polyketide production in dinoflagellates (Amphidinium, Dinoflagellata).* In: PloS one, **7**, 6: e38253.

Murray, S. A., Kohli, G. S., Farrell, H., Spiers, Z. B., Place, A. R., Dorantes-Aranda, J. J. & Ruszczyk, J. (2015): *A fish kill associated with a bloom of Amphidinium carterae in a coastal lagoon in Sydney, Australia*. In: Harmful Algae, **49**: 19-28.

Murray, S., Flø Jørgensen, M., Daugbjerg, N. & Rhodes, L. (2004): *Amphidinium Revisited. II. Resolving Species Boundaries in the Amphidinium Operculatum Species Complex (Dinophyceae), Including Descriptions of Amphidinium Trulla Sp. Nov. and Amphidinium Gibossum. Comb. Nov.* In: Journal of Phycology, **40**, 2: 366-382.

Nuzzo, G., Cutignano, A., Sardo, A. & Fontana, A. (2014): Antifungal amphidinol 18 and its 7-sulfate derivative from the marine dinoflagellate Amphidinium carterae. In: Journal of natural products, **77**, 6: 1524-1527.

Paredes, J., Aguilera-Belmonte, A., Olivares, B., Uribe, C., Urrutia, G., Seguel, M., Villanueva, F., Vargas, M. & Varela, D. (2016): *Morphological variability and genetic identification of ichthyotoxic species Pseudochattonella sp. isolated from severe outbreak in 2016 at the Northern Patagonian Fjord, southern Chile*. – Conference Poster.

Pitt, J. J. (2009): Principles and Applications of Liquid Chromatography-Mass Spectrometry in Clinical Biochemistry, A Review article. In: Clin Biochem Rev., **20**(1): 19-34.

Raine R, McDermott G, Silke J, Lyons K, Nolan G, Cusack C. (2010): *A simple short-range model for the prediction of harmful algal events in the bays of southwestern Ireland.* In: J. Mar. Syst. **83**, 150–57

Reddy, B. H., Vardhani, Chowdary, C. A., Sahiti (2010): Ultra Performance Liquid Chromatography: A Review. In: DOAJ, Article

Rhodes, L. L., Smith, K. F., Munday, R., Selwood, A. I., McNabb, P. S., Holland, P. T. & Bottein, M.-Y. (2010): *Toxic dinoflagellates (Dinophyceae) from Rarotonga, Cook Islands.* In: Toxicon : official journal of the International Society on Toxinology, **56**, 5: 751-758.

Sargent, M (Ed)., Sage A., Wolff, C., Mussel, C., Neville D., Lord, G., Saeed, M., Lad, R., Godfrey, R., Hird, S., Barwick, V. (2013): Guide to achieving reliable quantitative LC-MS measurements, RSC Analytical Methods Committee. ISBN 978-0-948926-27-3.

Satake, M., Cornelio, K., Hanashima, S., Malabed, R., Murata, M., Matsumori, N., Zhang, H., Hayashi, F., Mori, S., Kim, J. S., Kim, C.-H. & Lee, J.-S. (2017): Structures of the Largest Amphidinol Homologues from the Dinoagellate Amphidinium carterae and Structure-Activity Relationships. In: Journal of natural products, **80**, 11: 2883-2888.

Satake, M., Cornelio, K., Hanashima, S., Malabed, R., Murata, M., Matsumori, N., Zhang, H., Hayashi, F., Mori, S., Kim, J. S., Kim, C.-H. & Lee, J.-S. (2017): *Structures of the Largest Amphidinol Homologues from the Dinoflagellate Amphidinium carterae and Structure-Activity Relationships.* In: Journal of natural products, **80**, 11: 2883-2888.

Satake, M., Murata, M., Yasumoto, T., Fujita, T. & Naoki, H. (1991): *Amphidinol, a polyhydroxy-polyene antifungal agent with an unprecedented structure, from a marine dinoflagellate, Amphidinium klebsii.* In: Journal of the American Chemical Society, **113**, 26: 9859-9861.

Van Deventer, M., Atwood, K., Vargo, G.A., Flewelling, L.J., Landsberg, J.H., Naar, J.P. & Stanek, D. (2012): *Karenia brevis red tides and brevetoxin-contaminated fish: a high risk factor for Florida's scavenging shorebirds?* In: Bot. Mar. **55**: 31–37.

Wellkamp, M. (2020): *LC-MS/MS basierte Analyse von Amphidinolen und weiteren marinen Phycotoxinen* Master thesis, University of Applied Sciences Bremerhaven.

Wellkamp, M., García-Camacho, F., Durán-Riveroll, L. M., Tebben, J., Tillmann, U.and Krock, B. (2020): *LC-MS/MS Method Development for the Discovery and Identification of Amphidinols Produced by Amphidinium.* In: Marine Drugs, **18**, p.497.

Zimmermann, L.A., (2006): *Environmental regulation of toxin production, comparison of hemolytic activity of Amphidinium carterae and Amphidinium klebsii*, 83University of North Carolina, Wilmington, pp. 55 (MSc thesis).

List of images

List of figures

List of tables

Appendix

Appendix A : Overview about present sample strains and mass spectrometry / chromatography parameters

Table 20: Overview of the examined *Amphidinium* strains from the Ensenada Center for Scientific Research and Higher Education (CICESE) based in Ensenada, Mexico.

Strain	Species	Cell count
AA60* Big chunks of cell impossible to break	*A. operculatum*	Not possible
AA40	*A. theodori*	13.511.111
AA39	*A. massartii*	9.995.556
AA38	*A. theodori*	5.933.333
AA181	New isolates from Baja California, not identified yet	14.000.000
AA177		8.200.000
AA172		11.380.000
AA165		5.840.000
AA139		4.575.000
AA113		2.832.000
AA112		5.150.000
AA111		11.200.000
AA60	*A. operculatum*	22.312.500

Table 21: Culture conditions, cell count and various collection sites of the examined *Amphidinium* strains from the algal culture collection of UNCW, cultivating strains from worldwide locations

Strain	Species	Collection date	Collection site	Culture media & salinity	Temperature [°C]	Cell count
ARC101	*carterae*	2004-06-22	Little San Salvador Is., Bahamas	L2 & 39	20	100.080.000

Strain	Species	Collection date	Collection site	Culture media & salinity	Temperature [°C]	Cell count
ARC100	*carterae*	2004-06-22	Little San Salvador Is., Bahamas	L2 & 39	20	101.080.000
CCMP1684	*carterae*	Unknown	Unknown	L1 & 33	20	100.552.500
CCMP122	*carterae*	1980-06-01	Unknown	L1 & 36	20	100.273.750
CCMP2199	*carterae*	2002-05-09	Aqua Hediona Lagoon, Carlsbad, California	L1 & 36	20	100.732.500
CCMP119	*carterae*	1986-08-20	Knight Key, Florida, USA	L1 & 36	20	100.125.000
CCMP1748	*carterae*	1997-02-04	main Lagoon, Carrie Bow Key, Belize	L1 & 36	20	100.108.750
CCMP2980	*carterae*	2009-01-07	Marquesas Keys, Florida, USA	L1 & 36	20	100.555.000
ARC195	*carterae*	2008-12-10	La Parguera, PR	L1 & 36	20	105.600.000
CCMP2100	*carterae*	2001-10-22	Eilat, Israel	L1 & 36	20	127.875.000
ARC383	*carterae*	2014-12-15	Bahia Cofresi, Dominican Republic	L1 & 39	20	108.750.000

Strain	Species	Collection date	Collection site	Culture media & salinity	Temperature [°C]	Cell count
ARC98	*carterae*	2004-06-22	Little San Salvador Is., Bahamas	L2 & 39	20	100.406.250
ARC99	*carterae*	2004-06-22	Little San Salvador Is., Bahamas	L2 & 39	20	122.125.000
ARC410	*carterae*	2015-06-04	Korotoga, Fiji	L1 & 39	25	102.400.000
ARC411	*carterae*	2015-06-04	Korotoga, Fiji	L1 & 39	25	104.125.000
ARC412	*carterae*	2015-06-04	Korotoga, Fiji	L1 & 36	25	102.000.000
ARC413	*carterae*	2015-06-04	Korotoga Fiji	L1 & 36	25	120.750.000
ARC148	*carterae*	Unknown	Sargassum offshore NC	L1 & 36	20	103.035.648
CCMP2400	*carterae*	2004-05-21	New Pass Channel, Florida	L1 & 36	20	100.049.658
ARC102	*carterae*	2004-06-22	Little San Salvador Is., Bahamas	L2 & 39	20	104.250.000
ARC90	*tomasii*	2003-04-03	Coast of Florida	L1 & 36	20	130.875.000
ARC389	*tomasii*	2014-12-15	Bahia Cofresi,	L1 & 39	20	100.406.250

Strain	Species	Collection date	Collection site	Culture media & salinity	Temperature [°C]	Cell count
			Dominican Republic			
ARC197	*tomasii*	2008-12-10	Bahia Phosphorescent Bay, PR	L1 & 36	25	30.140.625
ARC387	*tomasii*	2014-12-15	Bahia Cofresi, Dominican Republic	L1 & 39	20	42.978.750
ARC388	*tomasii*	2014-12-15	Bahia Cofresi, Dominican Republic	L1 & 39	20	15.236.250
F11	*tomasii*	Unknown	Unknown	Unknown	Unknown	15.826.150
CCMP1741	*massartii*	1996-11-01	Elbow Cay, Belize	L1 & 36	20	101.251.850
CCMP2774	*massartii*	2006-12-19	Marquesas Keys, Florida	L1 & 36	20	112.022.100
CCMP1821	*massartii*	1997-12-30	Succotash Marsh, South Kingstown, RI	L1 & 36	20	109.812.500
CCMP1684	*massartii*	1900-01-01	N/A	N/A	N/A	100.552.500
ARC149	*massartii*	2006-07-01	Offshore N.C., Gulf Stream	L2 & 39	20	107.175.000

Strain	Species	Collection date	Collection site	Culture media & salinity	Temperature [°C]	Cell count
ARC342	*massartii*	2012-08-01	Palmyra atoll	L2 & 39	20	105.525.000
CCMP1342	*massartii*	1991-04-01	Knight Key, Florida	L1 & 36	20	101.397.000
CCMP2813	*massartii*	1900-01-01	Florida Keys National Marine Sanctuary, Marquesas Keys, Fl, USA	L1 & 36	20	108.062.500
ARC414	*massartii*	2015-06-04	Korotoga, Fiji	L1 & 39	25	138.937.500
ARC115	*fijiensis*	2005-06-25	Korotoga, Fiji	L2 or K39	20	98.971.875
ARC79	*fijiensis*	2005-06-25	Korotoga, Fiji	L2 or K39	20	104.182.500
ARC103	*gibbossum*	Unknown	Little San Salvador Is., Bahamas	L2 & 39	20	Unknown
ARC104	*gibbossum*	2004-06-22	Little San Salvador Is., Bahamas	L2 & 39	20	100.845.000
ARC105	*gibbossum*	2004-06-22	Little San Salvador Is., Bahamas	F/2 & 36	20	102.300.000

Strain	Species	Collection date	Collection site	Culture media & salinity	Temperature [°C]	Cell count
ARC106	*gibbossum*	2004-06-22	Little San Salvador Is., Bahamas	L2 & 39	20	97.146.250
ARC116	*gibbossum*	2005-08-01	La Parguera, PR	L2 & 39	20	85.606.400
CCMP2973	*gibbossum*	2008-01-25	south of Brewers Bay Beach, St. Thomas, U. S. Virgin Islands	L2 & 39	20	101.378.798
ARC68	*magnum*	2002-06-01	Grand Bahama Beach	K & 39	20	14.187.300
ARC73	*magnum*	2002-06-01	Grand Bahama Beach	L2 & 39	20	26.200.000
ARC69	*magnum*	2002-06-01	Grand Bahama Beach	L2 & 39	20	34.128.000
ARC70	*magnum*	2002-06-01	Grand Bahamas Beach	K & 39	20	21.853.675
ARC71	*magnum*	2002-06-01	Grand Bahama Beach	K & 39	20	16.863.948
ARC72	*magnum*	2002-06-01	Grand Bahamas Beach	K & 39	20	16.406.680

Strain	Species	Collection date	Collection site	Culture media & salinity	Temperature [°C]	Cell count
ARC150	*paucianulatum*	2006-06-08	Palma Sola Causeway; Clearwater, FL	K & 39	20	11.740.000
ARC117	*paucianulatum*	2005-07-25	Korotoga, Fiji	K & 39	20	19.456.684
ARC151	*paucianulatum*	2006-08-06	Palma Sola Causeway; Clearwater, FL	K & 39	20	32.940.000
ARC173	*theodori*	2007-02-01	Korotoga, Fiji	K & 39	20	35.905.500
ARC89	*thermaeum*	2003-03-31	Siesta Key, FL	K & 39	20	12.565.176
ARC386	*thermaeum*	2014-12-01	Bahia Cofresi, Dominican Republic	L1 & 39	20	106.636.625
ARC385	*thermaeum*	2014-12-01	Bahia Cofresi, Dominican Republic	L1 & 39	20	106.987.500

Table 22: Mass spectrometry parameters for the measurement of amphidinols

Ion source	
Capillary voltage [kV]	3.00
Cone voltage [V]	40
Desolvation temperature [°C]	600
Gas flow	
Desolvation gas flow [l/h]	1000
Cone gas flow [l/h]	150
Nebuliser gas flow [bar]	7.0
Further settings	
Autosampler-temperature [°C]	10
Column temperature [°C]	40

Table 23: Chromatography parameters for the measurement of amphidinols

Eluent composition	Eluent A: 500 ml ultrapure water (Merck) mixed with 252.5 µl NH4OH (25%) Eluent B: 450 ml acetonitrile, 50ml ultrapure water (Merck) mixed with 252.5 µl NH4OH (25%)
Eluent gradient	80% Eluent A to 20% Eluent B
Total duration [min]	5
Flow rate [ml/min]	0.2
Injection volume [µ]	0.500

Collision energy [eV]	75 85 for amphidinols over 1500 *m/z* during product ion scans
Scanning time [sec]	0.133
Scanning rate [points per peak]	12

Appendix B : Quantification of detected amphidinols

Table 24: Quantification of detected amphidinols from the species *A. operculatum* and unidentified new isolates, originating from Mexico, stated in fg/cell

Name	t_R [min]	AA60 *A. operculatum*	AA39 *A. massartii*	AA181 New Isolates	AA177 New Isolates	AA172 New Isolates	AA165 New Isolates	AA111 New Isolates
AM – 2	3,78	4		632	231	200	22	21
AM – 4	3,87			2	547	441		
AM – 5	4,07			1	406	317		
AM – 6	3,18	22						
AM – 7	3,3			250	79	45		
AM – 9	4,10			796	19	1		
AM – 11	3,43			5	5	2		
AM – 14	2,61	2		2	10			
AM – 15			1					
AM – 17	4,17			2			5	2
N7	4,20			2				
N8/N9	4,17			2				
N12	3,88				15	14		
N13	3,52				2	1		

Table 25: Quantification of detected amphidinols from the species *A. tomasii, A. gibbosum, A. massartii,* originating from the algal culture collection of UNCW, cultivating strains from worldwide locations, stated in fg/cell

Name	t_R [min]	ARC90 *A. tomasii*	ARC197 *A. tomasii*	ARC388 *A. tomasii*	ARC104 *A. gibbosum*	CCMP1741 *A. massartii*
AM – 2	3,78	7				
AM – 4	3,87	1				
AM – 7	3,3			45		
AM – 11	3,43	1				
AM – 17	4,17	2				
AM – 20 (S)	3,60		4			
AM – 20 (M)						5
LP – B / LP – C	2,82					16
LP – D	2,81	1			2	22
LS – A						543
LS – B / SP						612
N1						34
N12	3,88	61				
N13	3,52	9				
N14 – N16	4,48	1				

Table 26: Quantification of detected amphidinols from the species *A. massartii*, originating from the algal culture collection of UNCW, cultivating strains from worldwide locations, stated in fg/cell

Name	t_R [min]	CCMP2774 *A. massartii*	CCMP2813 *A. massartii*	CCMP1342 *A. massartii*	ARC149 *A. massartii*	ARC414 *A. massartii*
KAR – A	3,17				52	
KAR – B	3,96				4	
LP – D	2,81					5
LS – B / SP	2,97			20		
N8 – N11	4,04	3	9			

N14 – N16	2,96					3

Table 27: Quantification of detected amphidinols from the species *A. carterae*, originating from the algal culture collection of UNCW, cultivating strains from worldwide locations cations, stated in fg/cell

Name	t_R [min]	ARC101 *A. carterae*	ARC100 *A. carterae*	CCMP122 *A. carterae*	CCMP2199 *A. carterae*	CCMP119 *A. carterae*
AM – 2	3,98	1	8			
AM – 4	3,83		1			
AM – 6	3,95		0			
AM – 11	3,10		1			
AM – 17	3,06		16			
AM – 18	4,07			33		
AM – 19	3			3		
AM – 20 (M)	4,23			1		
AM – 22	3,81			30		
AM – A	4,17			35	0	
AM – B	3,32			3		
LP – D	2,81					0,25
LS	4,40			1		
N5 / N6	4,47			6		
N7	4,56			12		
N8 – N11	4,37			65		
N12	3,76	2	16	5		
N13	4,70	0	2	28		
N14 – 16	4,48			139		

Table 28: Quantification of detected amphidinols from the species *A. carterae*, originating from the algal culture collection of UNCW, cultivating strains from worldwide locations, stated in fg/cell

Name	t_R [min]	ARC195 *A. carterae*	CCMP2100 *A. carterae*	ARC383 *A. carterae*	ARC98 *A. carterae*	ARC99 *A. carterae*
AM – 2	3,98		24		16	21
AM – 4	3,83	1	217	2	3	5
AM – 5	3,93		1			
AM – 7	2,98		33			
AM – 9	4,31		1062	1	1	

Name	t_R [min]	ARC195 *A. carterae*	CCMP2100 *A. carterae*	ARC383 *A. carterae*	ARC98 *A. carterae*	ARC99 *A. carterae*
AM – 11	3,10		7		1	2
AM – 14	2,97		52			
AM – 17	2,97				1	
AM – 20 (M)	2,93	3		39		
LP – A	2,97	1		2		
LP – B / LP – C	3,16	17		133		
LP – D	2,81	37		250	2	3
LS – A	3,75	953		1937	1	
LS – B / SP	2,97	1513		1680		
N1	2,97	89		90		
N3	3,65			2		
N8 – N11	4,04		1			
N12	3,76		7		146	235
N13	3,78		1		20	33
N14 – N16	2,96				1	2

Table 29: Quantification of detected amphidinols from the species A. carterae, originating from the algal culture collection of UNCW, cultivating strains from worldwide locations, stated in fg/cell

Name	t_R [min]	ARC410 *A. carterae*	ARC411 *A. carterae*	ARC412 *A. carterae*	ARC413 *A. carterae*	CCMP2400 *A. carterae*
AM – 4	3,83	17			5	
AM – 9	4,31					2
AM – 12	3,87		5	5		
AM – 20 (M)	2,93	13			19	
CAR – E	4,39	2	4	2		
LP – A	2,97	1				
LP – B / LP – C	3,16	69			112	
LP – D	2,81	233			165	
LS – A	3,75	2696	4	2	1939	
LS – B / SP	2,97				1166	

N1	2,97				62	
N3	3,65	1				
N12	3,76	1				

Appendix C : Overview of measured EPI scans and description of measurement procedures

Table 30: Overview about strains and Q1-Masses detected in the neutral loss, full scan measurement mode and Q1-Masses of known amphidinols, which were measured using enhanced product ion scans to discover and identify possible amphidinol variations

Strain name	t_R [min]	Q1-Mass (*m/z*)
ARC173	4,22	1016
ARC412	3,73	1017
CCMP2199	4,40	1022
AA113	4,16	1028
ARC388	3,39	1032
ARC173	3,19	1033
AA113	4,16	1044
CCMP2774	2,89	1046
ARC101	4,15	1061
ARC411	3,06	1068
AA139	3,73	1074
CCMP2813	2,88	1090
ARC197	2,76	1092
ARC117	3,32	1105
ARC150	3,30	1106
AA113	3,75	1114
ARC151	2,57	1115
ARC411	2,74	1119
ARC150	3,10	1126
ARC89	3,27	1127
AA113	3,78	1135
AA111	2,93	1138
AA111	3,90	1140
CCMP2774	3,33	1152
CCMP1784	3,77	1180
1BF	2,89	1214
ARC101	3,89	1226
CCMP2973	4,12	1230
AA38	2,03	1238

Strain name	t_R [min]	Q1-Mass (*m/z*)
AA165	2,92	1242
AA165	2,93	1243
AA177	3,3	1254
AA111	3,80	1264
ARC383	2,97	1266
ARC101	3,40	1272
ARC383	3,21	1281
AA165	4,04	1290
ARC410	3,84	1296
AA39	2,90	1297
ARC115	2,88	1304
AA172	3,79	1305
ARC195	3,77	1322
CCMP2100	3,87	1324
ARC101	2,94	1328
CCMP1784	3,09	1329
ARC383	2,81	1330
ARC195	3,59	1332
AA60 (50 mL)	3,03	1334
ARC71	3,63	1336
ARC383	2,82	1344
CCMP2100	4,10	1350
CCMP2100	2,90	1358
CCMP2100	2,95	1360
CCMP122	4,17	1362
AA60	3,18	1368
ARC410	3,53	1378
CCMP122	4,07	1382
AA60	3,75	1384
CCMP2774	3,48	1386
AA165	3,90	1392
AA177	4,07	1394
AA165	3,90	1396
ARC410	2,93	1398
AA181	3,78	1398
CARM	4,58	1411
AA60	2,92	1418
CCMP1821	3,81	1420
ARC411	4,39	1422
ARC412	3,87	1426
CCMP122	3,20	1446

Strain name	t_R [min]	Q1-Mass (*m/z*)
ARC72	3,36	1459
CCMP122	3,11	1464
ARC149	3,99	1478
CCMP122	3,14	1484
CCMP2400	4,08	1484
AA60	2,92	1486
CCMP1821	3,84	1492
ARC411	4,35	1506
CCMP2400	3,14	1514
ARC411	3,26	1608
CCMP1342	2,90	1626
ARC411	3,39	1627
ARC388	3,75	1650
CCMP122	3,81	1668
ARC99	3,79	1725
ARC387	3,66	1730
AA172	3,77	1765

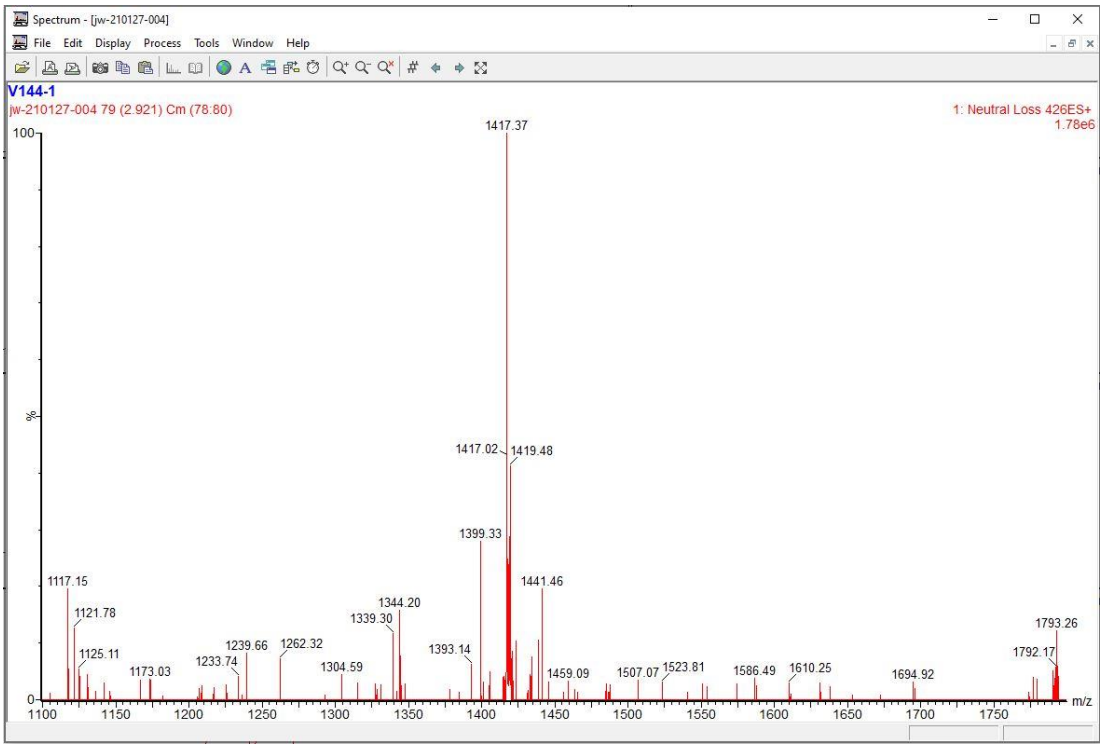

Figure 28: Corresponding spectrum of the neutral loss 426Da in strain AA60

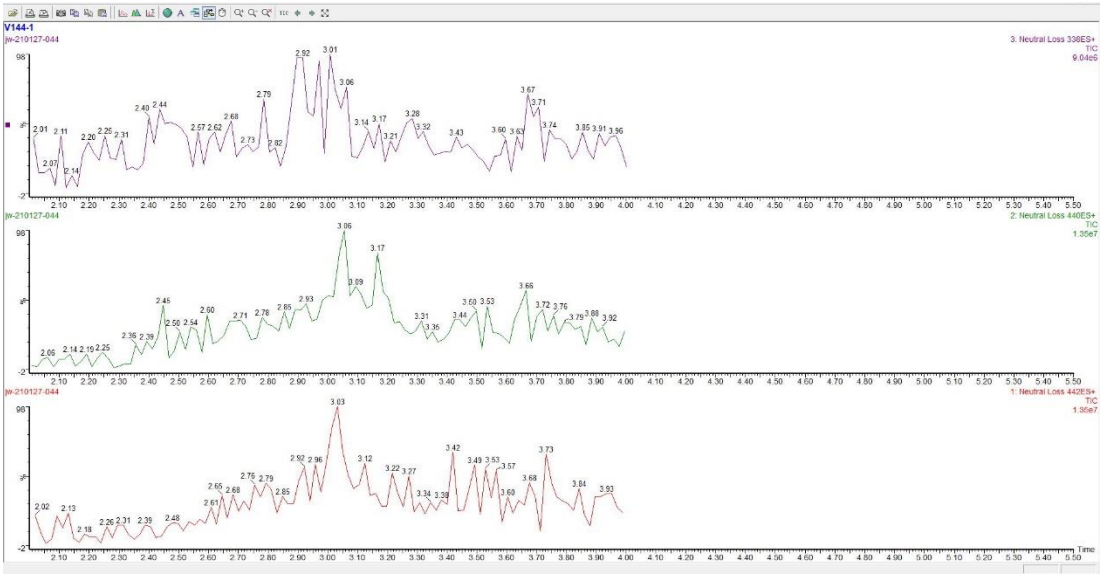

Figure 29: Overview about the chromatograms created by the three neutral losses (338Da, 440Da, 442Da) in strain AA60

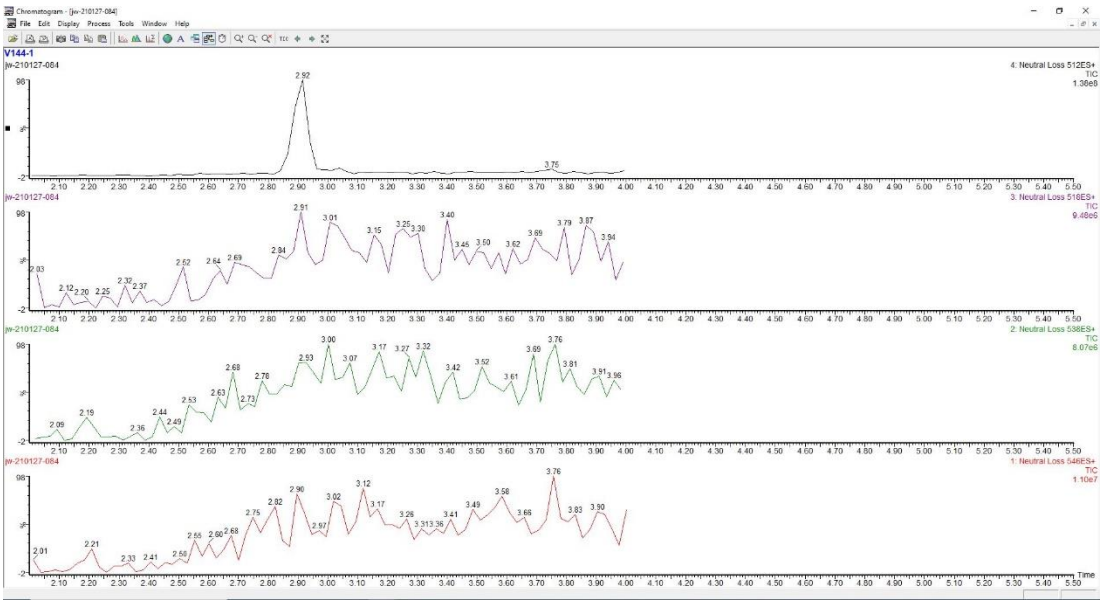

Figure 30: Overview about the chromatograms created by the four sulfated neutral losses (512Da, 518Da, 538Da and 546Da) in strain AA60

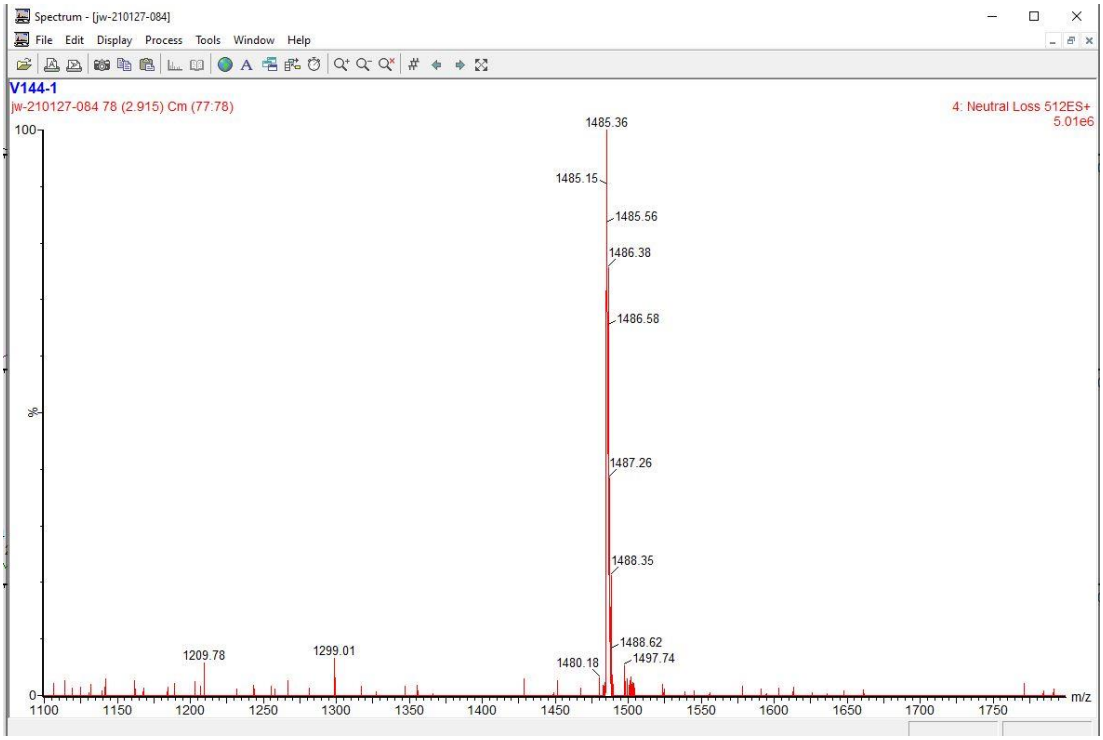

Figure 31: Corresponding spectrum of the neutral loss 512Da in strain AA60

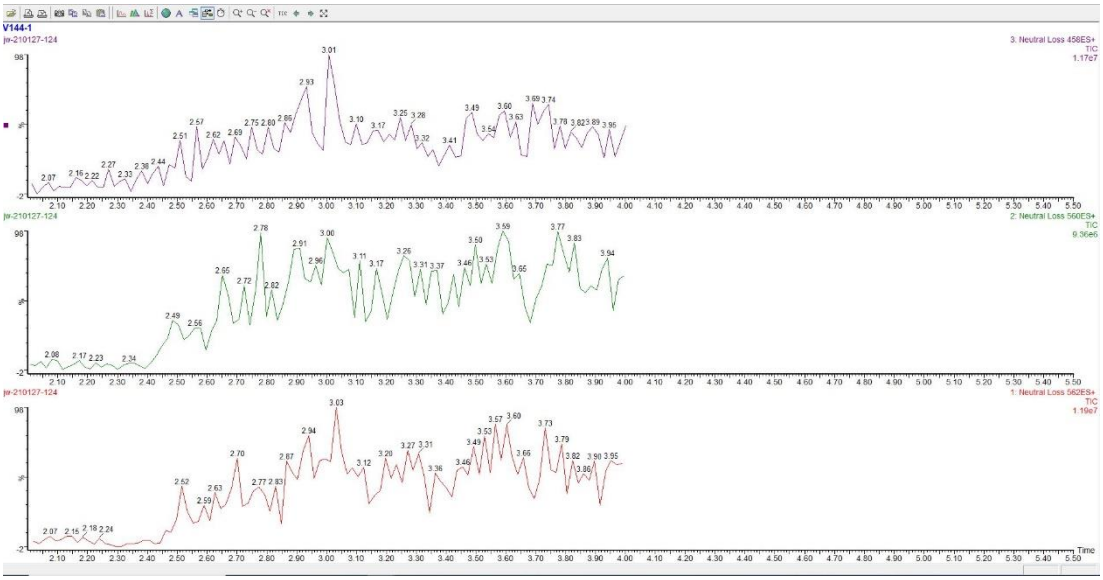

Figure 32: Overview about the chromatograms created by the three sulfated neutral losses (458Da, 560Da, 562Da) in strain AA60

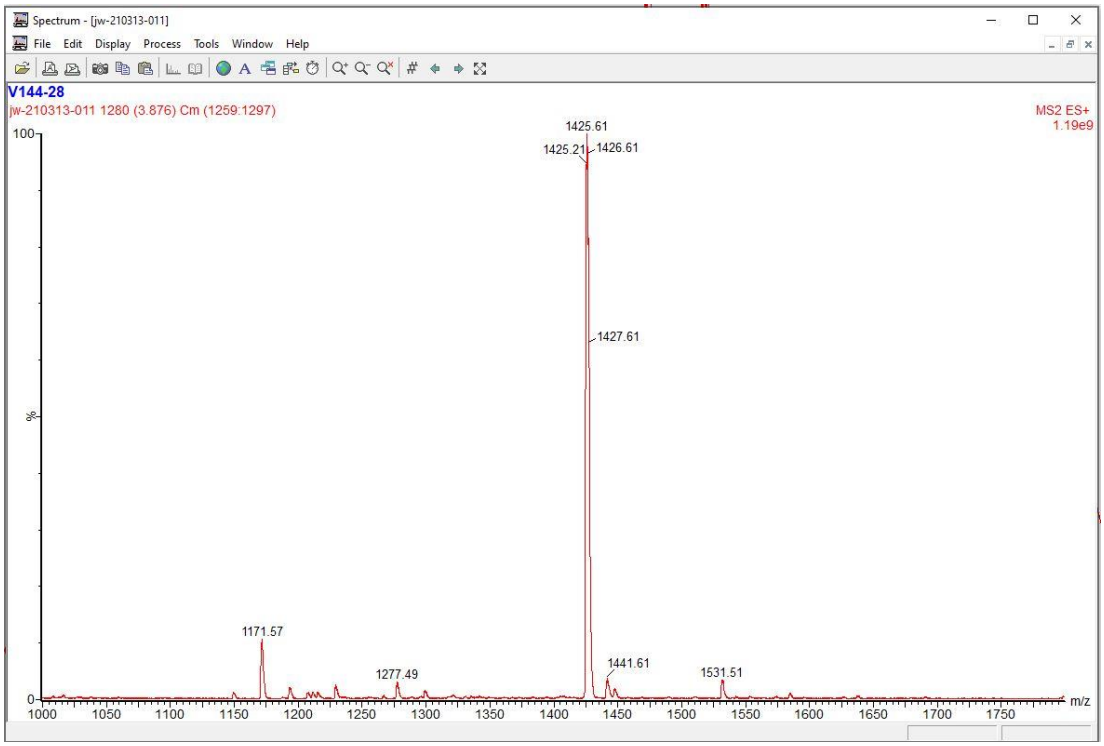

Figure 33: Corresponding spectrum of the peak occurring after 3,88 min in the full scan measurement of strain ARC411

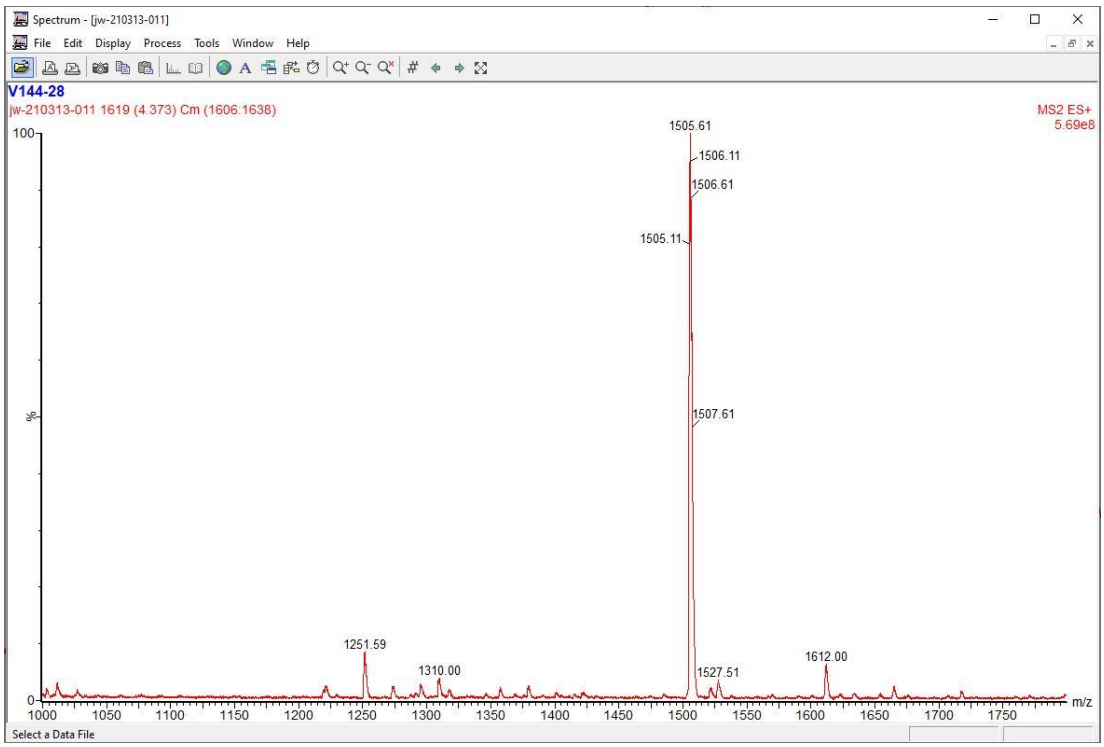

Figure 34: Corresponding spectrum of the peak occurring after 4,37 min in the full scan measurement of strain ARC411

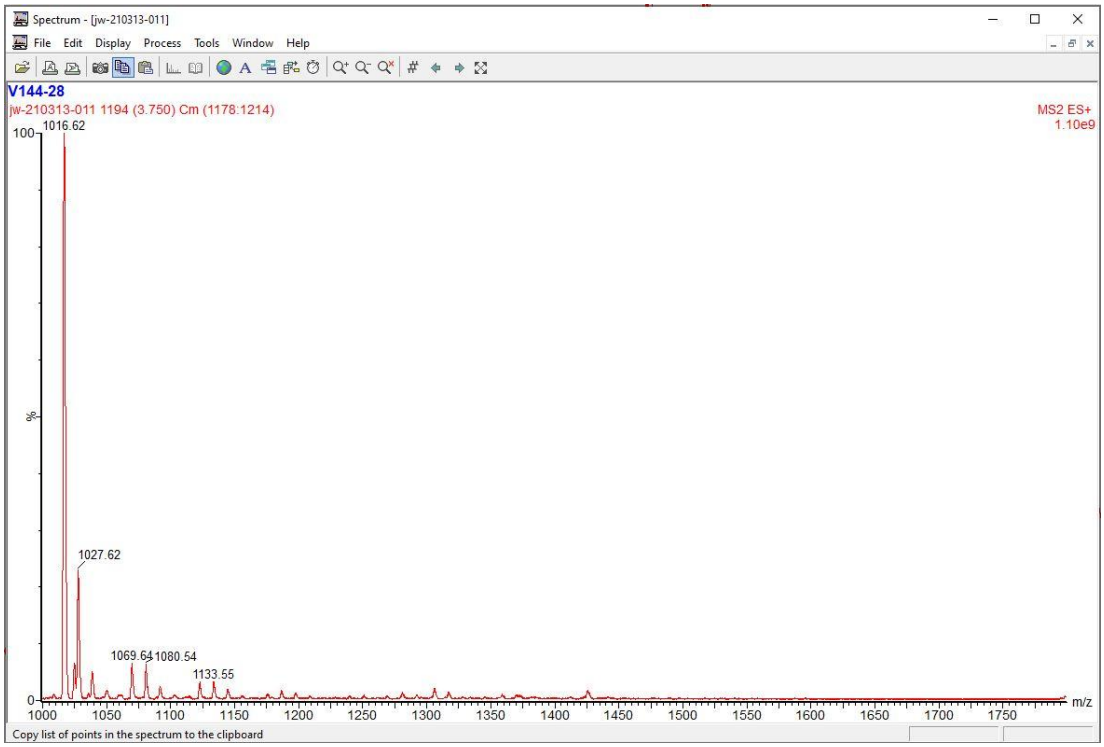

Figure 35: Corresponding spectrum of the peak occurring after 3,75 min in the full scan measurement of strain ARC411

Appendix D : Confirmation of detected amphidinols in the SRM measurement through enhanced product ion spectra

Table 31: Confirmation status of every detected amphidinol in the SRM measurement

Strain possessing highest abundancy	Amphidinol name and transition	t_R [min] SRM	t_R [min] EPI	Confirmation status
AA181	AM07 – 1254/742	3,3	3,04	Unclear
ARC383	LSP/SP – 1266/754	2,97	3,03	Not confirmed
CCMP2100	AM14 – 1288/742	2,61	No peak	Not confirmed

Strain possessing highest abundancy	Amphidinol name and transition	t_R [min] SRM	t_R [min] EPI	Confirmation status
ARC410	LSA – 1296/904	3,84	3,82	Confirmed
ARC100	AM17 – 1306/816	4,17	No Peak	Not confirmed
CCMP2100	AM04 – 1324/932	3,87	3,81	Confirmed
ARC383	LPD – 1330/904	2,81	2,81	Confirmed
ARC383	LPB/LPC – 1344/904	3,16	3,17	Confirmed
ARC383	AM20(M) – 1346/904	2,79	No peak	Not confirmed
CCMP2100	AM09 – 1350/932	4,10	4,03	Confirmed
CCMP122	AMA – 1362/964	4,17	4,19	Confirmed
AA60	AM06 – 1368/976	3,18	No Peak	Not confirmed
CCMP122	AM18 – 1382/964	4,07	4,07	Confirmed
AA177	AM05 – 1394/976	4,07	4,00	Confirmed
AA181	AM02 – 1398/1006	3,78	4,00	Confirmed

Strain possessing highest abundancy	Amphidinol name and transition	t_R [min] SRM	t_R [min] EPI	Confirmation status
ARC411	CarE – 1422/1030	4,39	4,42	Unclear
ARC412	AM12 – 1426/914	3,87	3,91	Not confirmed
ARC149	KarB – 1462/1064	3,96	4,00	Not confirmed
CCMP122	AMB – 1464/946	3,11	3,15	Confirmed
ARC149	KarA – 1480/1082	3,17	3,65	Not confirmed
CCMP122	AM19 – 1484/946	3,14	No peak	Not confirmed
CCMP2100	AM11 – 1500/988	3,43	3,22	Unclear
ARC197	AM20S – 1653/1260	3,60	3,83	Not confirmed
CCMP122	AM22 – 1668/1330	3,81	3,81	Confirmed

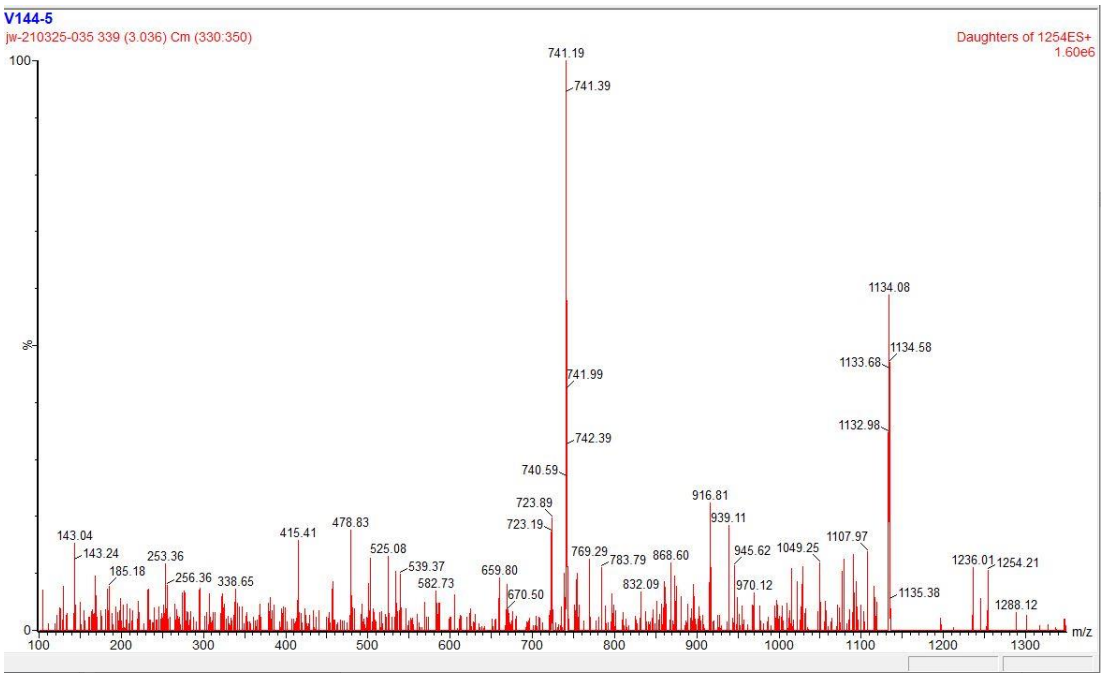

Figure 36: Enhanced product ion spectrum of 1254Da of the strain AA181, which could not confirm the substance at t_R=3,04 min as amphidinol 07 clearly

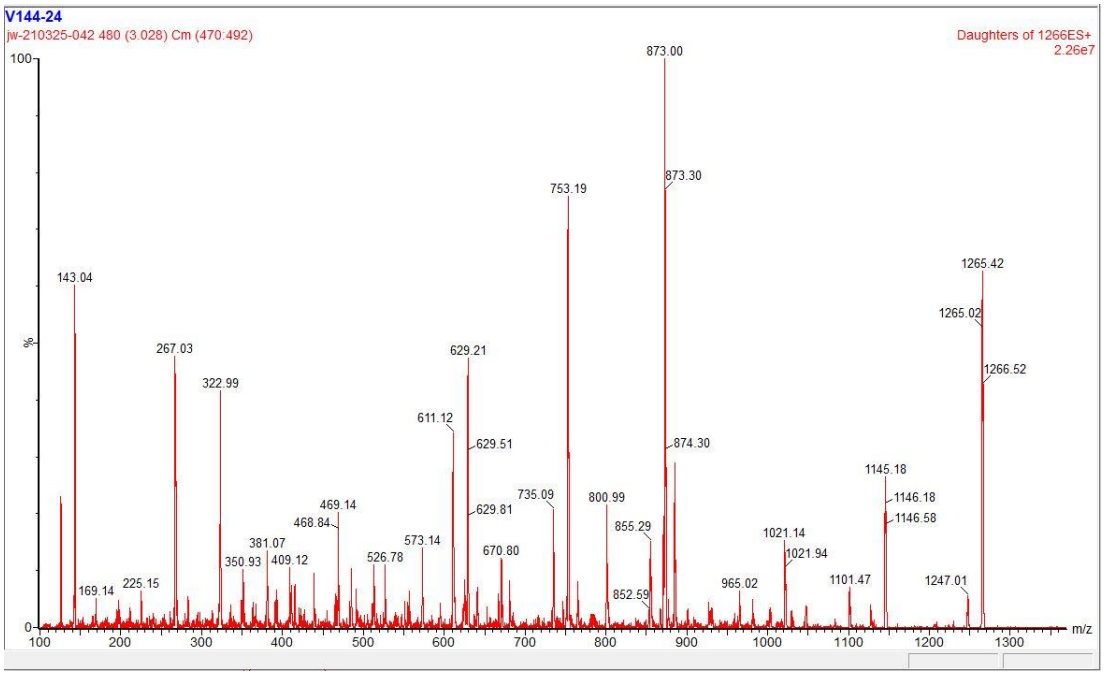

Figure 37: Enhanced product ion spectrum of 1266Da of the strain ARC383, which did not confirm the substance at t_R=3,03 min as LSB/SP

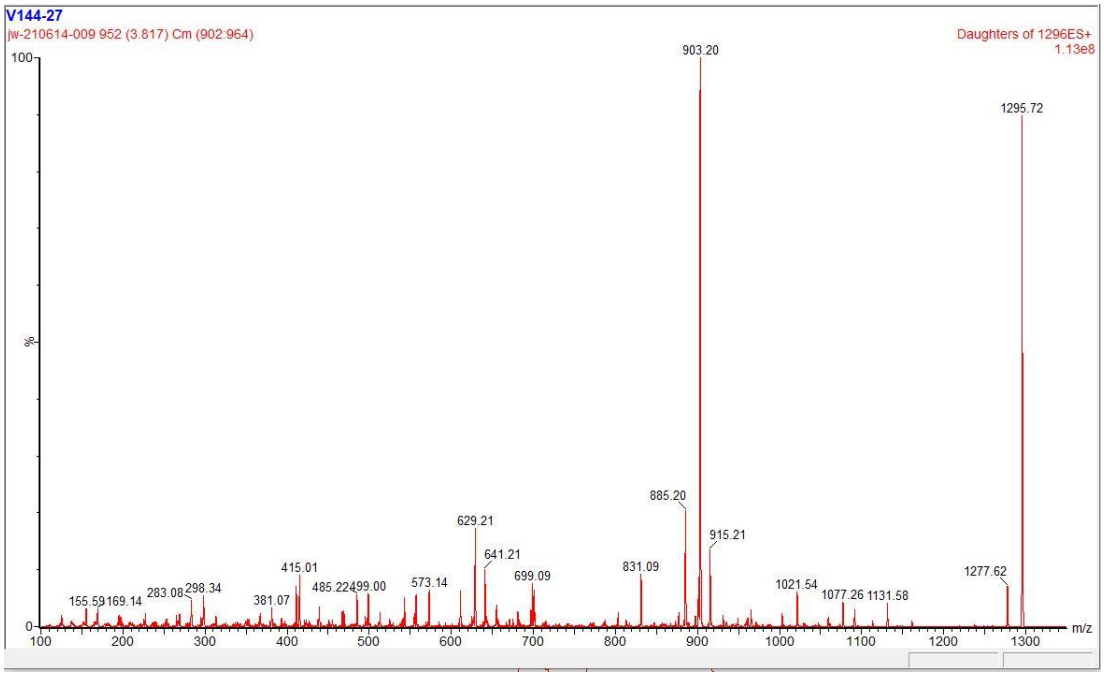

Figure 38: Enhanced product ion spectrum of 1296Da of the strain ARC410, which confirmed the substance at t_R=3,82 min as LSA

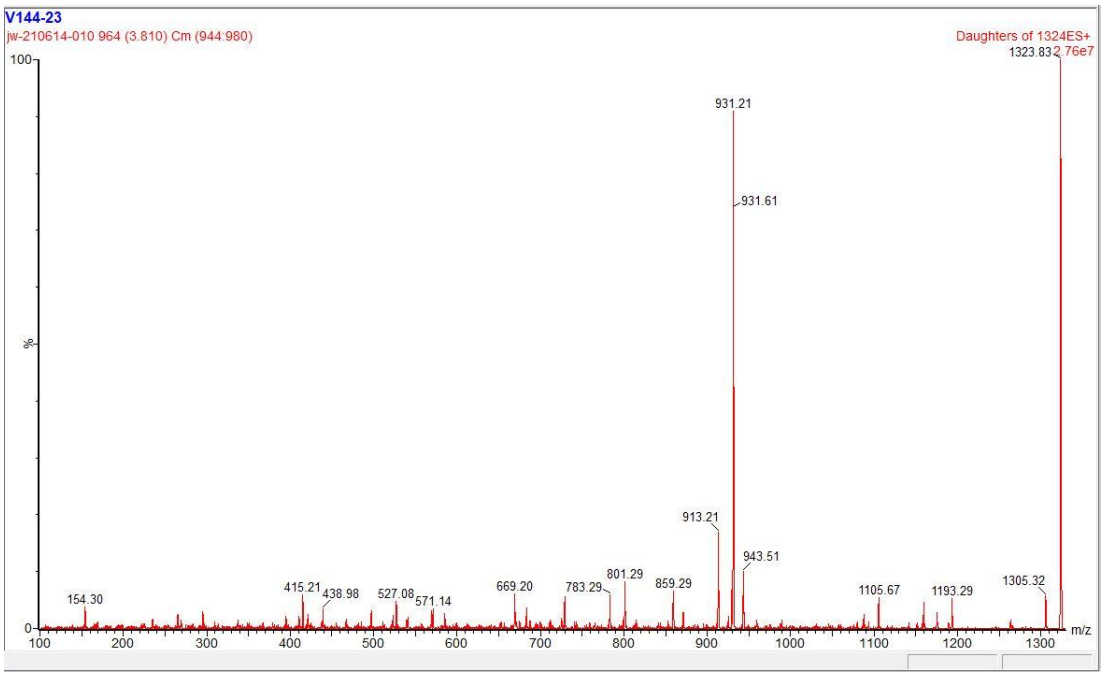

Figure 39: Enhanced product ion spectrum of 1324Da of the strain CCMP2100, which confirmed the substance at t_R=3,81 min as amphidinol 04

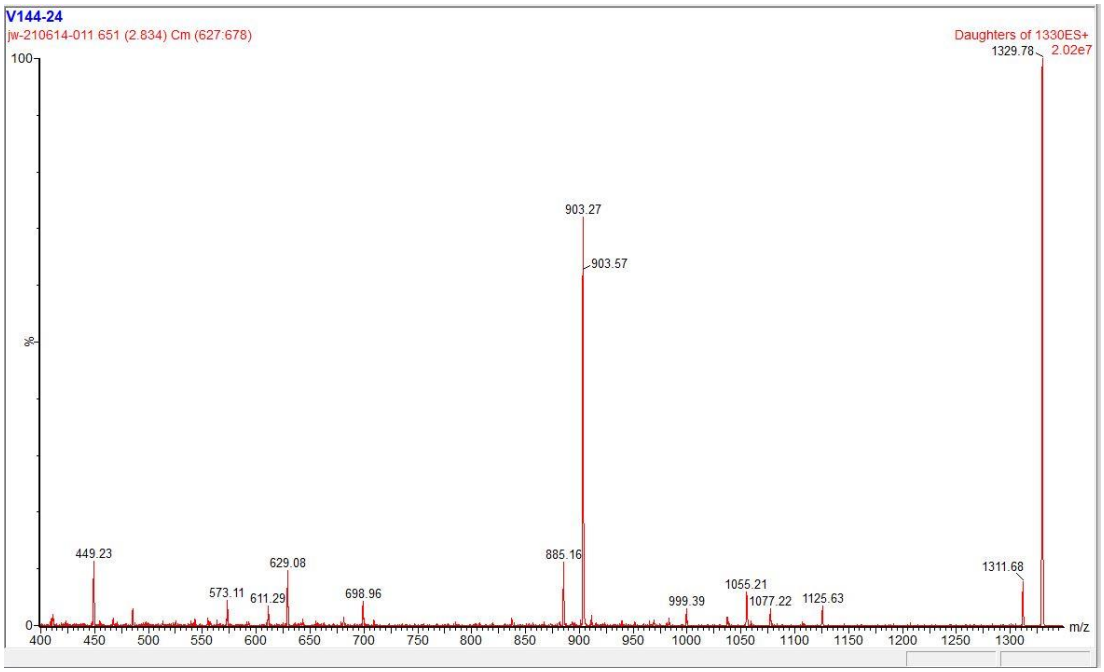

Figure 40: Enhanced product ion spectrum of 1330Da of the strain ARC383, which confirmed the substance at t_R=2,81 min as LPD

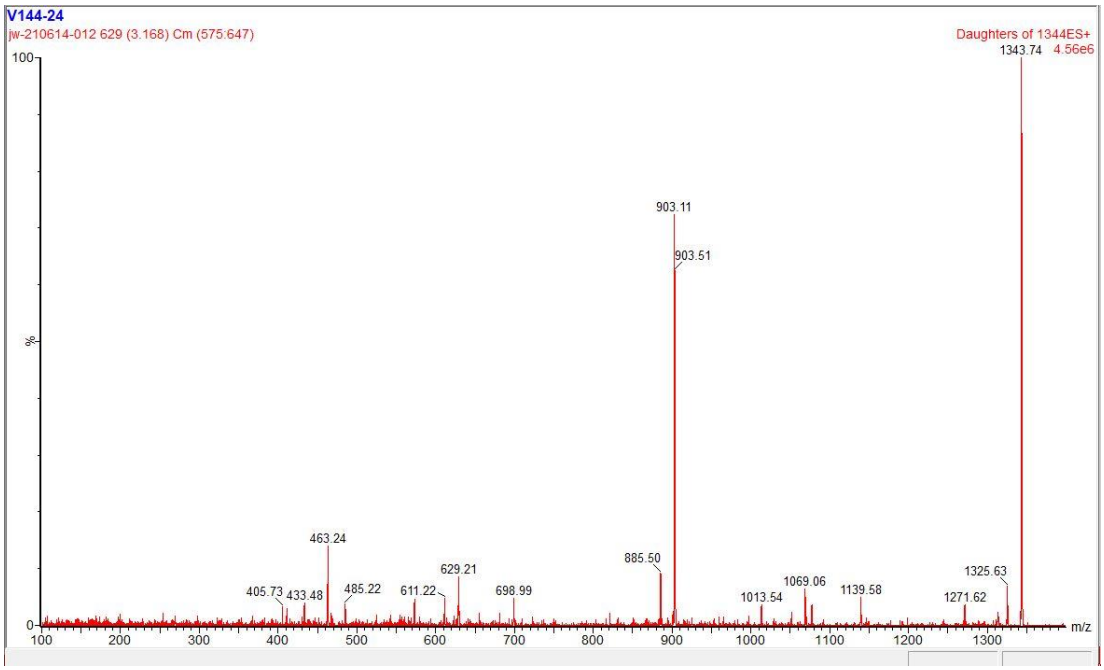

Figure 41: Enhanced product ion spectrum of 1344Da of the strain ARC383, which confirmed the substance at t_R=3,17 min as LPB/LPC

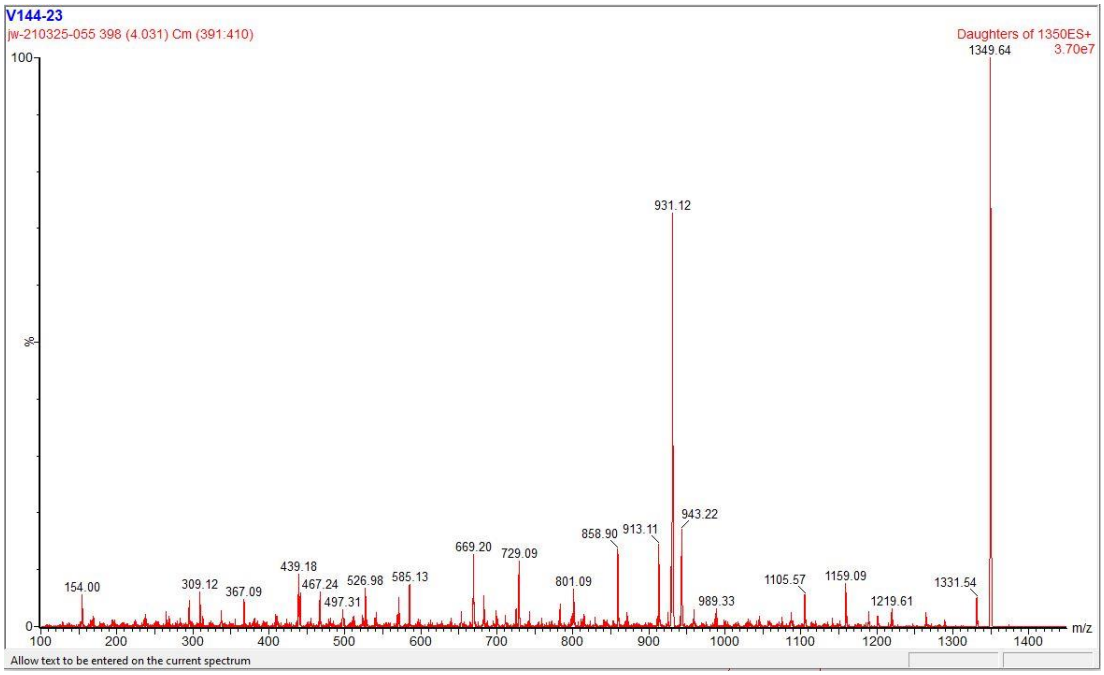

Figure 42: Enhanced product ion spectrum of 1350Da of the strain CCMP2100, which confirmed the substance at t_R=4,03 min as AM09

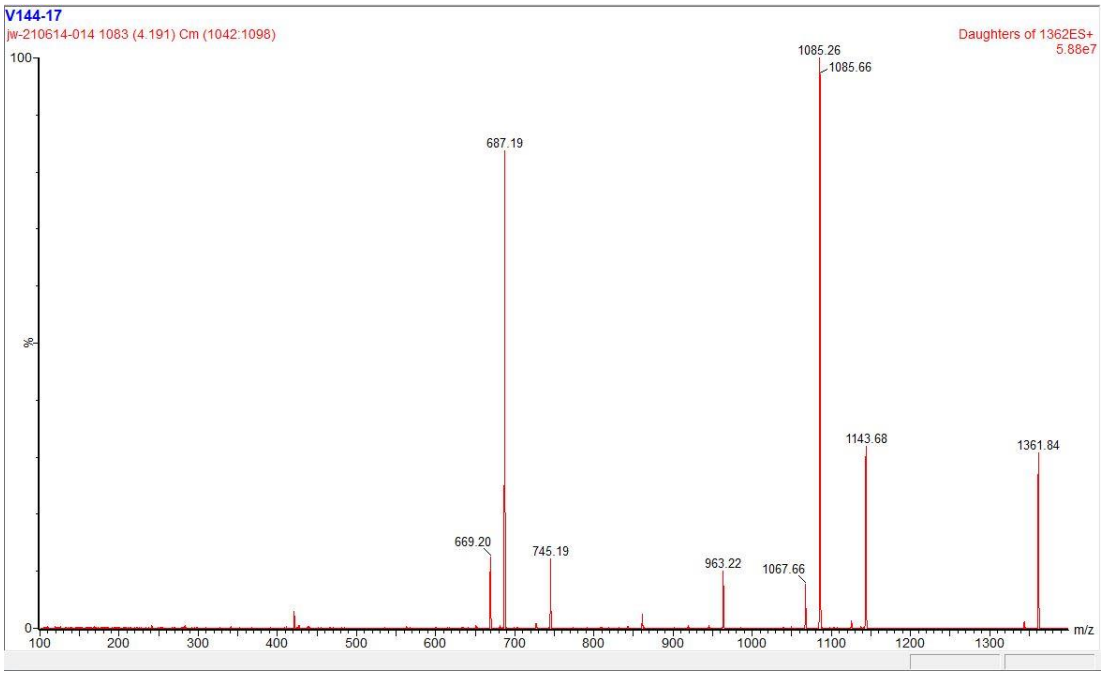

Figure 43: Enhanced product ion spectrum of 1362Da of the strain CCMP122, which confirmed the substance at t_R=4,19 min as AMA

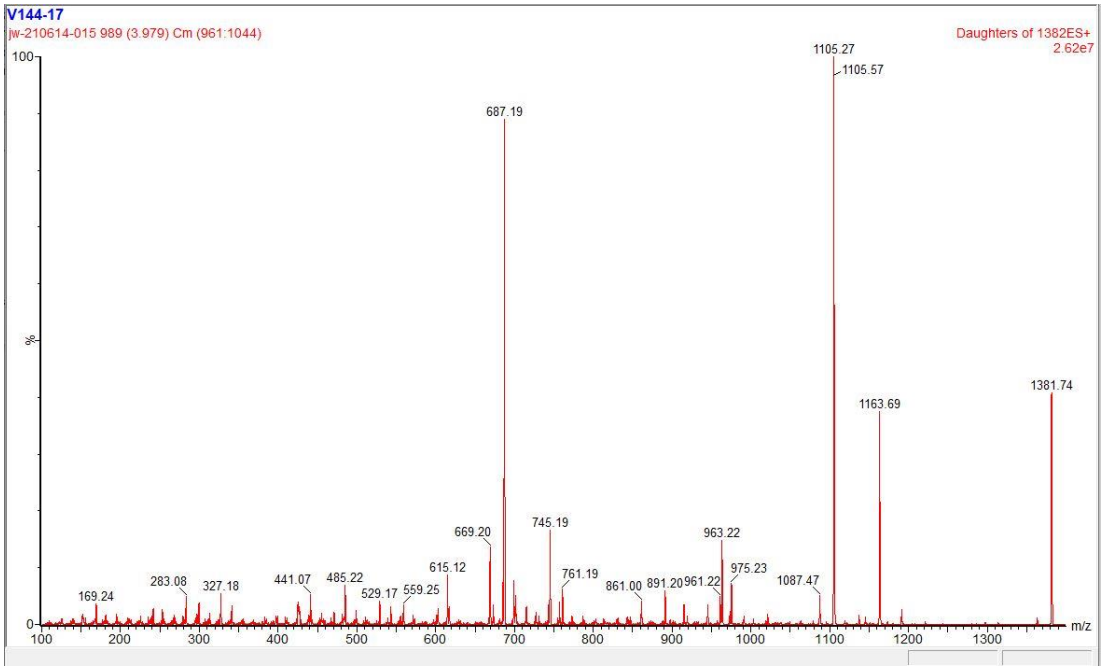

Figure 44: Enhanced product ion spectrum of 1382Da of the strain CCMP122, which confirmed the substance at t_R=4,07 min as AM18

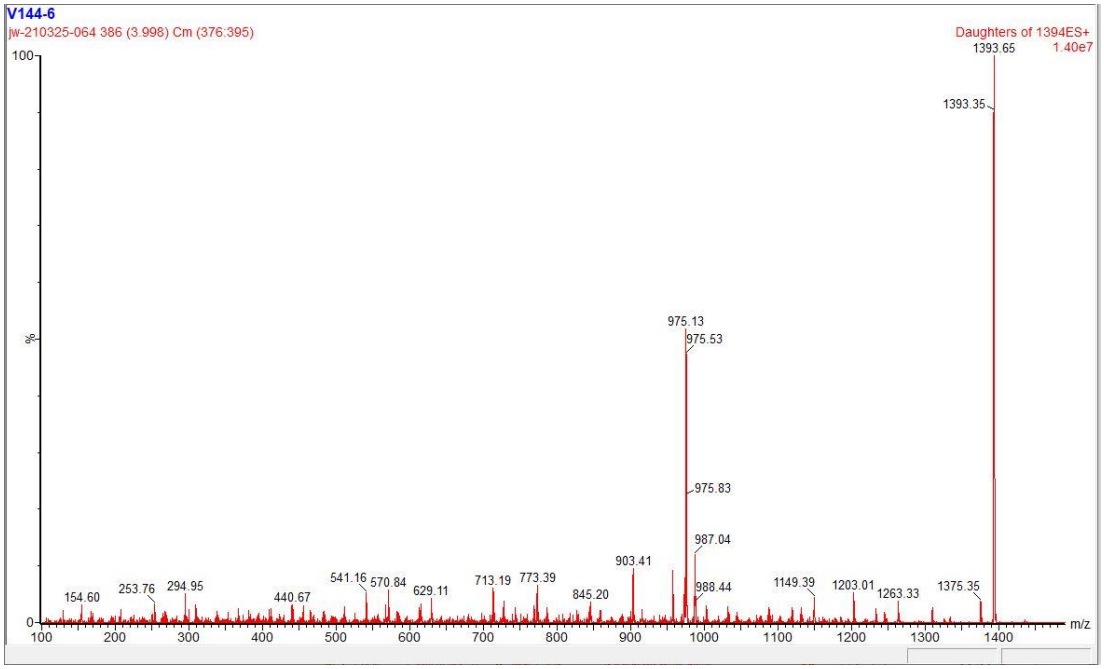

Figure 45: Enhanced product ion spectrum of 1394Da of the strain AA177, which confirmed the substance at t_R=4,00 min as AM05

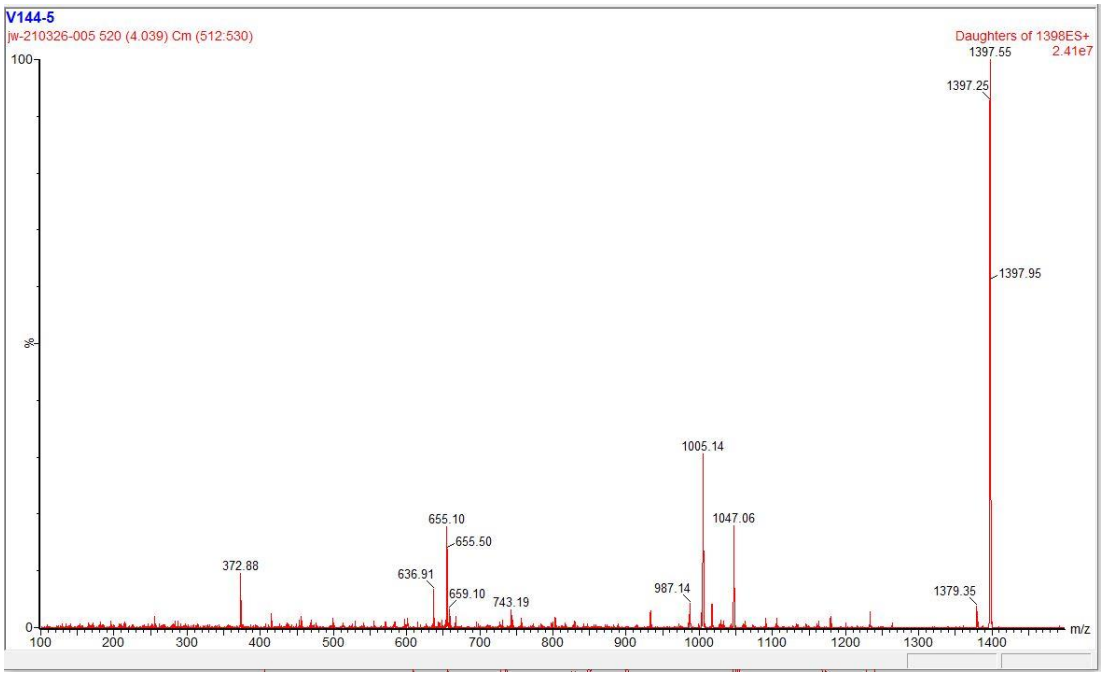

Figure 46: Enhanced product ion spectrum of 1398Da of the strain AA181, which confirmed the substance at t_R=4,00 min as AM02

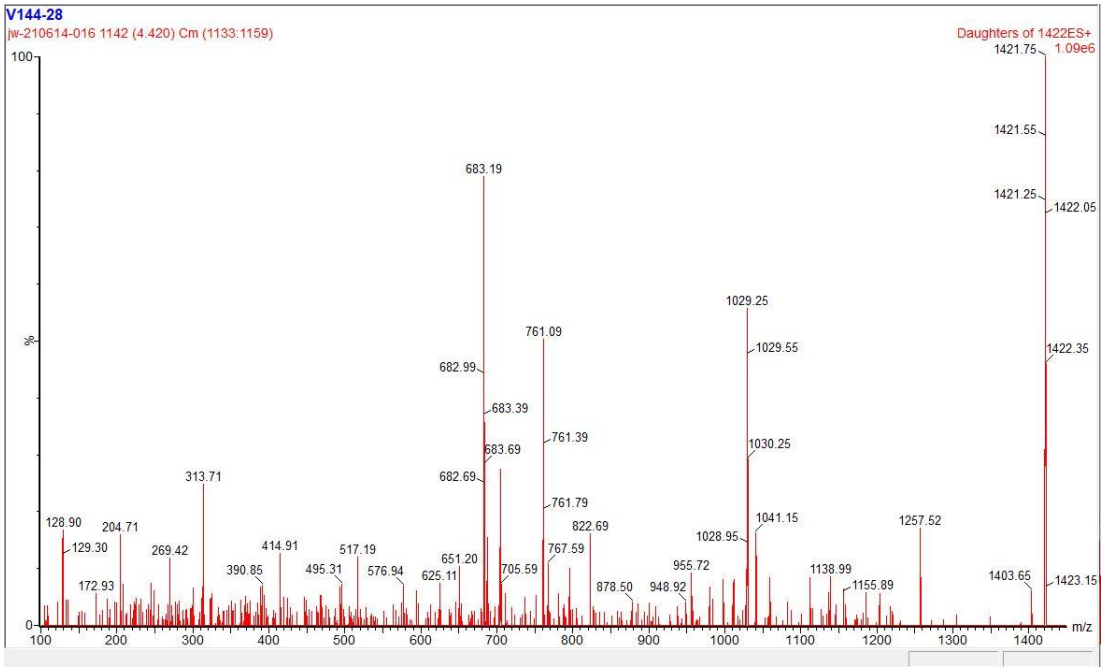

Figure 47: Enhanced product ion spectrum of 1422Da of the strain ARC411, which could not confirm the substance at t_R=4,42 min as CarE clearly

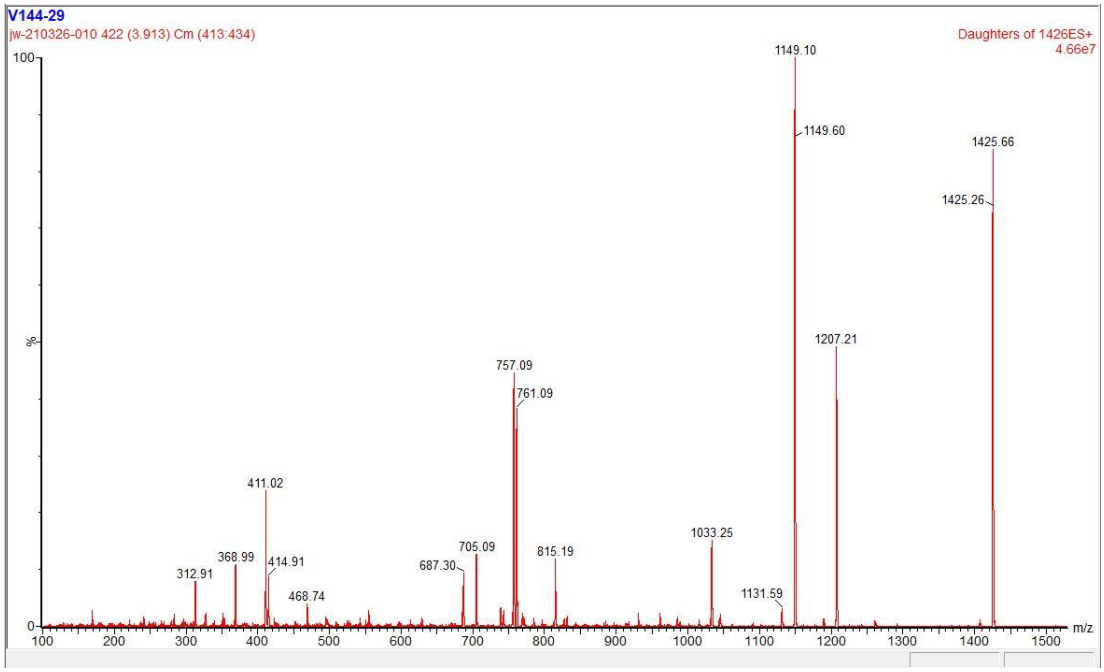

Figure 48: Enhanced product ion spectrum of 1426Da of the strain ARC412, which did not confirm the substance at t_R =3,91 min as AM12

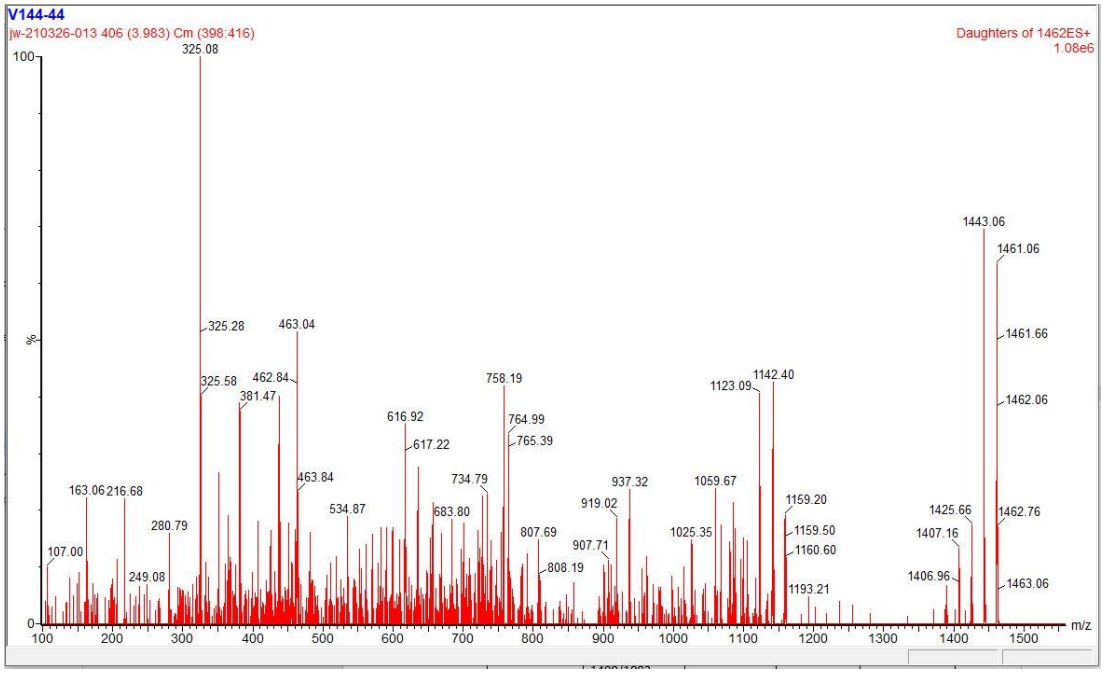

Figure 49: Enhanced product ion spectrum of 1462Da of the strain ARC149, which did not confirm the substance at t_R=4,00 min as KarB

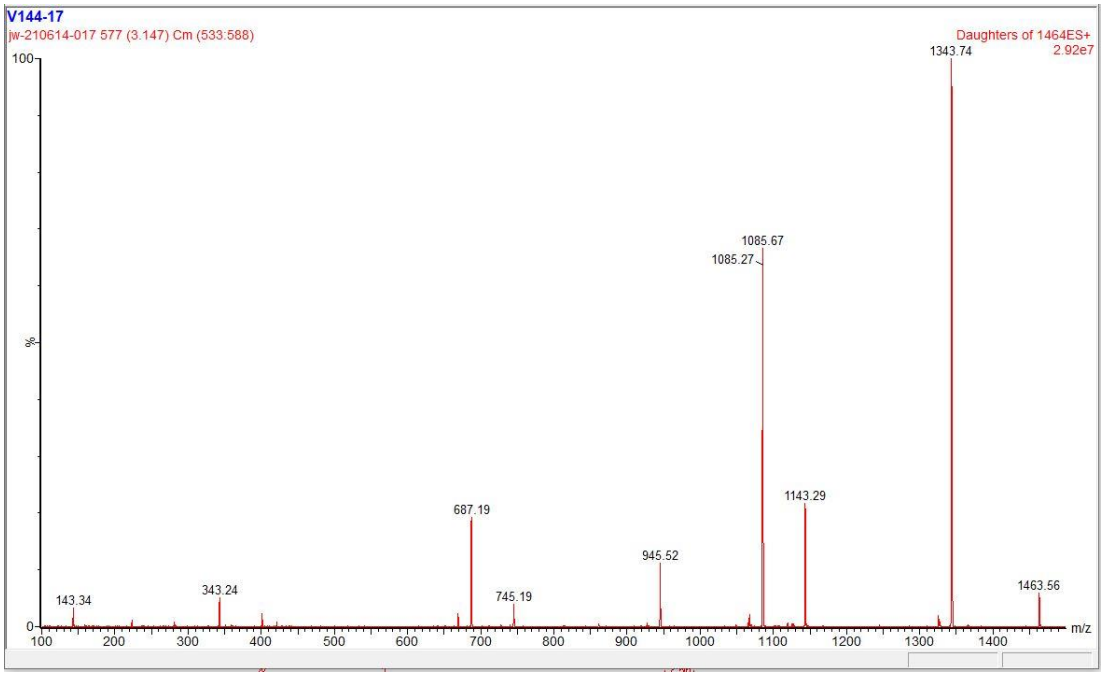

Figure 50: Enhanced product ion spectrum of 1464Da of the strain CCMP122, which confirmed the substance at t_R=3,15 min as AMB

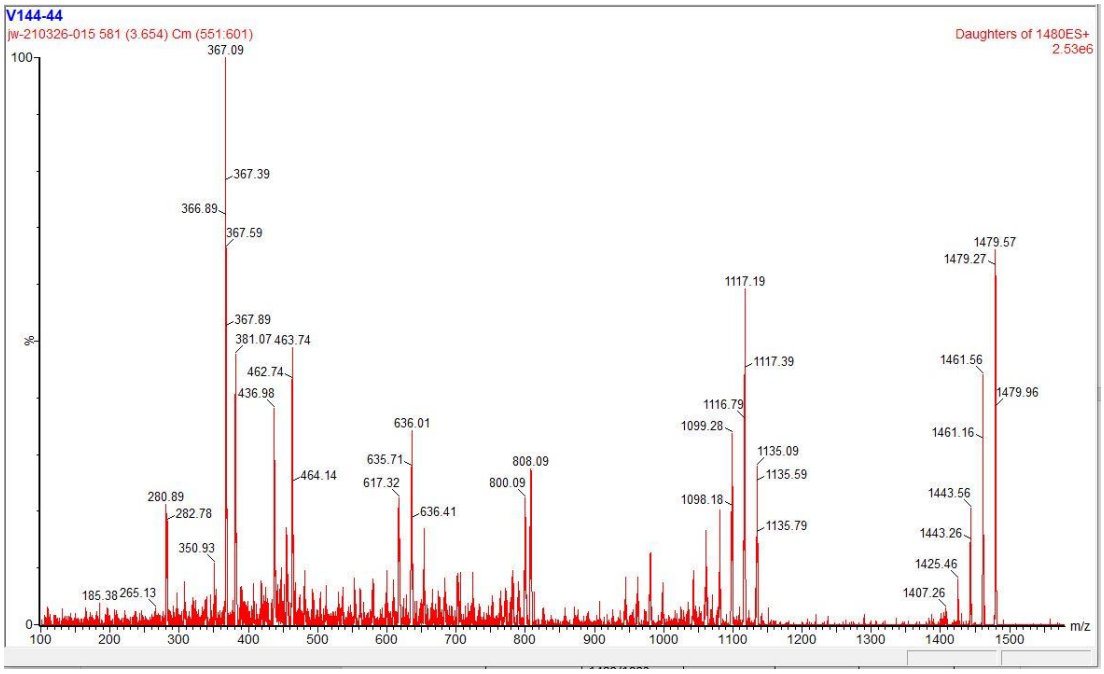

Figure 51: Enhanced product ion spectrum of 1480Da of the strain ARC149, which did not confirm the substance at t_R=3,65 min as KarA

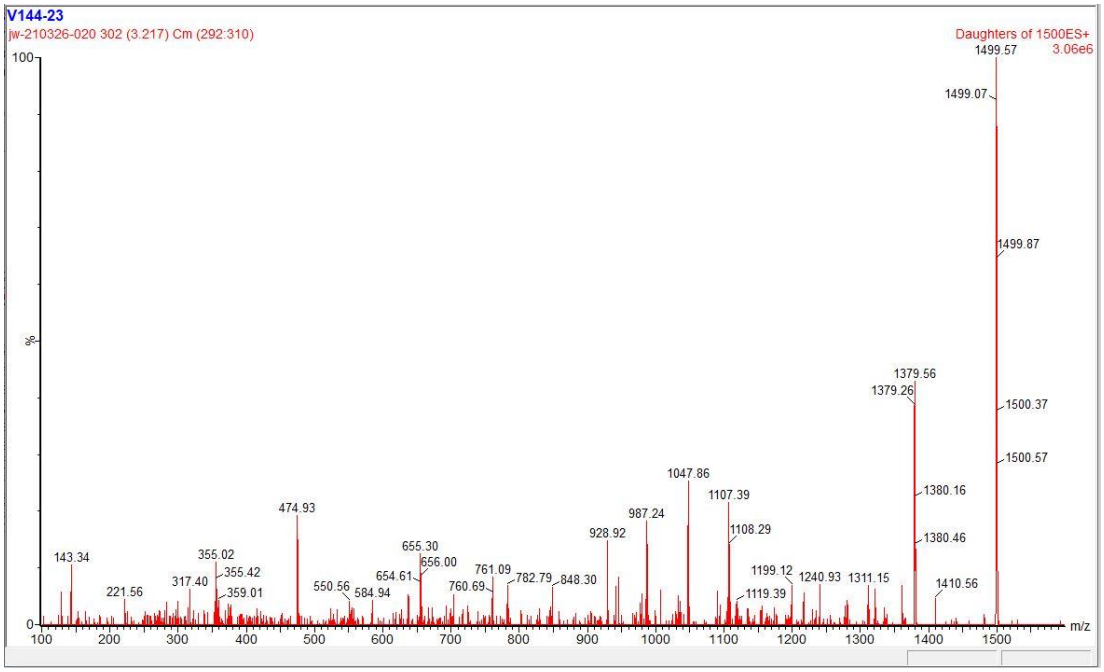

Figure 52: Enhanced product ion spectrum of 1500Da of the strain CCMP2100, which could not confirm the substance at t_R=3,22 min as amphidinol 11 clearly, due to the low abundance of peaks

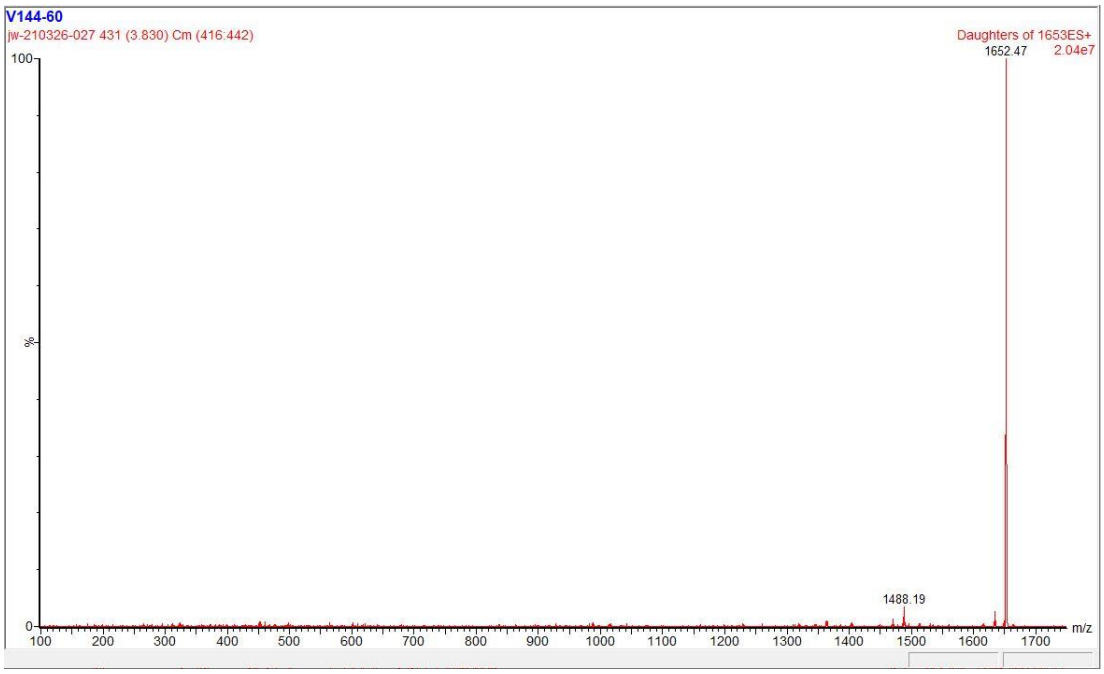

Figure 53: Enhanced product ion spectrum of 1653Da of the strain ARC197, which did not confirm the substance at t_R=3,83 min as AM20S

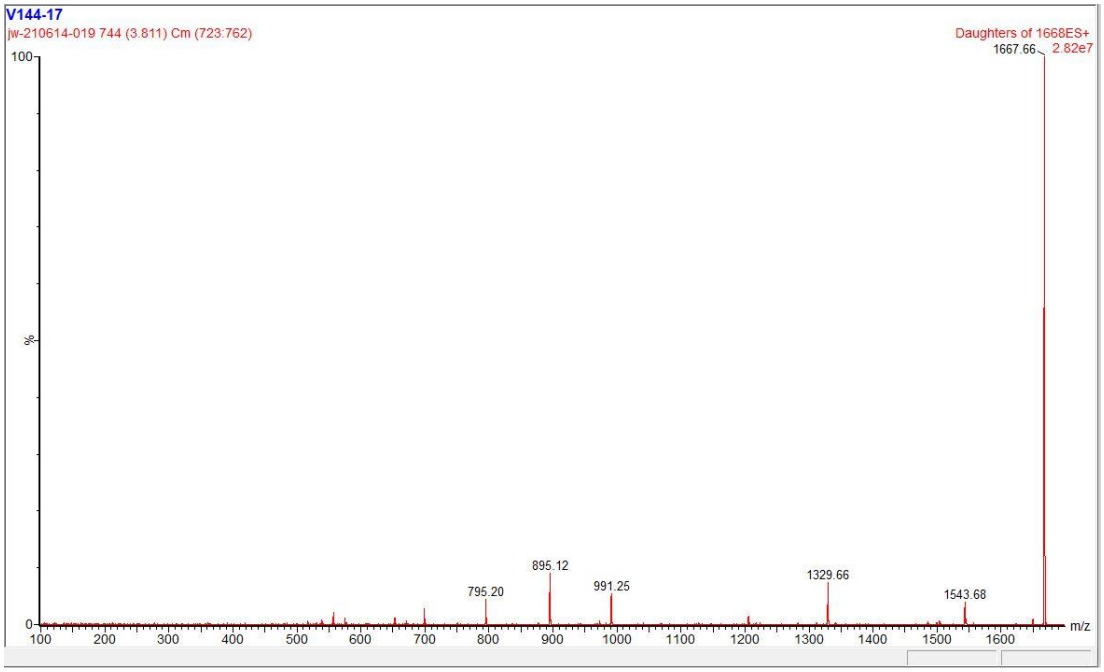

Figure 54: Enhanced product ion spectrum of 1668Da of the strain CCMP122, which confirmed the substance at t_R=3,81 min as AM22

Hochschule **RheinMain**
University of Applied Sciences
Wiesbaden Rüsselsheim

Affidavit

I hereby confirm that my bachelor thesis entitled "*Screening of several Amphidinium species and strains for amphidinols and related secondary metabolites*" is the result of my own work. I did not receive any help or support from third parties. All sources containing directly, or indirectly applied language and ideas are listed and marked as not my own in the thesis.
Furthermore, I confirm that this thesis has not yet been submitted in identical or in a similar form as part of another examination process.

Bremerhaven, 21.06.21

Jannik Weber